**KARADENİZ TECHNICAL UNIVERSITY**
**THE GRADUATE SCHOOL OF NATURAL AND APPLIED SCIENCES**

**DEPARTMENT OF CHEMISTRY**

# DEVELOPMENT AND APPLICATION OF A NOVEL COLORIMETRIC BLOOD CALCIUM MEASUREMENT METHOD

**MASTER'S THESIS**

**Amad Badal YOUNIS**

**SEPTEMBER 2024**
**TRABZON**

**KARADENİZ TECHNICAL UNIVERSITY**

**THE GRADUATE SCHOOL OF NATURAL AND APPLIED SCIENCES**

**DEPARTMENT OF CHEMISTRY**

# DEVELOPMENT AND APPLICATION OF A NOVEL COLORIMETRIC BLOOD CALCIUM MEASUREMENT METHOD

**Amad Badal YOUNIS**

**ORCID : - - -**

**This thesis is accepted to give the degree of**

**"MASTER OF SCIENCE"**

**By**

**The Graduate School of Natural and Applied Sciences at**
**Karadeniz Technical University**

**The Date of Submission : 04 / 09 /2024**

**The Date of Examination : 23 / 09 /2024**

**Supervisor : Prof. Dr. Murat KÜÇÜK**

**ORCID : - - -**

**Trabzon 2024**

## PREFACE

I would like to convey my sincere appreciation and respect to my extremely valued supervisor, Prof. Dr. Murat KÜÇÜK. He assisted and guided me during the entire process of preparing my master's thesis, supporting me every step of the way. In addition, I want to express my gratitude to my parents for their support and to my wonderful wife Areen Mohammed for being by my side no matter what. I also want to express my gratitude to my study group buddies from the Bioactivity Laboratory (BAL) for their assistance. Additionally, I want to thank the Turkiye Scholarship (YTB) for this wonderful chance and for providing me with all my education fees.

Amad Badal Younis YOUNIS

Trabzon 2024

## THESIS ETHICS STATEMENTS

This study titled " Development and application of a novel colorimetric blood calcium measurement method", which I presented as my Master thesis was carried out by myself and I completed it under the responsibility of my supervisor Prof. Dr. Murat KÜÇÜK from beginning to end. I collected the data/samples myself, I carried out the experiments/analyses in the Biochemistry Laboratory of Karadeniz Technical University, Department of Chemistry, and I fully present the information I received from other sources in the text and bibliography, that I acted by scientific research and ethical rules during the study process, and that in case the opposite occurs, I declare that I accept all legal consequences. 04/09/2024

Amad Badal Younis

**CONTENTS**

**Page No**

Yüksek Lisans Tezi

# ÖZET

Yeni bir kolorimetrik kan kalsiyum ölçüm yönteminin geliştirilmesi ve uygulanması

Amad Badal YOUNIS

Karadeniz Teknik Üniversitesi
Fen Bilimleri Enstitüsü
Kimya Anabilim Dalı
Danışman: Dr. Murat KÜÇÜK
2024, 88 Sayfa

o-Cresol Ftalein Komplekson (CPC) yöntemini kullanan, kolorimetri kullanarak serumdaki kalsiyumun ölçülmesine yönelik yeni bir yaklaşım ortaya kondu. Bu yöntem, geleneksel ultraviyole-görünür (UV-Vis) spektrometrisinin yerini, daha basit ve uygun maliyetli akıllı telefon tabanlı kolorimetrik dijital görüntü tekniğiyle değiştirmektedir. Bu yöntem için belirlenen optimal koşullar arasında yeşil renk modelinin en etkili olarak kullanılması, görüntüleme kamerası ile örnek çözelti arasında 25 cm mesafenin korunması ve ışık kaynağının örnek çözeltilerden 3 cm uzağa konumlandırılması yer almaktadır. Optimum koşullar altında tayin katsayısı, 20 mg/dL'ye kadar doğrusal dinamik aralığında 0,9917 idi. Yöntemin kesinliği, yüzde bağıl standart sapmaya dayalı olarak %5'in altındaydı. Tespit sınırı (LOD) ve tayin sınırı (LOQ) sırasıyla 0,46 mg/dL ve 1,56 mg/dL olarak belirlendi; bu değerler serumdaki kalsiyum seviyelerini ölçmek için yeterlidir. Yöntemin doğruluğu, UV-Vis yöntemi kullanılarak yapılan bağımsız bir deneyle doğrulandı. İki yöntem önerilen yaklaşımın güvenilirliğini vurgulayan güçlü istatistiksel uyum gösterdi.

**Anahtar Kelimeler**: CPC Yöntemi, Kan Kalsiyumu, Dijital Görüntü İşleme, Image J, Kolorimetri.

MASTER'S THESIS

**SUMMARY**

Development and application of a novel colorimetric blood calcium measurement method

Amad Badal YOUNIS

Karadeniz Technical University
The Graduate School of Natural and Applied Sciences
Chemistry Department
Supervisor: Prof. Murat KÜÇÜK
2024, 88 Pages

A new approach for measuring calcium in serum using colorimetry is introduced, which utilizes the o-Cresol Phthalein Complexone (CPC) method. This method replaces traditional ultraviolet-visible (UV-Vis) spectrometry with a more straightforward and cost-effective smartphone-based digital image colorimetric technique. The optimal conditions determined for this method include using the green color model as the most effective, maintaining a distance of 25 cm between the detection camera and the sample solution, and positioning the light source 3 cm from the sample solutions. Under the optimum conditions, the coefficient of determination was 0.9917 within a linear dynamic range up to 20 mg /dL. The precision of the method based on the percent relative standard deviation was below 5%. The detection limit (LOD) and quantitation limit (LOQ) were determined to be 0.46 mg/dL and 1.56 mg/dL, respectively, which are adequate for measuring calcium levels in serum. The method's accuracy was confirmed through validation with an independent experiment using a UV-Vis method. The two methods demonstrated strong statistical agreement, underscoring the reliability of the proposed approach.

**Key Words:** CPC-Method, Blood Calcium, Digital Image Processing, Image J, Colorimetry.

## FIGURES INDEX

**Page No**

## TABLES INDEX

**Page No**

## ABBREVIATION INDEX

| | |
|---|---|
| EXF | Extracellular fluid |
| PTH | Parathyroid hormone |
| MEN | Multiple Endocrine Neoplasia |
| ISE | Ion Selective Electrode |
| DICP | Digital Image Colorimetry Processing |
| RGB | Red Green Blue |
| HSB | Hue, Saturation, Brightness |
| CMYK | Cyan, Magenta, Yellow, Black |
| CUPRAC | Cupric Reducing Antioxidant Capacity |

# 1. INTRODUCTION

## 1.1. Body Fluid Compartments

The body is made up of 60–70% water. The solute content of each bodily water compartment determines how water is distributed inside it. The extracellular fluid and the intracellular fluid make up the two primary compartments that contain all of the bodily fluid (shown in Figure 1), and the extracellular fluid comprises both blood plasma and interstitial fluid (Hall, 2015, Vasudevan et al., 2013).

An additional fluid compartment, termed transcellular fluid, exists in the human body. This compartment encompasses cerebrospinal fluid, along with the fluid present in synovial, peritoneal, pericardial, and intraocular spaces. While its composition may occasionally diverge markedly from that of plasma or interstitial fluid, it is generally regarded as a distinct subtype of extracellular fluid. The aggregate volume of transcellular fluids typically ranges between one and two liters (Hall, 2015).

The body water content of a 70-kg adult male is approximately 42 liters, equivalent to 60% of his body weight. This percentage is subject to variation based on factors such as obesity, age, and gender. Specifically, the proportion of total body weight constituted by fluids diminishes progressively with advancing age. The aging-related decrease in bodily water content is partially attributable to the tendency for an increased proportion of body fat as individuals age. This elevation in body fat percentage subsequently diminishes the overall water content of the body. Women often have a higher percentage of body fat than males do, hence their total body water makes up roughly 50% of their body weight on average. The percentage of total body water in preterm and newborns varies between 70 and 75 percent of their body weight. As a result, we should be aware that there are differences in "average" bodily fluid compartments based on factors including age, gender, and body fat percentage (Hall, 2015).

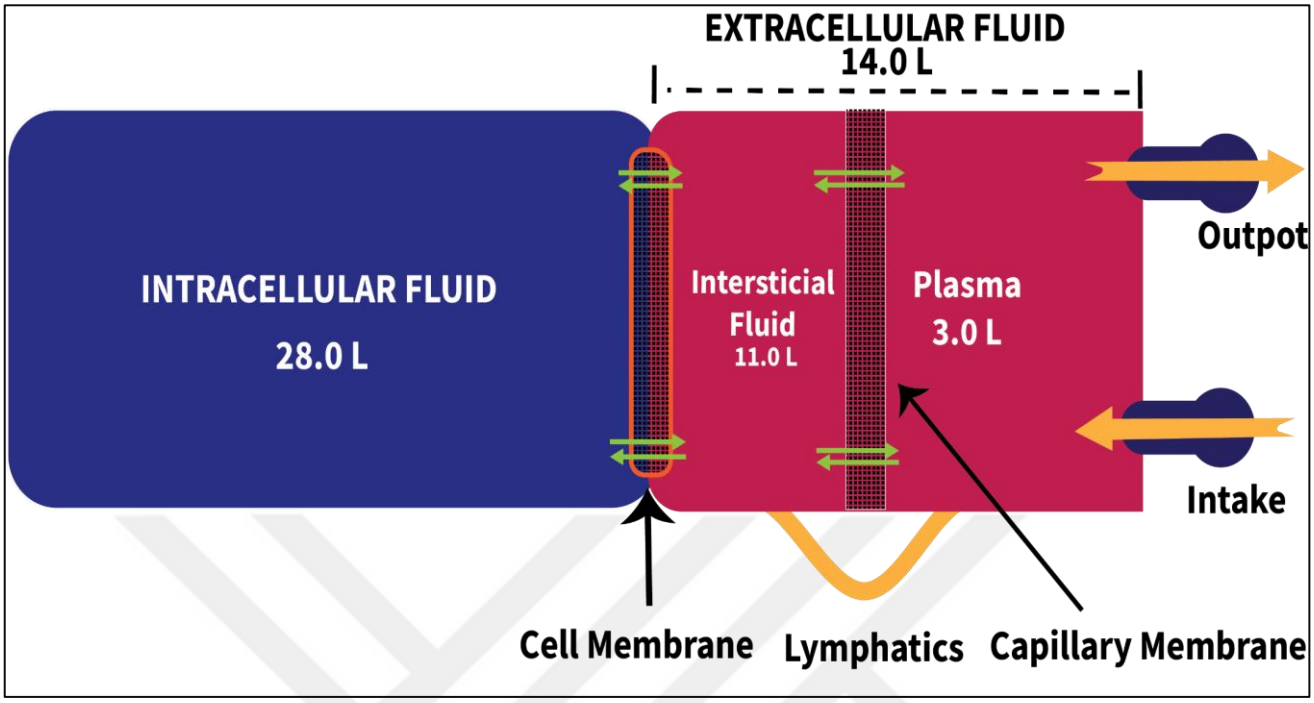


Figure 1. An overview of the main bodily fluid compartments and the membranes dividing them, as well as the management of bodily fluids. The amounts displayed are for an adult male weighing an average of 70 kg.

### 1.1.1. Intracellular Fluid

The 42 liters of fluid within the body consist of approximately 28 liters of intracellular fluid (Figure 1), distributed within each of the body's estimated 100 trillion cells. Consequently, in an "average" individual, intracellular fluid constitutes approximately 40% of their total body weight. The fluid within each cell comprises a distinct blend of numerous components, yet the concentrations of these chemicals remain uniform throughout the cell. Remarkably, the composition of cell fluids exhibits striking similarity across a diverse spectrum of organisms, spanning from humans to the most primitive microbes. Consequently, the intracellular fluid within each cell is regarded as a unified and extensive fluid compartment (Hall, 2015).

### 1.1.2. Extracellular Fluid

Extracellular fluid is the term used to refer to all fluids that are not inside of cells. When combined, these liquids make up around 20% of the body weight or 14 liters in the case of a 70-kg man. The interstitial fluid, which comprises over three-quarters (11 liters) of the extracellular fluid, and the plasma, which comprises about one-fourth, or around 3 liters, of the extracellular fluid, are the two major compartments of the extracellular fluid. Plasma constantly exchanges materials with the interstitial fluid through the capillary membrane pores. Except for proteins, nearly all of the solutes in the extracellular fluid are extremely permeable through these pores. Because of this continuous mixing of extracellular fluids, the compositions of the interstitial and plasma fluids are similar, except for proteins, which are more concentrated in the plasma (Hall, 2015).

### 1.1.3. The Components of Extracellular and Intracellular Fluids

Comparisons between the contents of the intracellular fluid and the extracellular fluid, which includes the plasma and interstitial fluid, are presented in Figure 2 and Table 1. Plasma's ionic composition and interstitial fluid are similar, but the concentration of positively charged ions, or cations, is slightly higher (around 2 percent) in the plasma than in the interstitial fluid due to the Donnan effect. In contrast, because the negatively charged anions are repelled by the plasma proteins' negative charges, negatively charged ions (anions) often have a somewhat higher concentration in the interstitial fluid than in the plasma.

Table 1. Concentration of electrolytes in body fluid compartments.

| **Solutes** | **Plasma** (mEq/L) | **Interstitial Fluid** (mEq/L) | **Intracellular Fluid** (mEq/L) |
|---|---|---|---|
| **Cations:** | | | |
| Sodium | 140 | 146 | 12 |
| Potassium | 4 | 5 | 160 |
| Calcium | 5 | 3 | - |
| Magnesium | 1.5 | 1 | 34 |

Table 1 Continue

| | | | |
|---|---|---|---|
| **Anions**: | | | |
| Chloride | 105 | 117 | 2 |
| Bicarbonate | 24 | 27 | 10 |
| Sulphate | 1 | 1 | - |
| Phosphate | 2 | 2 | 140 |
| Protein | 15 | 7 | 54 |
| Other anions | 13 | 1 | - |

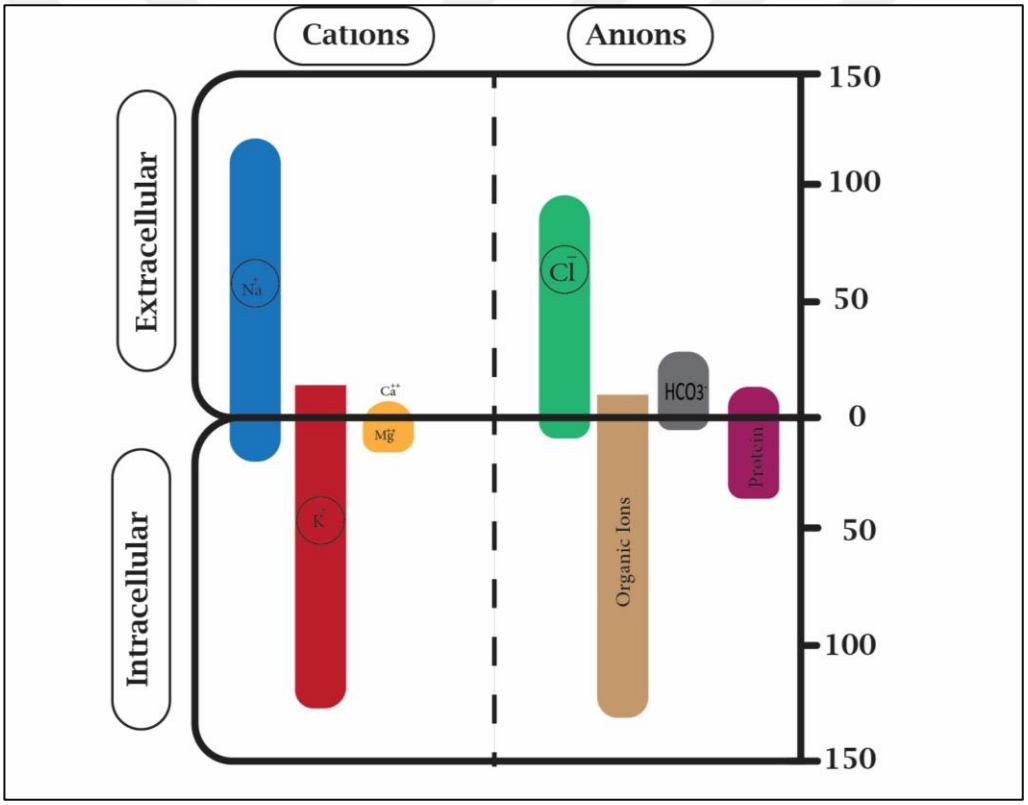


Figure 2. Main anions and cations found in extracellular and intracellular fluids.

### 1.1.4. The Components of Intracellular Fluid

The cell membrane, which serves as the boundary between intracellular fluid and extracellular fluid, exhibits high permeability to water while maintaining impermeability to most of the body's electrolytes. Compared to extracellular fluid, the intracellular fluid contains very little sodium and chloride ions and nearly none calcium ions. On the other

hand, it contains moderate levels of magnesium and sulfate ions, along with considerable concentrations of potassium and phosphate ions, all of which have low concentrations in the extracellular fluid. Additionally, cells have a high protein content, almost four times that of plasma (Figure 2).

### 1.2. Blood

Blood is made up of both intracellular (found in red blood cells) and extracellular (found in plasma) fluids, Red Blood Cells, and White Blood Cells precipitate from blood when it is centrifuged after mixing with an anticoagulant. We refer to the supernatant as plasma. Plasma makes up between 55 and 60 % of blood. However, because blood is kept in its chamber the circulatory system is regarded as a different fluid compartment.

Adults typically have 4.5 to 5 liters of blood, or 7% of their body weight, in circulation. For general health but especially important to the regulation of cardiovascular dynamics is the blood volume. Red blood cells makeup 40 % of blood and plasma makes up about 60 % of it, however individual differences in these percentages can occur based on several factors, including gender and weight (Toribio, 2011).

### 1.3. Blood Electrolytes

Electrolytes are essential minerals that play critical roles in maintaining various physiological processes necessary for life. These minerals include sodium ($Na^+$), potassium ($K^+$), calcium ($Ca^{2+}$), chloride ($Cl^-$), magnesium ($Mg^{2+}$), phosphate ($PO_4^{3-}$), and bicarbonate ($HCO_3^-$). They are found in the blood and other body fluids, carrying an electric charge that is crucial for many bodily functions (Shrimanker and Bhattarai, 2019).

#### 1.3.1. Functions of Key Electrolytes

Sodium ($Na^+$) regulates fluid balance, nerve function, and muscle contractions, while potassium ($K^+$) is crucial for nerve transmission and muscle contraction, particularly in the heart. Chloride ($Cl^-$) maintains fluid balance and forms a component of stomach acid. Bicarbonate ($HCO_3^-$) buffers to maintain normal blood pH levels. Phosphate ($PO_4^{3-}$) is vital for energy production, bone formation, and cell signaling. Magnesium ($Mg^{2+}$) supports

muscle and nerve function, blood glucose control, and bone health. Together, these electrolytes are essential for various physiological functions and overall health. Normal range and Imbalance Implications of some key electrolytes are summarized in Table 2 below (Mount, 2008, Smith, 2010, Schrier, 1990).

Table 2. Normal range and Imbalance Implications of some key electrolytes.

| **Electrolytes** | **Normal Range** | **Hyper Effect** | **Hypo Effect** |
|---|---|---|---|
| Sodium | 135-145 mEq/L. | thirst, weakness, and in seizures and coma | nausea, headache, confusion, and seizures |
| Potassium | 3.5-5.0 mEq/L | fatigue, weakness, and cardiac | muscle weakness, cramps, and arrhythmias |
| Chloride | 96-106 mEq/L. | fatigue, weakness, and excessive thirst | metabolic alkalosis, shallow breathing, and muscle spasms |
| Bicarbonate | 22-28 mEq/L. | Alkalosis, in vomiting, muscle twitching, and hand tremors | Acidosis, rapid breathing, confusion, and fatigue |
| Phosphate | 2.5-4.5 mg/dL | Can lead to itching and, with chronic elevation, cardiovascular disease | muscle weakness, respiratory failure, and hemolysis |
| Magnesium | 1.7-2.2 mg/dL. | Can result in nausea, hypotension, and in severe cases, cardiac arrest | Can cause muscle cramps, seizures, and cardiac arrhythmias |

### 1.4. Calcium

In the human body, calcium is one of macro element of vital importance, the average body has between 1000 to 1500 g of calcium in total, of all of wich 99% are concentrated in the bone as the mineral phase of bone's hydroxyapatite ($Ca_{10}(PO_4)_6(OH)_2$) crystal, with the remainder being found in body fluids such as plasma and extracellular fluid. According to age-specific body requirements, humans ought to take 120–1500 mg of calcium per day, to be clearer, a child needs approximately 1200 mg per day. More specifically, a child needs approximately 1200 mg per day, and an adult needs 500 mg. In certain circumstances, such as pregnancy and lactation, daily requirements may be increased to 1500 mg. About 20% of this is obtained by drinking water with calcium, while the remaining 80% is obtained through food intake (Favus et al., 2006, Li and Zhai, 2020, Vasudevan et al., 2013). Insufficiency of calcium is considerd to be harmful to human health since it is not only the building block for bone development and directly affects growth but also serves other key physiological purposes in the human body (Li and Zhai, 2020).

#### 1.4.1. Distribution of Calcium in the Body

In the human body, total calcium is mostly distributed in bone and the extracellular fluid (ECF). In the mineral phase of bone, hydroxyapatite crystals make up 99% of total calcium. These crystals help the bone's ability to support mechanical weight bearing, supporting the body against gravity, protecting internal organs (heart, brain, spinal cord, and lungs), and serving as a niche for blood-forming substances, as well as acting as a reservoir of $Ca^{2+}$ that can be quickly mobilized to support the various biological systems that depend on calcium for cofactors and regulators (Favus et al., 2006, Toribio, 2011).

The majority of the remaining calcium 0.9% calcium exists in the endoplasmic reticulum and plasma membrane of cells, 0.1% of the total body's calcium mass is found in the extracellular fluid including blood, which has a total calcium concentration of roughly 2.5 mmol/L, and the cytoplasm of cells contains extremely little calcium around 100 nM, mostly in the form of ions (Baker and Worthley, 2002). Three main forms of serum total calcium concentration (0.001M) are found: 50% ionized, 40% protein-bound, and 10% mainly complexed to citrate and $PO_4^{3-}$ ions, Calcium's biological effects are achieved by its

ionized form, which is readily exchanged with calcium stores in bone, blood, and intracellular spaces (Favus et al., 2006).

### 1.4.2. Homeostasis

Calcium concentration is regulated and remains stable, and the balance system is continuously adjusting to deliver enough calcium from the intestine and kidney into the extracellular fluid (ECF) and blood, and then to bone to fulfill changing skeletal growth requirements without disturbing the serum-ionized Ca concentration [$Ca^{2+}$]. This refers the fact that skeletal calcium requirements and diet calcium intake differ significantly during the life cycle and from day to day (Favus et al., 2006). The blood's ionized calcium never changes more than 5% in a healthy, typical body, and this mechanism is maintained mostly by the action of Parathyroid Hormone (PTH) and Vitamin D (Baker and Worthley, 2002).

## 1.5. Absorption of Calcium

Absorption occurs in the first and second segments of the duodenum. Calcium is absorbed by active transport, proceeding against a concentration gradient, and it necessitates energy (Vasudevan et al., 2013). Ca absorption from the intestinal tract includes saturable “transcellular” transport and nonsaturable “paracellular” transport. The percentage of intestinal absorption is directly related to the amount of food intake, diets low in calcium can lead to high absorption rates of up to 95%, whereas diets rich in calcium have lower absorption rates of around 40%. High-calcium food while having poor absorption rates, may elevate blood calcium levels due to nonsaturable intestinal absorption. Diets with low calcium may lead to normal levels of calcium in the blood due to the body's response mechanisms such as parathyroid hormone, bone resorption, renal calcium reabsorption, and enhanced synthesis of 1,25-dihydroxy vitamin D (Rosol and Capen, 1997).

The saturable transcellular process is mostly found in the duodenum and is carrier-mediated and reliant on vitamin D. It mainly occurs in the duodenal region of the small intestine, but can also be present in the cecum and colon. Saturable transport involves the entry of calcium into intestinal epithelial cells via calcium channels, its movement and stabilisation in the cytoplasm, and its release by a $Ca^{2+}$-ATPase on the basolateral side.(Bronner, 2003, Rosol and Capen, 1997).

The paracellular passive mechanism is unsaturable and operates over the whole length of the intestine. Unsaturable calcium transport relies on the calcium concentration in the intestinal lumen. When the amount of calcium in the food is raised, a significant portion of the calcium in the intestines becomes unavailable for absorption that is not restricted by absorption due to the formation of calcium salts or complexes with anions (Bronner, 2003, Rosol and Capen, 1997).

### 1.5.1. Factors Causing Higher Absorption

I. Vitamin D: in its active form, 1,25-dihydroxy vitamin D, promotes the transcellular transport of calcium by increasing the production of the carrier protein Calbindin in the cells of the intestine, thus raising calcium absorption.
II. Parathyroid hormone: enhances calcium transfer from intestinal cells.
III. Acidity: promotes the absorption of calcium.
IV. Lysine and arginine: improve calcium absorption.

### 1.5.2. Factors Causing Reduced Absorption

I. Oxalates: found in some green plants lead to the creation of insoluble calcium oxalates.
II. Malabsorption syndromes: result in the failure to absorb fatty acids, leading to the production of insoluble calcium salts of fatty acids.
III. Phosphate: excessive levels of phosphate will result in the formation of calcium phosphate precipitate.

## 1.6. Factors Regulating Blood Calcium Level

The normal limited range of blood calcium can be controlled with proper actions.

### 1.6.1. Vitamin D

Vitamin D is a collective designation for a class of fat-soluble vitamins (Baker and Worthley, 2002). Vitamin D is obtained by applying ultraviolet radiation, 7-dehydrocholesterol or ergosterol can be converted into vitamin D. There are two forms of

vitamin D: vitamin D2, also known as ergocalciferol, and vitamin D3, also known as cholecalciferol. Ergocalciferol is produced from irradiated fungus or yeast. Cholecalciferol is produced in the skin or found naturally in fatty fish such as salmon or mackerel. Both forms of vitamin D can be used to enrich food, but only cholecalciferol can be produced naturally and endogenously in the skin (Khazai et al., 2008).

7-dehydrocholesterol, a compound in a more common route of cholesterol production, is found in the Malpighian layer of the skin. Ultraviolet radiation (290-315 nm) in the epidermis causes the bond between positions 9 and 10 of the steroid ring to break. So, the ring B is opened, to generate the provitamin secosterol. The cis double bond between the 5$^{th}$ and 6$^{th}$ carbon atoms undergoes isomerization to a trans double bond by rotating on the 6$^{th}$ carbon atom, resulting in the formation of vitamin D3 or cholecalciferol Figure 3. Therefore vitamin D is known as the sunny vitamin (Vasudevan et al., 2013). Various factors such as skin color, age, sunscreen usage, time of day, season, and location might influence the production of vitamin D3 in the skin (Khazai et al., 2008).

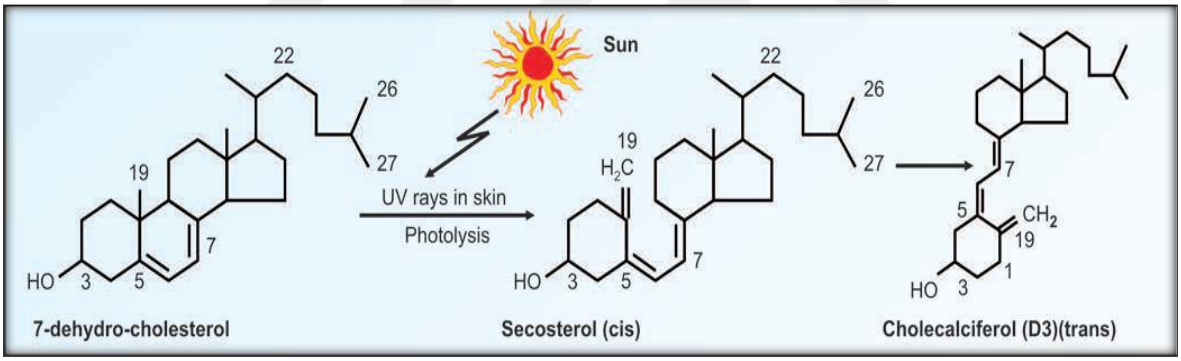


Figure 3. Production of Vitamin D3 by sunlight

Calcitriol enhances the intestinal absorption of calcium and phosphorus. Calcitriol enters the intestinal cell and links to a cytoplasmic receptor. The hormone-receptor complex binds to DNA, leading to the activation and subsequent transcription of certain genes responsible for producing Calbindin. A higher concentration of calcium-binding protein enhances the absorption of calcium. Therefore, blood calcium levels tend to increase (Vasudevan et al., 2013).

### 1.6.2. Parathyroid Hormone (PTH)

Parathyroid hormone (PTH) is a big polypeptide composed of 84 amino acids. Its molecular weight is around 9500. It comes out as prepro-PTH with 115 amino acids. Within the endoplasmic reticulum and Golgi apparatus. It undergoes modifications with the removal of 25 amino acids to create pro-PTH. Then pro-PTH is broken to produce PTH with 84 amino acids and stored in secretory granules, but the storage of PTH spans for around 1 hour, and in the plasma, half-life is 10 minutes. Parathyroid hormone (PTH) is broken down by hepatic Kupffer cells, and its fragments are eliminated by the kidneys. The plasma concentration of PTH ranges from 1.0 to 6.5 pmol/L (Baker and Worthley, 2002, Vasudevan et al., 2013).

The first 35 amino acids of PTH have biological functions. The release of the hormone is regulated by negative feedback via ionized calcium levels in the bloodstream. Parathyroid hormone binds to a receptor protein which is on the surface of target cells. This stimulates adenyl cyclase, leading to a rise in intracellular calcium levels. Parathyroid hormone (PTH) has its effects directly at three main sites: bone, kidney, and intestines. PTH's three effects all result in elevated serum calcium concentration. PTH in the bone leads to demineralization or decalcification, PTH in the kidney reduces calcium excretion and increases phosphate excretion, as well as in the intestines Parathyroid hormone (PTH) promotes the conversion of 25-hydroxycalciferol to calcitriol by 1-hydroxylation in the kidney. This enhances the absorption of calcium from the intestines indirectly (Figure 4) (Vasudevan et al., 2013).

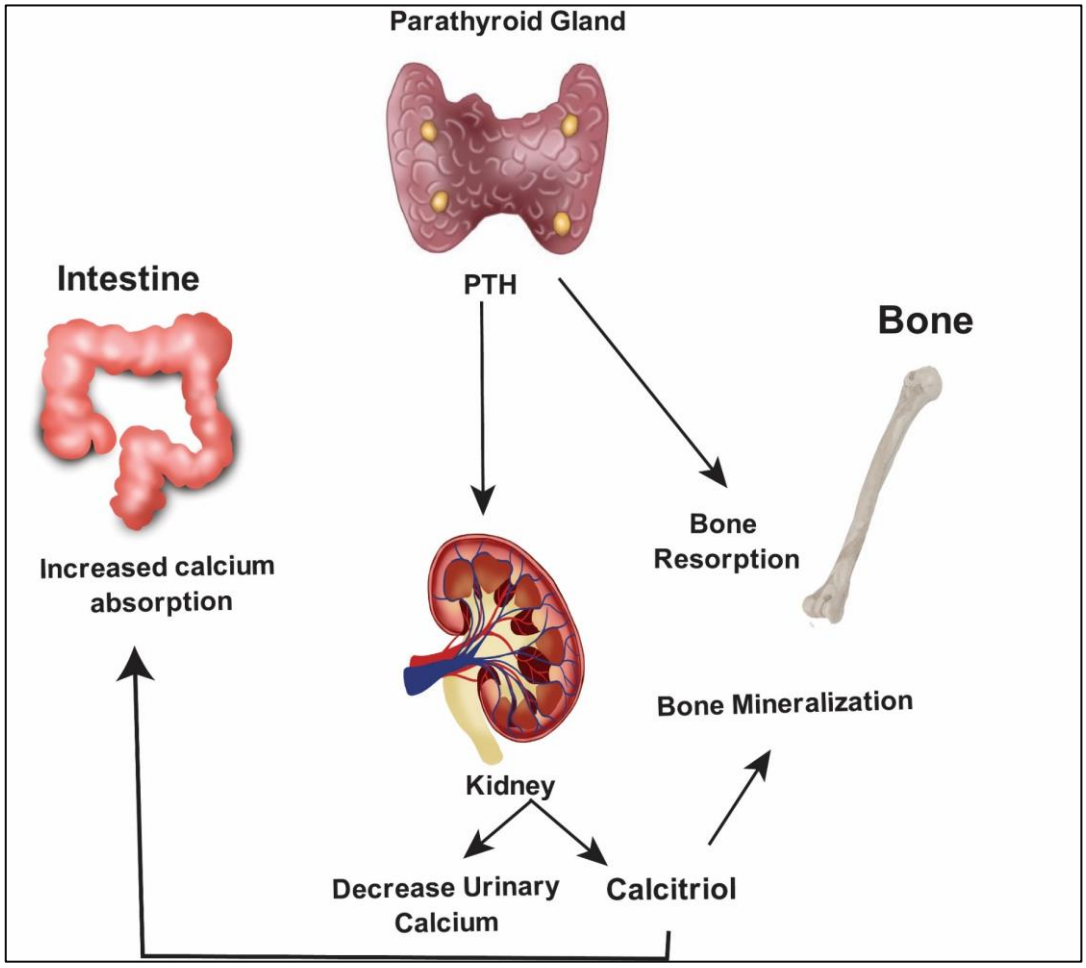


Figure 4. Calcium regulation

### 1.6.3. Calcitonin

Calcitonin is a 32-amino acid polypeptide hormone with a molecular weight of 3500 and a half-life of about 10 minutes. Clear cells or parafollicular of the thyroid are responsible of secretion of Calcitonin. Calcitonin secretion is regulated by serum calcium, gastrin, glucagon, and biological amines. Typically, when the plasma calcium level exceeds 2.45 mmol/L. Its primary function seems to be the regulation of hypercalcemia, calcitonin reduces the concentration of calcium in the bloodstream. It prevents the absorption of bone. It inhibits osteoclast activity and enhances osteoblast activity. Calcitonin may be released in some pathological circumstances, such as medullary carcinoma of the thyroid, where its levels are

elevated, making it a tumor marker. The amount is elevated in multiple endocrine neoplasia (MEN). Elevated levels of calcitonin in the blood may also be caused by abnormal synthesis of calcitonin from cancerous tumors in the lung and bronchus (Baker and Worthley, 2002, Vasudevan et al., 2013).

Association among Calcitonin, Calcitriol, and PTH can regulate calcium levels. They work together via this technique, when blood calcium levels decrease, parathyroid hormone (PTH) production increases and calcitonin secretion decreases, resulting in bone demineralization and increased calcium entry into the blood. Higher blood calcium levels reduce PTH and stimulate the secretion of calcitonin, leading to greater calcium uptake into bones, these principles are outlined in Figure 4 and

Table 3. Overview of the impact of three primary variables on serum calcium.

| | **Vitamin D** | **PTH** | **Calcitonin** |
|---|---|---|---|
| Serum calcium | Increased | Increased | Decreased |
| Primary action | Absorption | Demineralization | Opposes demineralization |
| Absorption of calcium | Increased | Increased | - |
| Bone resorption | Decreased | Increased | Decreased |
| Result of excess | Hypercalcemia + | Hypercalcemia ++ | Hypocalcemia |

### 1.7. Implications of Changed Calcium Concentrations In The Body Fluids

The body does not immediately react negatively when the amount of phosphate in the extracellular fluid is increased from much below normal to two or three times normal. On the other hand, small variations in the concentration of calcium ions in the extracellular fluid can have profound, instantaneous physiological impacts. Furthermore, long-term hypophosphatemia or hypocalcemia significantly reduces bone mineralization (Toribio, 2011).

### 1.7.1. Hypercalcemia

When the plasma calcium level is more than 11 mg/dl, it is denoted by the term. The central nervous system suffers from depression and slows down its reflex functions when there is an excess of calcium present in bodily fluids. Further, elevated calcium ion concentration shortens the heart's QT interval, suppresses hunger, and induces constipation all likely as a result of decreased gastrointestinal tract muscle wall contractility.

Hyperparathyroidism is the primary reason. An ectopic disease that secretes PTH or a parathyroid adenoma may indicate the cause of this, and hypercalcemia has numerous causes, such as Paget’s disease, Metastatic carcinoma of bone, Dehydration, Milk-alkali syndrome, and some Drugs like Thiazide diuretics, Excess vitamin D or vitamin A, and Lithium therapy (Toribio, 2011).

### 1.7.2. Hypocalcemia

Hypocalcemia occurs when the serum calcium level is less than 8.8 mg/dl. There will be slight tremors if the serum calcium level is less than 8.5 mg/dl. If it is less than 7.5 mg/dl, tetany, a potentially dangerous illness, will arise. The nervous system becomes more irritable when calcium ion concentrations drop below normal because this situation increases neuronal membrane permeability to sodium ions, making action potential initiation easy.

Peripheral nerve fibers become so excitable at plasma calcium ion concentrations roughly 50% below normal that they start to discharge spontaneously. This sets off nerve impulse trains that travel to the peripheral skeletal muscles and cause tetanic muscular contraction. Tetany is consequently brought on by hypocalcemia. Additionally, because it increases brain excitability, it can occasionally result in seizures.

Tetany often develops when the blood calcium concentration drops from 9.4 mg/dl, which is the normal level, to roughly 6 mg/dl, which is just 35% below the normal level. Tetany is typically fatal at 4 mg/dl. The hand tetany typically develops before tetany in the majority of other body parts. Carpopedal spasm is a descriptive name for it (Toribio, 2011, Vasudevan et al., 2013).

### 1.8. Blood Calcium Determination Methods

Serum calcium levels can be determined using a variety of techniques. A number of the frequently used techniques are as: Atomic Absorption Spectroscopy (Willis, 1960), Flame Photometry (Severenghaus and Ferrebee, 1950), Ion-Selective Electrode (ISE) Method (Dash et al., 2022), Titration (Winarno et al., 2021), Fluorometric Method, and Colorimetric Methods (Stern and Lewis, 1957, Morgan et al., 1993).

#### 1.8.1. Colorimetric Methods for Blood Calcium Determination

These techniques use color reagents, which react with calcium ions to change color, the color change's intensity is then determined using spectrophotometry or by the proposed methodology. The utilization of computational software is advocated. There are two widely used colorimetric methods, o-Cresol Phthalein Complexone, and Arsenazo III method.

#### 1.8.2. CPC Method

Calcium analysis in a sample is crucial for clinical diagnostics and is carried out using a variety of reagents and instruments. The CPC “o-Cresol Phthalein Complexone” (Figure 5) method is widely used in clinical laboratory testing and general chemical analysis (Biswas et al., 2023). When in an alkaline solution, CPC reacts with calcium to create a colored complex. The absorbance measured at 570 nm corresponds directly to the concentration of calcium present in the specimen. The color of the CPC reagent is a result of lactone ring formation in the phthalein molecule, this has been favored by divalent compound metals and results in an increase in pH (Stern and Lewis, 1957).

Diethylamine can be used as the buffer solution in this process to ensure the stability of the color complex that is produced, and Magnesium ions are the main factor that interfere with calcium in this method; the reagent typically contains 8-hydroxyquinoline to get rid of the magnesium, thus, the technique for determining calcium becomes more selective (Olansky et al., 1977, Lorentz, 1982).

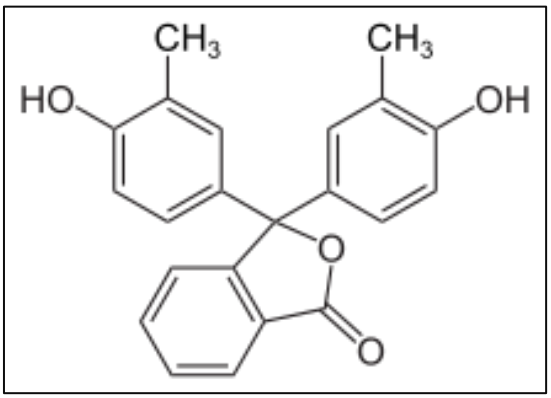


Figure 5. o-Cresolphthalein

### 1.8.3. Arsenazo III

Several metals have been determined colorimetrically using Arsenazo III (Figure 6), a selective ligand. Nonetheless, the most popular use of it in clinical laboratories has been for measuring serum calcium. Where the requirement for an effective method of measuring low calcium ion concentrations in biological systems arises from the role of micromolar quantities of calcium ions in several physiological processes. Due to the Arsenazo III reagent being more selective for calcium than magnesium as a competition interference in an acidic medium, it has been modified almost exclusively for use in serum calcium determinations. Michaylova and Ilkova (Michaylova and Ilkova, 1971), first reported using Arsenazo III as a ligand reagent for the determination of calcium in magnetite. The complex is identified by variations in absorbance at a particular wavelength, often around 650 nm (Caglar et al., 2006, Morgan et al., 1993).

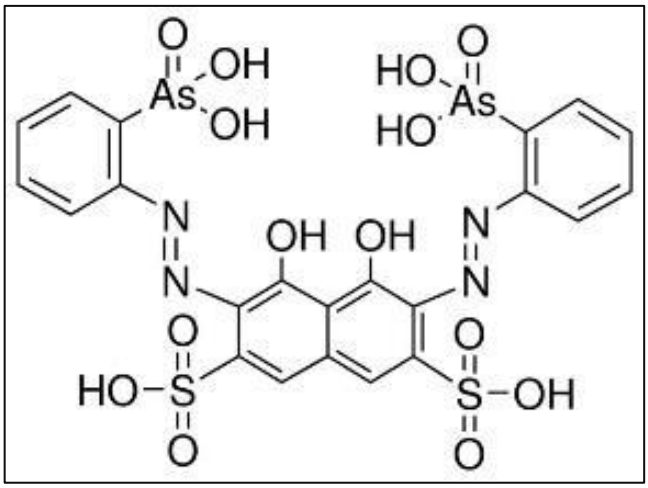


Figure 6. Arsenazo III calcium sensitive dye

### 1.9. Electromagnetic spectrum

The entire range of electromagnetic radiation arranged according to wavelength or frequency is known as the electromagnetic spectrum. The electromagnetic waves that make up each of the several bands that make up the spectrum are given distinct names. These include radio waves, microwaves, infrared, visible light, ultraviolet, X-rays, and gamma rays, ranging in frequency from low to high (Figure 7). The properties of the electromagnetic waves in each of these bands vary, including their production processes, interactions with matter, and beneficial uses.

The study of how matter interacts with or emits electromagnetic radiation is made possible by spectroscopy. Spectroscopy comes in a variety of forms based on the wavelength range being measured. The ultraviolet and visible portions of the electromagnetic spectrum are used in UV-Vis spectroscopy. The lower energy infrared region of the spectrum is used in infrared spectroscopy (Dadi et al., 2022).

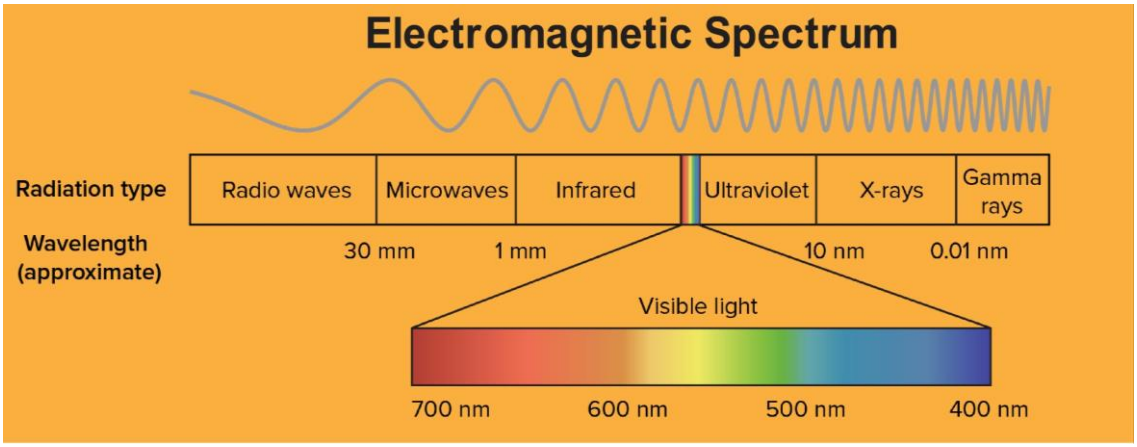


Figure 7. The electromagnetic spectrum

### 1.10. Ultraviolet-visible Spectroscopy

UV-Vis spectroscopy serves as a technique to observe and quantify the interactions occurring between ultraviolet (UV) and visible light wavelengths and various chemical compounds within the spectral range spanning from 200 to 780 nanometers.One of the most spectroscopic methods is ultraviolet-visible (UV-Vis) spectroscopy, which has become incredibly popular over the years due to a multitude of methodology advancements and applications to an infinite number of samples in a variety of fields, including environmental, food, pharmaceutical, and agricultural sciences. The method takes advantage of the various physical reactions that light and analytes have within the sample, including diffraction, refraction, absorption, scattering, and reflection (Zhong and Wang, 2019, Ríos-Reina and Azcarate, 2022).

#### 1.10.1. Developments in UV-Vis Spectrometric Analysis

An analytical method known as UV-Vis spectroscopy can monitor and quantify how many molecules interact with UV and visible light in the corresponding wavelength ranges of 200–350 and 350–780nm respectively. This method makes use of many physical processes that occur between the light and the compound or compounds in the sample, including absorption, scattering, diffraction, refraction, and reflection (Figure 8). Particularly, UV-Vis light absorption is limited to certain chromophores with defined molecular functional groups, being principally controlled by their composition and concentration. From this phenomenon, the Beer-Lambert law has been described to correlate

the quantity of the incident light absorbed by the absorbing substance or molecule present in a matrix, its concentration, and the light path length. As a result, countless quantitative analytical techniques have been created to ascertain and measure the target molecule's concentration in a broad range of mixture (Ríos-Reina and Azcarate, 2022).

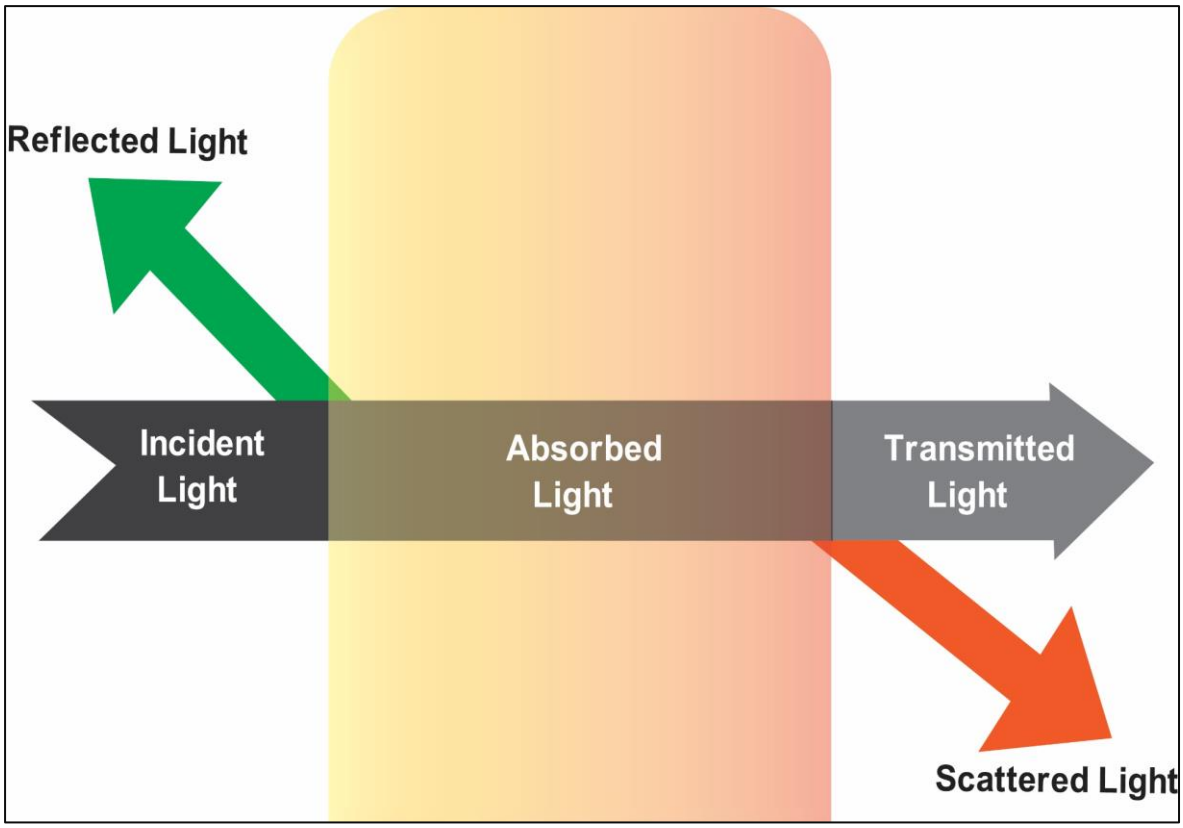


Figure 8. Intraction between light and analyte

### 1.10.2. Instrumentation

Several key components and sections make up the UV-visible spectrophotometry device, and these sections all function together to measure the amount of light absorbed by the samples. These sections included the Source of light, Sample holder, Monochromator, and Detector (Figure 9) (Dadi et al., 2022).

Tungsten filament lamps are the most common type of light source for visible light, whereas hydrogen and deuterium lamps are utilised for UV light. Sample holders are created out of quartz or regular glass and are used for both UV and visible cuvettes. Quartz or silica

cells are normally used in the ultraviolet region, whereas glass cells can be used in the visible zone. The normal length of the route of these cuvettes is typically 1 cm (Dadi et al., 2022, Ríos-Reina and Azcarate, 2022).

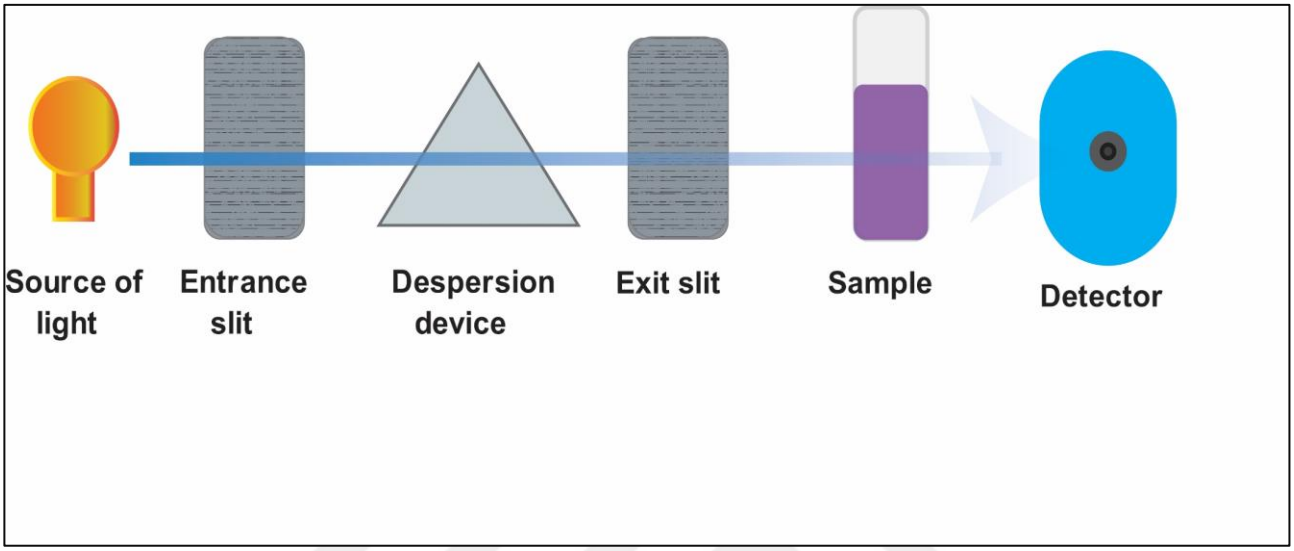


Figure 9. Schematic of UV -Vis Spectrophotometer.

### 1.11. Digital Image Colorimetry Processing

Recently, there has been an increasing interest in integrating image processing programs and mobile apps into chemical research to provide efficient, rapid, and low-cost analysis. These programs and mobile applications are used for colorimetry, as well as additional functions such as fluorimetry, chemiluminescence, and electrochemical inquiry (Elagamy et al., 2023). A lot of studies have been done on Digital Image Colorimetry Processing (DICP) as a flexible approach for qualitative and quantitative analysis of many sample types such as pesticides (Zhao et al., 2023), heavy metals (Sivakumar and Lee, 2021), antibiotics (Cao et al., 2022), environmental materials (Vargas-Muñoz et al., 2023), and food products (Yam and Papadakis, 2004).

(DICP) involves capturing images with a smartphone and analyzing colors using mobile applications such as Red Blood Cells color detector, color meter, Photo Metrix, or image processing software like Image J, Adobe Photoshop, or Matlab within the suitable color scheme. The color quantification data were used to determine the quantity of the

analyte. Smartphones are favored over digital cameras for image capture in (DICP) because of their mobility, user-friendly interface, enhanced camera capabilities, and the accessibility of mobile applications (Elagamy et al., 2023).

### 1.11.1. ImageJ

ImageJ is an excellent tool for processing pictures and performing analyses. It is utilized in more than 1,000 professional research articles in fields ranging from biological sciences to astronomy and physics. In life sciences, it is used to quantify medical pictures to help discover disease signs.

ImageJ is an open-source image processing software created by the National Institutes of Health (NIH) for analyzing scientific pictures. Image J has been widely used in many biological research to measure cellular and subcellular constituents. It has been successfully used to analyze several types of medical pictures such as dental imaging, tumor differentiation, and brain tissue imaging (Elagamy et al., 2023). It has several uses in analyzing biomolecule components in the body's fluids, like serum total protein (Markus et al., 2023), cholesterol (Nguyen et al., 2020), serum uric acid (Elagamy et al., 2023).

Image J has various advantages over other image processing software, including the accessibility and simplicity of use of basic provided capabilities, even for those with no previous knowledge of image analysis, is freely accessible, and it has an engaged and helpful user community. Furthermore, it works on a variety of computer systems and can handle the majority of regularly used picture formats. Image J functions include color splits, reducing noise, elimination of backgrounds, smoothing out, sharpening, contrast adjustment, area recognition, and intensity quantification (Schindelin et al., 2015, Elagamy et al., 2023).

### 1.11.2. ImageJ Protocol

The ImageJ program can be downloaded for free from the official website at https://imagej.net/ij/download.html where users can select the appropriate version for their computer system, whether it is Windows or MacOS. The installation process is straightforward, making it easy for users to quickly set up and start utilizing this powerful image-processing software.

Once the installation is complete, you can open ImageJ, which will display a window as shown in Figure 10. To open a photo, you can either use the shortcut Ctrl+O or click on

'File' and then 'Open' like (Figure 11). After the photo is opened, it can be converted to specific color models by navigating to the 'Image' menu, selecting 'Color', and then choosing 'Split Channels'. This process will automatically convert the photo into three separate color channels: Red, Green, and Blue (Figure 12).

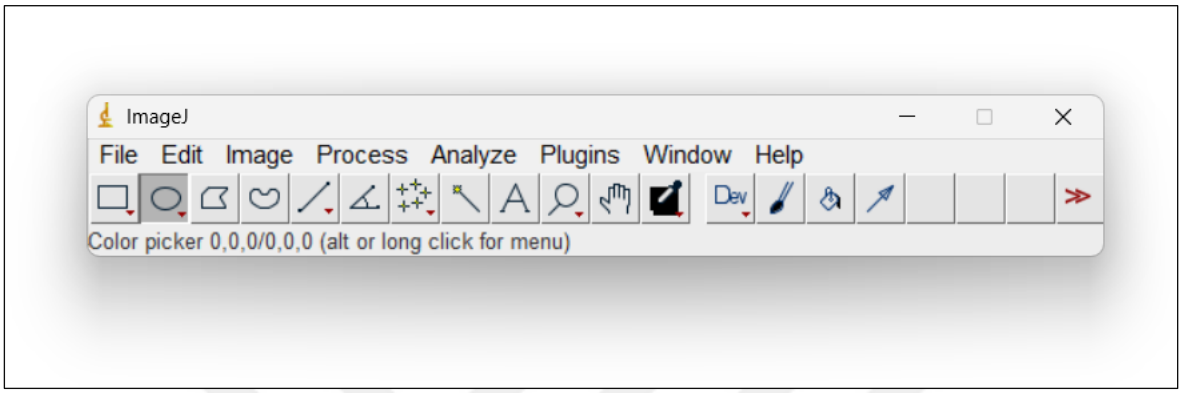


Figure 10. Image window face.

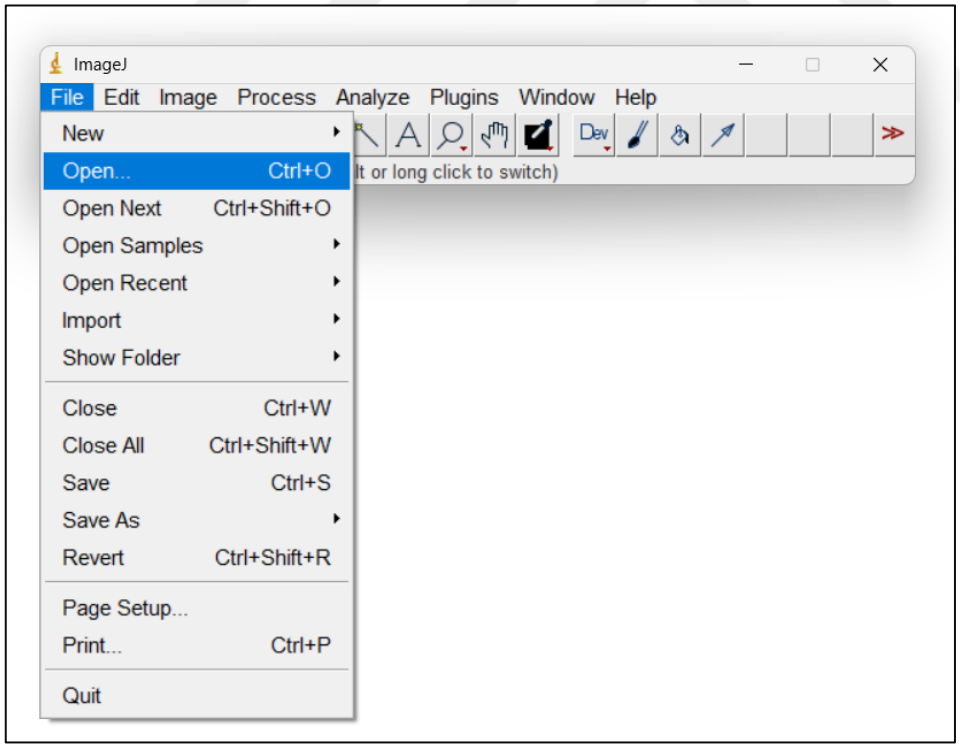


Figure 11. Image J file menu.

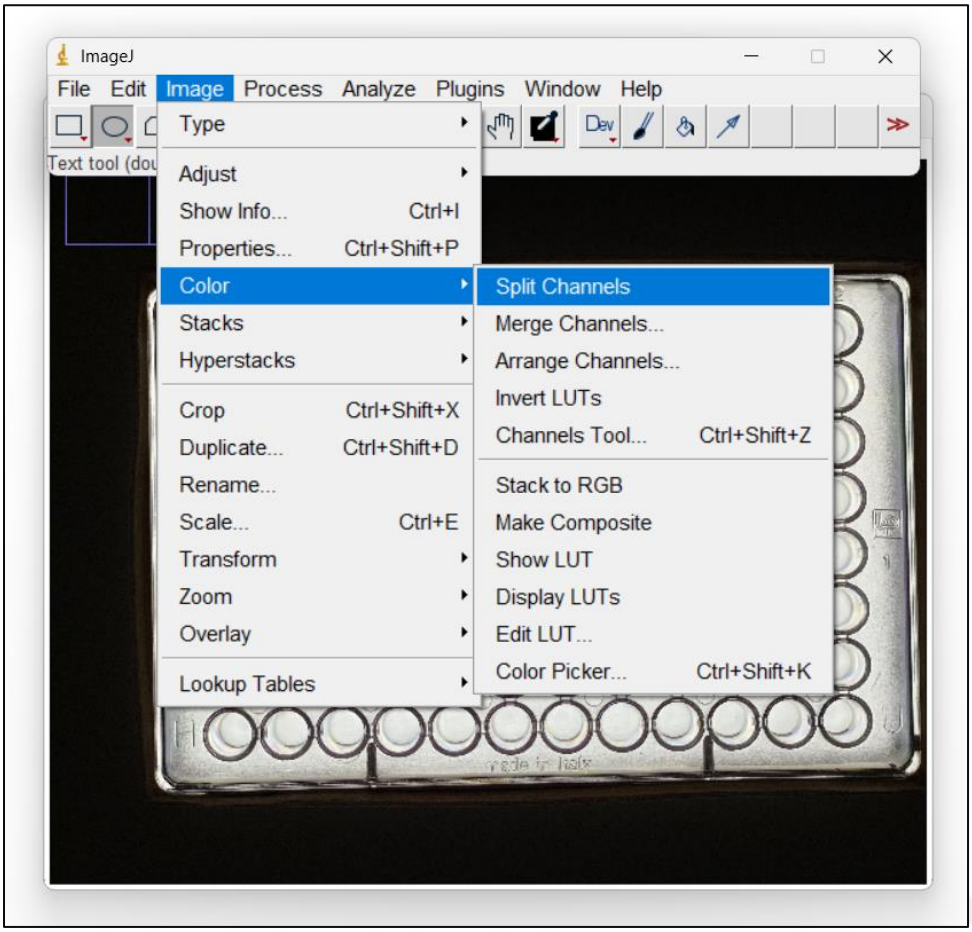


Figure 12. Image J spliting the color.

If you want to convert the photo to other color models, such as the HSB or LAB stack model, this can also be done easily. Simply click on 'Image' in the menu bar, then select 'Type', and choose the desired color model with a single click (Figure 13)

After selecting the color model, you can use the Oval or Rectangle tool in the toolbar to select the region of interest. Once the region is selected, press the 'M' key on the keyboard to proceed and analysis the selected area (Figure 14).

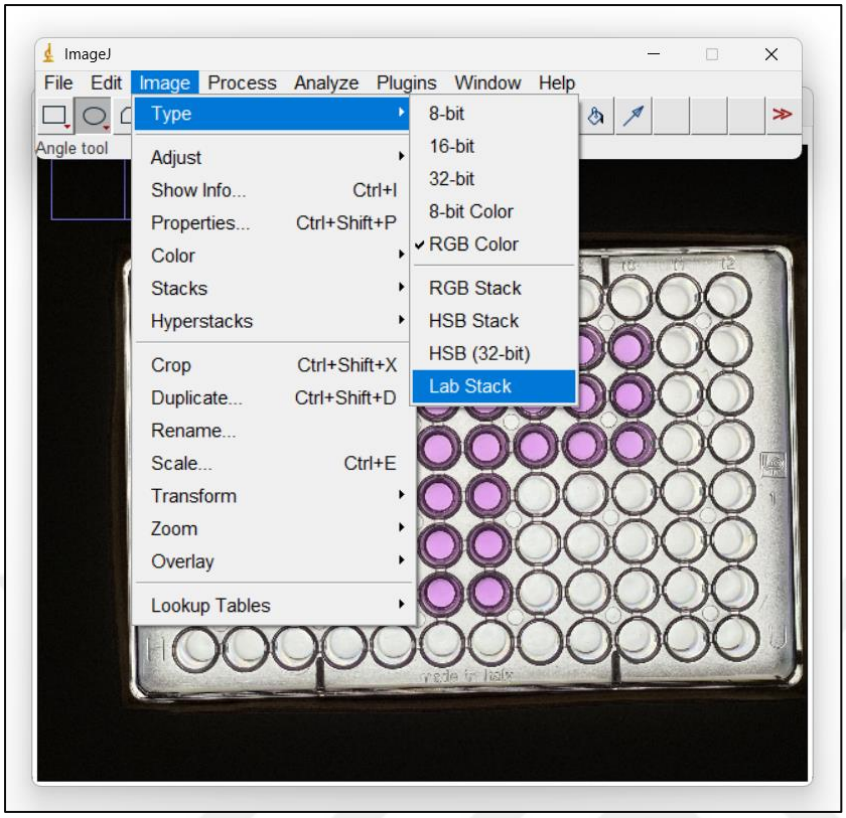


Figure 13. Converting the photo to other type and models.

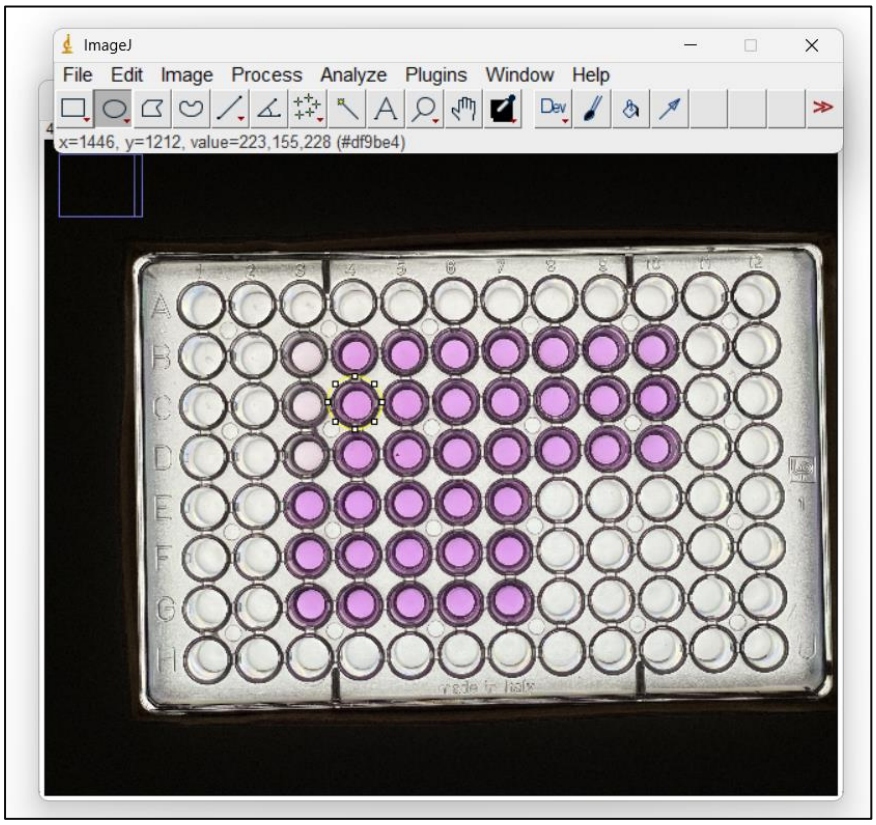


Figure 14. Analysis with Image J.

## 1.12. Color Models

There are many other color models readily available, but four are chosen in this thesis to define color, and color measurements. The color models that are commonly used are the RGB , $L^*a^*b^*$, HSB (hue, saturation, and brightness), and CMYK (cyan, magenta, yellow, and black). Of them all, the $L^*a^*b^*$ model has the widest range, covering every color in the CMYK and RGB range (Yam and Papadakis, 2004).

### 1.12.1. RGB Color Model

The RGB color model defines the amounts of red, green, and blue light in a specific color using the components red (R), green (G), and blue (B) respectively. In a 24-bit image, each component is represented by a number ranging from 0 to 255. An image with a higher bit rate, such as a 48-bit image, has a wider value range. The combination of these components results in a single color.

The eye interprets a color that is created when red, blue, and green in any photons are combined at their highest intensities as white Figure 15. Though the pixels on a display are too close together for the human eye to distinguish between the three colors, the colors are still theoretically red, green, and blue. The color appears black to the eye when the values of all components are 0, which denotes a lack of light. RGB is the most widely used color model since it can store and display a wide spectrum of colors (URL-1, 2024).

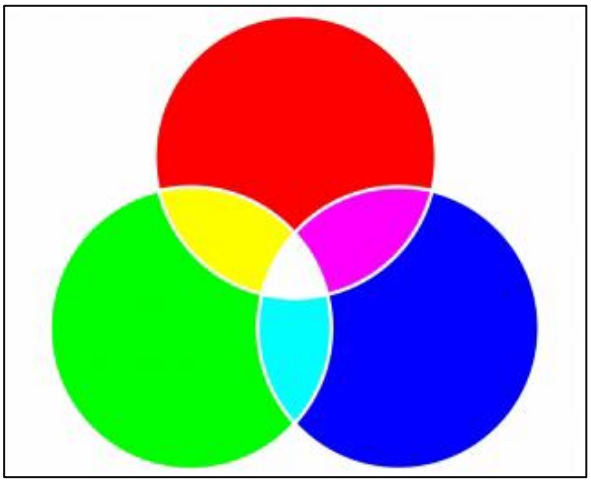

Figure 15. RGB model and White is the outcome of mixing the three RGB colors at their highest intensity ratios.

### 1.12.2. LAB Color Model

The $L^*a^*b^*$ model is a calculation that represents all conceivable colors that humans are capable of seeing. The Commission International d'Eclairage (CIE) created the model as an international standard for color measurement in 1976. The $L^*a^*b^*$ Figure 16 color is made up of two chromatic components (ranging from -120 to +120): the $a^*$ component (from green to red) and the $b^*$ component (from blue to yellow), as well as a luminance or brightness component (L value ranging from 0 to 100). While RGB and CMYK models depend on the device, $L^*a^*b^*$ color is independent of the devices. Regardless of the input or output device such as a digital camera, scanner, monitor, or printer—the $L^*a^*b^*$color model gives constant color. Many studies and research on food are frequently done using the $L^*a^*b^*$color model (Yam and Papadakis, 2004).


Figure 16. Lab color model

### 1.12.3. HSB Color Model

Hue (H), saturation (S), and brightness (B) are the three components of color defined by the HSB color model (Figure 17). HSB is sometimes referred to as HSV (hue, saturation, and value). Hue is a color's pigment and is measured in degrees to indicate where it falls on the conventional color wheel. As an example, 0 degrees is represented by red, 60 degrees by yellow, 120 degrees by green, 180 degrees by cyan, 240 degrees by blue, and 300 degrees by magenta. According to the HSB color model, saturation indicates how vibrant or dark a color is. Saturation values are expressed as percentages with a restricted range of 0 to 100;

the higher the value, the more vibrant the color. The last component of HSB color model is Brightness, which indicates how much white is present in the color, similar to Saturation levels, Brightness values are percentages with a range of 0 to 100; the higher the value, the brighter the color (URL-1, 2024).

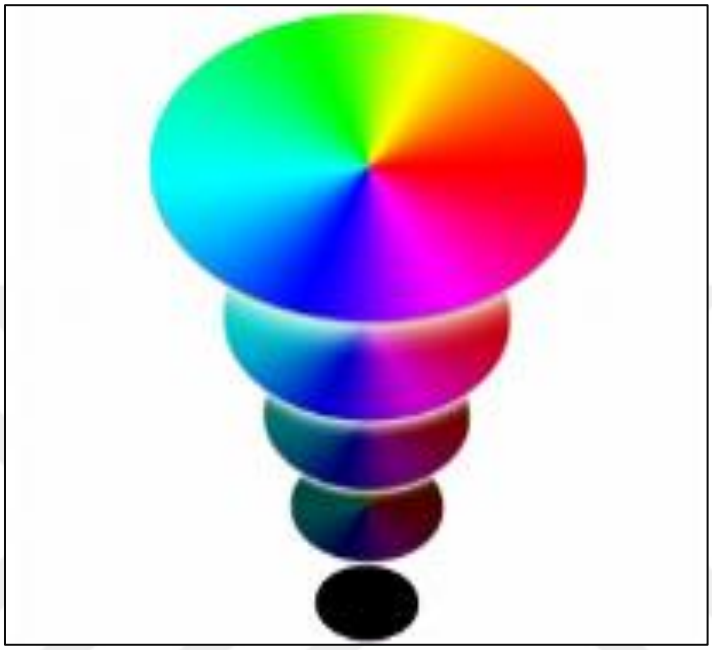

Figure 17. HSB color model

### 1.12.4. CMYK Color Model

Cyan (C), magenta (M), yellow (Y), and black (K) are the color components that make up the CMYK color model, which is used in printing. These components' values, which represent percentages, vary from 0 to 100. A appear, such as white paper, is painted with color that is, ink in subtractive color models like CMYK. Afterwards, the color "subtracts" surface brightness. Black is the resultant color when the values of the color components (C, M, and Y) are all 100. In the event where every component has a value of zero, the surface remains uncolored, revealing the white paper in this instance. As black ink is more neutral and darker than combining equal parts cyan, magenta, and yellow, it is included in the color model for printing the white poses. Sharper text is produced with black ink, particularly when printing. Furthermore, using black ink typically costs less than using colored ink (URL-1, 2024).

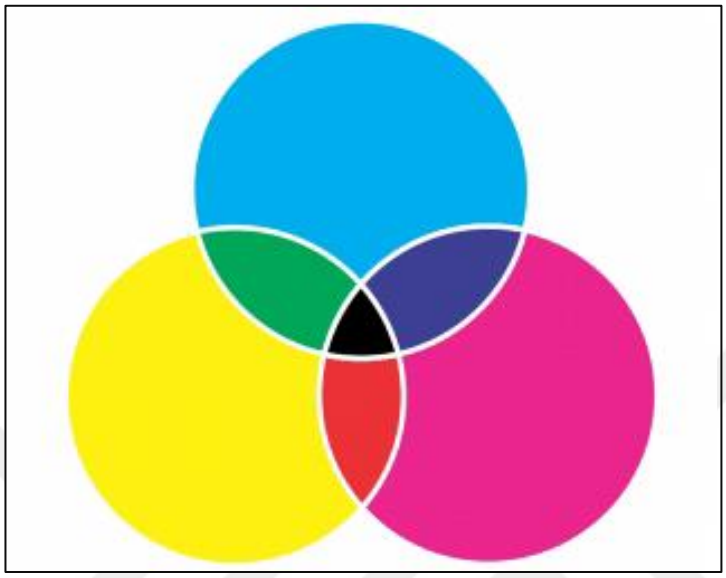

Figure 18. CMYK Color Model, Black, according to the CMYK color model, is created by mixing the three CMY colors at their maximal intensities.

## 1.13. Application of Image J

### 1.13.1. Determination of Serum Proteins

Based on the biuret method, colorimetric measurement of proteins in serum is developed. UV-visible spectrometric (UV-Vis) detection was replaced with the easy and cost-effective smartphone digital image colorimetric (SDIC) method by using the free software ImageJ (Figure 19). All necessary parameters for the analytical method have been optimized and validated in this study. The coefficient of determination under optimal conditions was 0.9982, with a dynamic range that was linear of 0.022 to 0.35 g/dl. Based on the percent relative standard deviation, the method's precision was less than 5%. The quantification of total protein, albumin, and globulin in serum was determined to be achievable with sufficient limits of detection and quantitation of 0.007 and 0.022 g/dL, respectively. The suggested SDIC method's correctness was demonstrated when it was

validated by an independent experiment relying on a UV-Vis method. Both methods showed strong statistical agreement (Markus et al., 2023).


Figure 19. Diagrammatic illustration of the colorimetric method for digital images using Image J

### 1.13.2. Determination of Serum Uric Acid

Using Image J for color quantification, a novel method for the quantitative measurement of uric acid is devised. Uric acid reduces the phosphotungstate reagent in an alkaline media, resulting in the color tungsten blue Equation 1. The concentration of uric acid and the intensity of blue color have a linear connection. This was used to quantify color using digital image colorimetry (DIC) with image J. Pictures taken with a smartphone were analyzed for related uric acid concentrations that had been processed using spectrophotometer.

Equation 1. Method reaction

$$\text{Uric acid} + \text{phosphotungstate} + Na_2CO_3 \longrightarrow \text{Allantoin} + \textbf{tungsten blue} + CO_2$$

### 1.13.3. Measurement of Glucose

Another instance of the application of Image J is the detection of Glucose in blood samples. Research has been conducted on a colorimetric biosensor for the detection of glucose, utilizing chitosan cryogel as a supporting material for the immobilization of enzymes. Detection relied on the conversion of glucose to hydrogen peroxide by glucose oxidase, followed by the utilization of titanium (IV) oxysulfate to quantify hydrogen peroxide, as indicated by the development of a yellow hue. Subsequently, alterations in color

corresponding to varying concentrations were captured using a commercial scanner and subjected to analysis through ImageJ software (Fatoni et al., 2019).

### 1.13.4. CUPRAC Antioxidant Measurement Method

The Cupric Reducing Antioxidant Capacity (CUPRAC) method stands as one of the most extensively employed techniques for antioxidant evaluation. Nonetheless, its reliance on a spectrophotometer, akin to numerous other methodologies, represents a notable drawback. But in this study as another example of application of Image J, the determination of Cupric Reducing Antioxidant Capacity was executed through color analysis utilizing the Image J program on a computer, thereby obviating the necessity for a spectrophotometer. The newly devised colorimetric CUPRAC assay was then applied to assess various standard antioxidants and plant extracts. Reaction mixtures were deposited onto TLC plates Figure 20, and the resultant colors were subsequently captured using scanner images and transferred to the computer. The Image J program was employed to determine the CTEAC (Cupric Reducing Antioxidant Capacity) value for each sample (Akar and Burnaz, 2019).

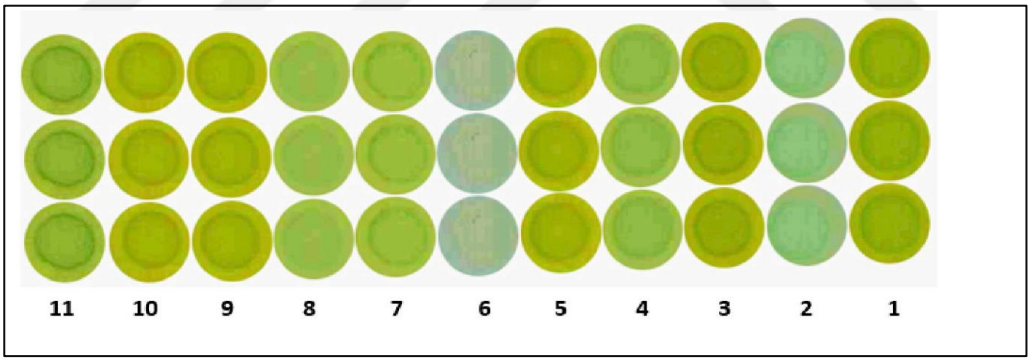


Figure 20. Image depicting the antioxidant standards analyzed using the colorimetric method on a Thin Layer Chromatography (TLC) plate.

### 1.13.5. Total Cholesterol Determination

Presently, hypercholesterolemia stands as a prevalent metabolic disorder afflicting millions of individuals and contributing to approximately 12 million fatalities in developed nations, while also serving as a primary causative factor for mortality in developing regions. The measurement is conducted employing a spectrophotometer, which relies on the analysis

of color concentration directly correlated with cholesterol levels. With the advancements in computing, numerous analysis techniques are being enhanced through the integration of computers as aids to clinical diagnosis, and cholesterol determination method is one of those examples (de Oliveira et al., 2018).

A digital image of cholesterol samples was taken using an ELISA plate (Figure 21). The picture was then turned into grayscale. The wells in this picture were divided into segments, and the grey levels within each segment were measured using a scale from 0 to 255. The cholesterol concentration determined by the spectrophotometer reading was then linked with this measurement. The results of this study show a strong relationship between the use of image processing techniques and conventional approaches (de Oliveira et al., 2018).

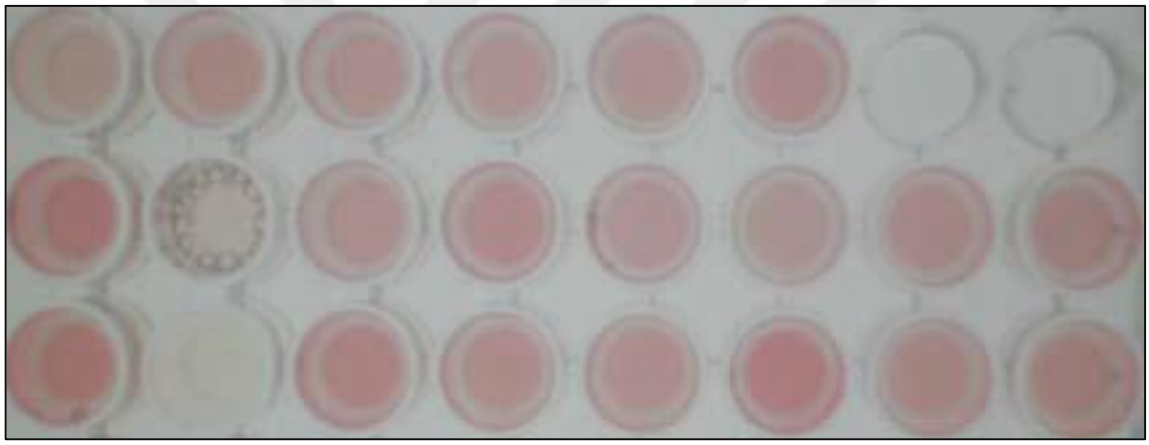

Figure 21. An example showing samples of cholesterol on an ELISA plate (de Oliveira et al., 2018).

# 2. EXPERIMENTAL

## 2.1. Instrument and Equipment

The substances and materials used in this experimental study were obtained from Karadeniz Technical University (KTU) Faculty of Science Department of Chemistry Biochemistry Research Laboratories. Table 4 provides details on the devices used and their producer companies who purchased them.

Table 4. Devices and Brands Used in the Study.

| **Device Name** | **Brand** |
|---|---|
| Micropipette (1000 mL) | Gilson |
| Micropipette (100 mL) | Gilson |
| Analytical balance | Mettler-Toledo |
| Magnetic stirrer with heater | IKA |
| Freezer | Vestel |
| Vortex mixer | IKA |
| Oven | Nüve |
| UV-vis spectrophotometer | Perkin Elmer, Lambda 25 |
| Tablet screen | Ipad Air 5 |
| Camera | Iphone 11 promax |

### 2.2. Chemicals Used

The chemicals used in the studies are listed in Table 5 along with the names of the companies that supplied them.

Table 5. Chemicals and Brands

| Chemical Name | Company |
|---|---|
| Calcium CPC method Kit | BIOLABO® |
| Magnesium Nitrate Hexahydrate | Merck |
| Calcium Nitrate Tetrahydrate | Merck |
| HCl | Merck |

### 2.3. Developing Method

The determination of calcium concentration is a critical task in various fields, ranging from medical diagnostics to environmental monitoring. Traditional methods often rely on expensive spectrophotometers, which can be cost-prohibitive and require specialized training. In this study, we present a novel approach utilizing the open-source image analysis software ImageJ for the precise quantification of calcium levels. By harnessing the power of digital image processing techniques, we developed a reliable and accessible method that offers comparable accuracy to conventional spectrophotometric assays. Our approach not only simplifies the analytical process but also reduces the financial barrier to entry, making calcium determination more accessible to a broader range of researchers and practitioners. Furthermore, the versatility of ImageJ allows for easy adaptation to various sample types and experimental conditions, enhancing its applicability across different research domains.

#### 2.3.1. Preparation of Standard Solution

One significant development in the development of a serum calcium monitoring method is the use of o-Cresol Phthalein Complexone dye. Because the o-CPC dye pairs with calcium to form a stable colored complex, and because this approach is frequently employed

in general chemical analysis and clinical laboratory testing. Using Image J software, the reaction of color with concentration was carefully evaluated by using various standard solutions as a preliminary work of the study.

In the experiment, a standard solution of Calcium ions at a concentration of 100 mg/dl was meticulously prepared as a stock solution from calcium nitrate tetrahydrate, by dissolving 590.35 mg of calcium nitrate tetrahydrate in 100 ml of distilled water, to prepare working standard solutions, the stock solution was diluted with the required quantities of distilled water. Each solution, ranging from 0 to 100 mg/dl, was meticulously applied to ascertain the response of detection color and determine the linear range. Through this systematic approach, the experiment aimed to unveil the relationship between calcium ion concentration and detection color response within the established linear range, crucial for accurate detection and quantification in analytical applications.

Initially, this methodological approach ensures the accuracy and consistency of the data and facilitates the creation of a robust calibration curve, both of which are necessary for the precise measurement of serum calcium levels. By methodically examining colorimetric reactions, this technology has the potential to increase the efficacy and efficiency of serum calcium determination, which could result in advancements in medical research and diagnostics.

### 2.3.2. Instrumentation Development

A specialized colorimetric wood box was constructed for capturing photos of sample solutions, featuring a design that ensures complete closure to block any ambient light, creating a very dark environment ideal for photography (Figure 22). To provide consistent lighting, the bottom of the box includes a designated slot to securely hold an iPad, which, when its screen is turned on and set to display a white background, serves as the box's light source. This setup guarantees uniform illumination of the samples, crucial for accurate colorimetric analysis.

Inside the box, there is an additional shelf designed to function as a sample holder, positioned above the light source. This shelf is equipped with a mechanism that allows it to move, enabling the adjustment of the distance between the light source and the sample solution. This adjustable feature is crucial for fine-tuning the lighting conditions, ensuring

optimal illumination, and enhancing the accuracy of the colorimetric analysis by allowing precise control over the light intensity reaching the sample.

Above the sample holder shelf, there is an additional shelf designed to securely hold a smartphone camera detector. This upper shelf is equipped with an adjustable mechanism that allows it to move up and down, providing the flexibility to modify the distance between the sample solution and the camera detector. This adjustability is essential for capturing high-quality images, as it enables precise focusing and framing of the sample, thereby ensuring accurate and reliable colorimetric analysis.

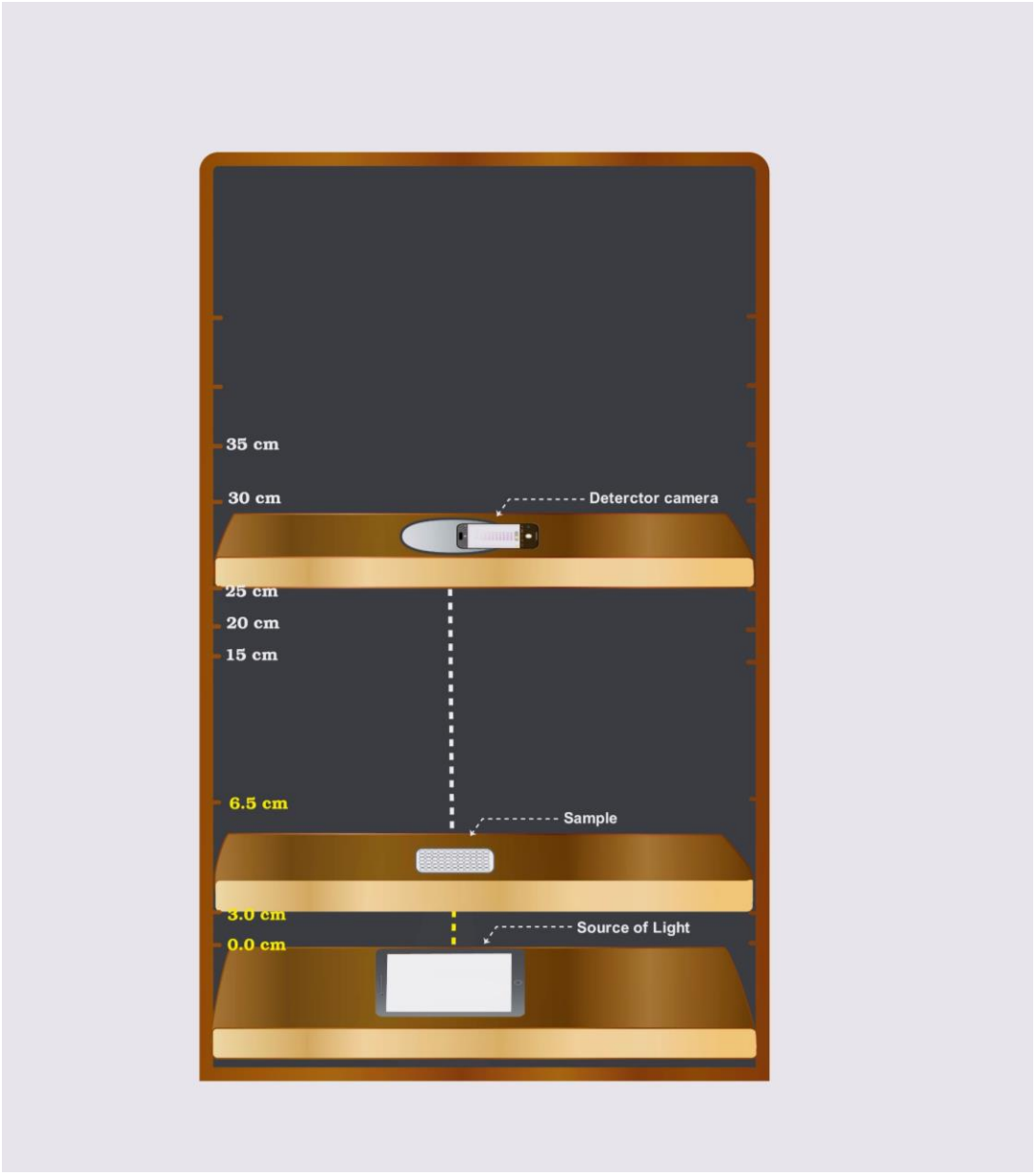


Figure 22. Schematic diagram of the colorimetric box.

### 2.3.3. Data Processing and Converting Color Channel

Following the acquisition, digital images of blank and standards solutions were taken in 3024 x 4032 resolutioin, then promptly transferred in JPG file format to the cloud using Microsoft OneDrive, facilitating seamless access from a personal computer (PC) for subsequent processing with ImageJ software. In ImageJ, the images underwent conversion into four distinct color models: RGB, HSB, LAB, and CMYK. This meticulous process was undertaken to discern the most appropriate color model for the study, enabling precise analysis and interpretation of color variations within the samples. By exploring multiple color models, the study aimed to optimize the selection for accurate and reliable color-based analysis, crucial for the study's objectives and outcomes.

## 2.4. Optimization

In pursuit of achieving optimal reproducibility and heightened sensitivity in analyte detection, a comprehensive optimization study was undertaken, encompassing critical parameters known to significantly influence experimental outcomes. This investigation rigorously examined various facets, including the refinement of color models, the optimization of environmental conditions during the acquisition process (such as dark or light modes), meticulous calibration of distances between the camera and the solution under examination, as well as between the light source and the plate containing the solution. Furthermore, careful consideration was given to the selection of plate type, the precise volume of solution utilized, incubation duration, and the maintenance of the solution throughout the incubation period. Such methodical scrutiny across multiple variables underscores a steadfast commitment to enhancing the efficacy and reliability of analytical procedures within the developing method.

### 2.4.1. Optimization of Mixture Solution Container

A series of experiments was conducted to assess the suitability of various solution containers for photographic analysis, specifically comparing UV-visible cuvettes with Microwell plates (Figure 23) under identical environmental conditions. Despite similarities in performance, preference was given to the Microwell plate due to its requirement of smaller

reagent volumes, thus offering cost efficiency and environmental benefits. Furthermore, the microwell plate demonstrated an additional advantage in its capacity to accommodate multiple samples concurrently, thereby expediting the analytical process and enabling the simultaneous analysis of a greater number of samples within a single photo.

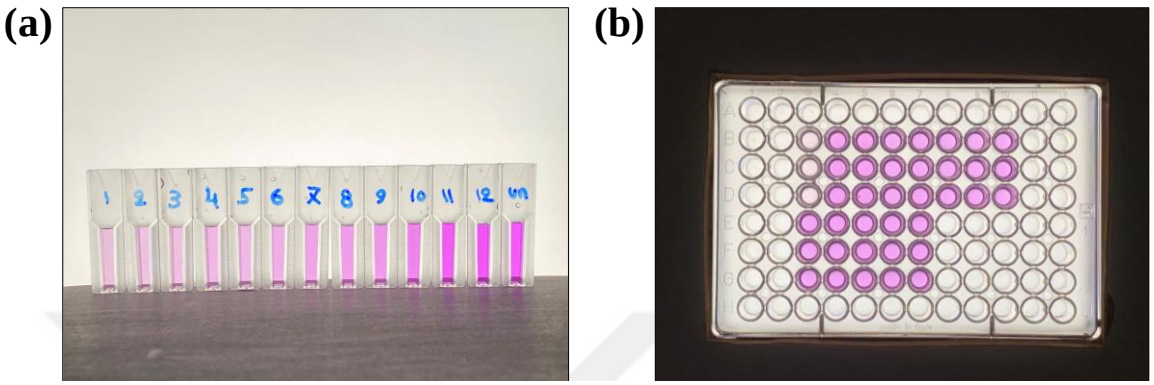


Figure 23. (a) Cuvette (b) Microwell plate tubes used for taking photo.

### 2.4.2. Optimization of Capturing Condition

The investigation encompassed a series of initial experiments designed to capture digital photographs under diverse environmental conditions, specifically within a standard room environment and a specially constructed containment box. To ensure the accuracy and reliability of the imaging process, the study included the measurement of a calcium standard solution at a concentration of 10.0 mg/dl, repeated five times. A calibration curve was established using both a calibrator and a blank solution. Following this, the mixture solution was transferred to a microwell plate for imaging. Photographs were then taken both inside the containment box and in the standard room setting. The results were subsequently compared by analyzing the percentage relative standard deviation (%RSD), allowing for an assessment of the consistency and precision of the imaging conditions in different environments.

### 2.4.3. Selecting the Color Channel

Upon capturing a photograph and transferring it to the computer, various options for color models are available in Image J for photo analysis. We investigated four specific

models: RGB, HSB, CMYK, and the LAB color model. Subsequently, for each model, we meticulously selected the most relevant color channel based on the characteristics of our solution color. For instance, it was observed that green exhibited a superior response compared to red and blue channels; hence, we opted for the green channel in the RGB model, saturation in the HSB model, magenta in the CMYK model, and A (representing the green-magenta axis) in the LAB color model. This approach ensured the selection of the most appropriate color channel for accurate and precise analysis tailored to the specific requirements of our study.

### 2.4.4. Solution Volume

In the proposed method, we examined the significance of solution volume as a parameter. Traditional spectrophotometric techniques for determining calcium typically necessitate a minimum solution volume of 1000 µl. However, through our optimization process, specifically in redesigning the solution holder to utilize a Microwell plate configuration, we were able to significantly reduce the required solution volume to just 150 µl. This particular type of plate is capable of accommodating a maximum solution volume of 250 µl. Subsequently, following a detailed experimental assessment, we determined that a solution volume of 150 µl was optimal for our purposes.

Following the completion of reaction time, we prepared a series of Calcium standard solutions and a Blank solution. Subsequently, the solution mixtures were transferred into a microwell plate comprising four different wells, each varying in solution volume (100, 150, 200, and 250 µl). Analysis of the collected data revealed a discernible correlation between the increase in solution volume and the augmentation of color intensity, accompanied by a reduction in Green value and Magenta value and increasing Saturation and $a^*$ value (Figure 24). Notably, all four parallel experiments exhibited consistent calibration performance, as evidenced by the similarity in coefficient of determination (R squared) values across the parallels. Consequently, we concluded that optimizing the method with a solution volume of 0.15 µl would be most advantageous. This optimization not only enhances the method's cost-effectiveness but also aligns with environmentally friendly practices, thereby underscoring another inherent benefit of this approach.

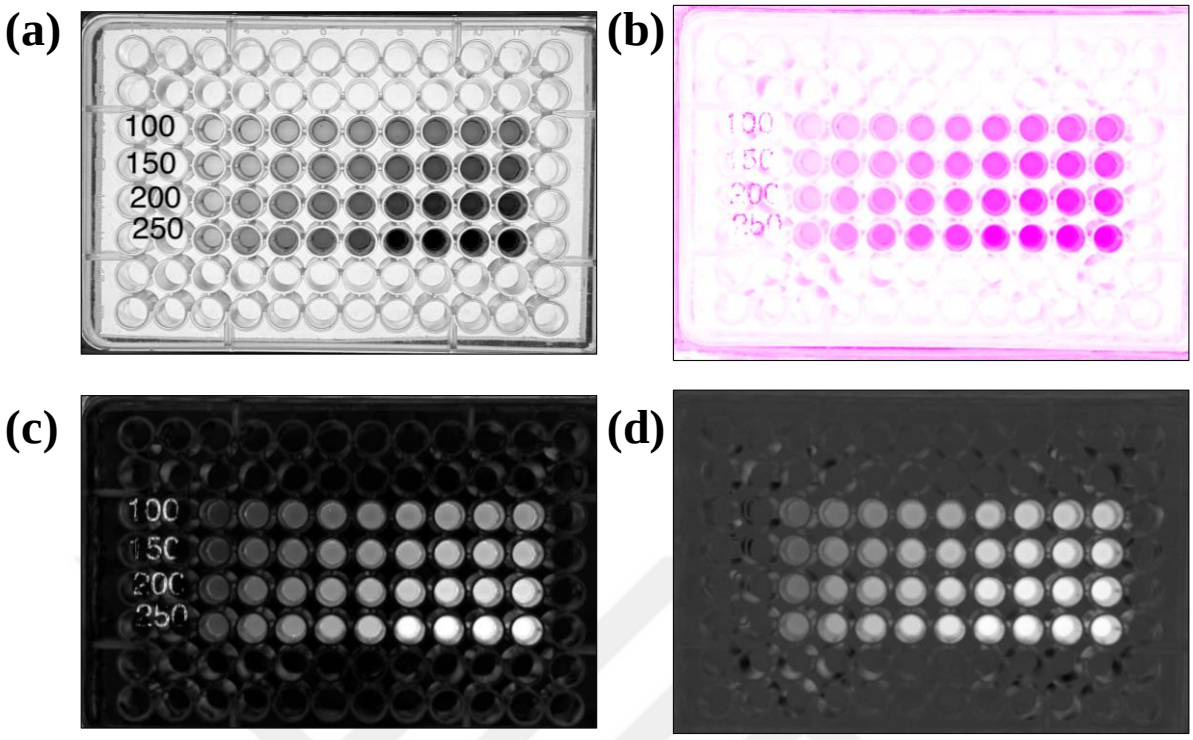


Figure 24. Microwell plate contain four different series of standard solutions from 100 to 250 µl of mixture solution: (a) Green, (b) Magenta, (c) Saturation, and (d) a color mode.

### 2.4.5. Distance Between Detection Camera and the Sample Solutions

The quality of images captured by standard digital cameras is often influenced by several factors, including aperture size, camera sensor quality, and inherent resolution capabilities. In the case of smartphone cameras, these features remain consistent, thus rendering the autofocus functionality highly dependent on the distance between the camera and the target object. Consequently, an investigation into the impact of camera-to-sample solution distance was conducted within the range of 15.0 to 35.0 centimeters. Below 15.0 centimeters, a noticeable degradation in image sharpness was observed, accompanied by an inability to capture all cells within the microwell plate in a central position relative to the camera sensor as is clear in (Figure 25 a). Optimal autofocus performance, ensuring all cells were accurately aligned with the camera, was achieved at a distance of 25.0 centimeters, which was subsequently utilized for all subsequent analyses.

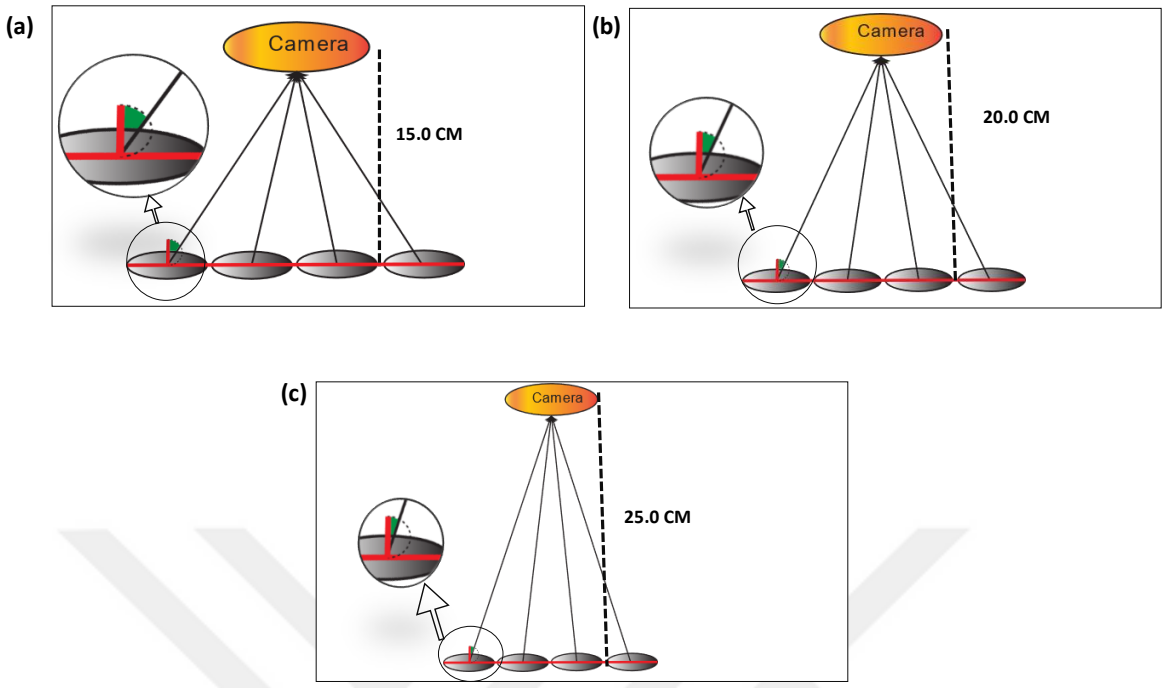


Figure 25. The distance between the Camera detector and the Solution. (a) 15.0 cm distance between camera and solution, (b) 20.0 cm, (c) 25.0 cm.

### 2.4.6. Distance Between Source of Light and the Sample Solutions

In the development of a calcium determination method, the distance between the light source and the sample solution plays a pivotal role in achieving accurate and reliable results. Employing an iPad Air 5 as the light source, I undertook a systematic investigation to optimize this critical parameter. Through experimentation spanning distances from 0.0 to 6.5 cm, it became evident that variations within this range did not substantially affect sensitivity, suggesting a degree of robustness in the method. However, an intriguing observation arose when the sample plate was positioned directly onto the screen: a discernible loss of clarity was noted. This phenomenon highlights the necessity not only to optimize the distance between the light source and sample but also to consider the physical arrangement of the experimental setup to mitigate potential sources of error in calcium determination.

### 2.4.7. Reaction Time Optimization

The interaction between calcium ions ($Ca^{2+}$) and o-Cresolphthalein was conducted through incubation either within a test tube or as a small droplet within a microwell plate. The experimental outcomes revealed the formation of a chromogenic complex resulting from the interaction between o-Cresolphthalein and calcium ions ($Ca^{2+}$) within a duration ranging from 5 to 10 minutes. To comprehensively evaluate the progression of the reaction, three distinct standards (representing low, normal, and high concentrations) were employed. The assessment spanned a duration of 120 minutes, facilitating the monitoring of reaction kinetics for both incubation methods. Through this optimization study, it was observed that readings or analyses of the solution could be reliably conducted 10 minutes from the onset of the reaction, with a stable observation window extending up to one hour. However, beyond the one-hour mark, a decline in absorbance was noted, accompanied by increased fluctuations in color value as assessed via ImageJ software.

## 2.5. Validation

During method development, it's crucial to ensure that the tests we use are reliable and accurate. This means carefully examining different parts of the method to confirm it's trustworthy. In this study, I focus on validating various parameters to improve the method's reliability and validation status.

### 2.5.1. Linear Range

After optimizing the main part of the proposed method, we had a specific test to determine the Linear Range of the proposed method and compared results with those of the traditional method, which required a spectrophotometer, based on the many preliminary works and specific work it is observed that the proposed method has a wider range. By using standard solutions of calcium ions in a concentration range of 0.0 to 100 mg/dl, an external aqueous calibration curve was produced to assess the analytical performance of the method.

### 2.5.2. Determination of LOD and LOQ

The analytical performance of the method was rigorously assessed by constructing an external aqueous calibration curve, which involved using a standard calibrator solution of calcium ions alongside a blank. To determine the method's precision and sensitivity, a standard solution with a concentration of 10 mg/dL was analyzed, allowing for the calculation of the standard deviation. The limit of detection (LOD) and limit of quantitation (LOQ) were subsequently determined using the formulas 3Sb/m and 10Sb/m, respectively. In these formulas, Sb denotes the standard deviation of the intercept, while m represents the slope of the regression equation, ensuring the method's capability to reliably detect and quantify calcium ions at low concentrations.

### 2.5.3. Repeatability and Precision

The evaluation of precision and repeatability in analytical methods is essential for ensuring the reliability and robustness of experimental outcomes. In this study, the precision and repeatability of a method for quantifying calcium concentration were assessed through the calculation of the percent relative standard deviation (% RSD) for both intra- and inter-day measurements. The experimental procedure involved the utilization of a 10 mg/dl calcium standard solution obtained from BIOLABO, from which ten parallel solutions were prepared. These solutions were then subjected to analysis using the same equipment and setup to minimize experimental variability. By applying the % RSD formula, the repeatability of the method was determined and subsequently compared with that of a conventional technique employing a UV-visible spectrophotometer.

### 2.5.4. Recovery

In any analytical method, the evaluation of matrix effects is paramount to assess the reliability and accuracy of analytical methods, particularly in complex sample matrices such as biological fluids. In this study, the matrix effect associated with a calcium assay method was systematically investigated through an addition-recovery test. This approach involved the deliberate introduction of known concentrations of calcium ions from a standard reference matrix into a serum sample. Subsequently, the proposed calcium assay method was applied to analyze the spiked samples, enabling the assessment of any potential

deviations in measurement accuracy induced by matrix effects. The evaluation of absolute recovery, achieved by quantifying the percentage yield of the spiked concentrations, served as a robust indicator of the method's capability to accurately quantify analytes in the presence of complex sample matrices.

### 2.5.5. Selectivity and Specificity

Blood samples underwent coagulation to eliminate fibrinogen and other clotting components, yielding serum upon centrifugation. Serum, a clear solution, was separated from the precipitated debris, including red blood cells, white blood cells, and platelets. It constituted dissolved hormones, metabolic waste, proteins, carbohydrates, and electrolytes within an aqueous medium. Previous studies have indicated that the o-Cresol Phthalein Complexone method, employed for serum calcium assessment, offers superior simplicity, accuracy, and diminished susceptibility to interference compared to alternative techniques.

In the o-Cresol Phthalein Complexone (o-CPC) method, magnesium ions pose a significant challenge as they competitively interfere with the measurement of calcium. However, this interference can be effectively managed by adjusting the pH of the solution. To assess the ability of the optimized o-CPC method to accurately determine serum calcium levels, a thorough investigation was conducted using a spiking experiment with a standard solution of magnesium ions. This involved deliberately adding known concentrations of magnesium ions to serum samples to evaluate their potential impact on the accuracy of calcium measurements. Subsequent analysis of calcium concentration before and after spiking allowed for the detection and quantification of any deviations caused by magnesium interference. This experimental procedure plays a crucial role in validating the reliability and effectiveness of the method in accurately quantifying serum calcium levels, particularly in the presence of interfering substances. Such meticulous evaluation is indispensable for ensuring the clinical relevance and accuracy of biochemical assays in diagnostic applications.

## 2.6. Applied on Real Serum Samples

The proposed method underwent rigorous optimization and validation processes to ensure its efficacy and accuracy. Following these crucial stages, the method was successfully

developed and implemented for the analysis of serum calcium levels in more than 40 real specimens collected from Farabi Hospital. This empirical application underscores the practical utility and relevance of the method in clinical settings. Moreover, a comparative analysis was conducted utilizing UV-visible spectrophotometry, allowing for an evaluation of the proposed method's performance against an established technique. Such comparative assessments are essential for validating the reliability and precision of novel analytical methodologies within scientific research and medical diagnostics.

### 2.6.1. Samples Collection Process

Taking a serum sample is a routine procedure typically performed by healthcare personnel. For this study, FARABI HOSPITAL provided these processes and the patients were chosen without regard to their age or gender. Initially, the patient was seated comfortably, and the area for blood extraction, usually the inner elbow, was exposed. The provider then confirms the patient's identity before applying a tourniquet to enhance vein visibility. After sterilizing the site with an alcohol swab, the provider uses a sterile needle attached to vacuum tubes for venipuncture, collecting blood for testing. Depending on the required tests and sufficient blood collection, the needle is withdrawn, and pressure is applied to the puncture site to prevent bleeding. Tube was meticulously labeled with the patient's details to ensure accurate processing. Subsequently, the samples are transported to a laboratory where, in the case of serum samples, they undergo clotting before centrifugation, separating the serum from other blood components. These meticulous steps guarantee the safety and precision of the sample collection process.

# 3. RESULTS AND DISCUSSION

## 3.1. Optimization

### 3.1.1. Optimization of Capturing Condition

The study comprised a sequence of experimental studies intended to obtain digital images in various settings, including a regular room setting and a containment box that was built to specification (Figure 26). The data indicates that taking photos inside the box is more reliable for most color models, as evidenced by improved %RSD values in (Table 6). This increased reliability is attributed to the controlled environment within the box, which eliminates ambient light and reduces light scattering. By removing these variables, the consistency and accuracy of the color measurements are significantly enhanced, leading to more precise and repeatable results.

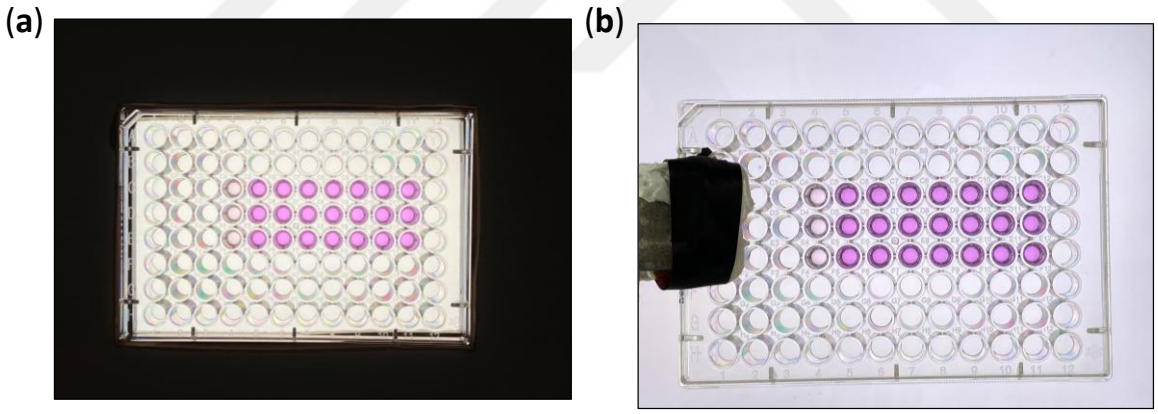


Figure 26. (a) plate inside the box, (b) plate outside the box.

Table 6. %RSD value of different color models and conditions.

| | %RSD | | | |
|---|---|---|---|---|
| | Green | Saturation | a | Magenta |
| Inside box | 1.23 | 0.69 | 0.82 | 0.56 |
| Outside | 1.34 | 0.62 | 0.86 | 0.61 |

### 3.1.2. Selecting the Color Channels

After taking a picture and importing it into the computer, Image J offers several color model choices for photo analysis. The four specific models that we looked into were the LAB color model (Figure 27), CMYK (Figure 29), HSB (Figure 28), and RGB (Figure 30).

After converting the photo to various color models and analyzing each one, it was observed that certain channels exhibited a more intense response compared to others. This observation was confirmed by drawing calibration curves and calculating the R-squared values for each color channel. The channels with higher R-squared values demonstrated a stronger correlation and more reliable intensity response, validating the differences in channel behavior across the different color models.

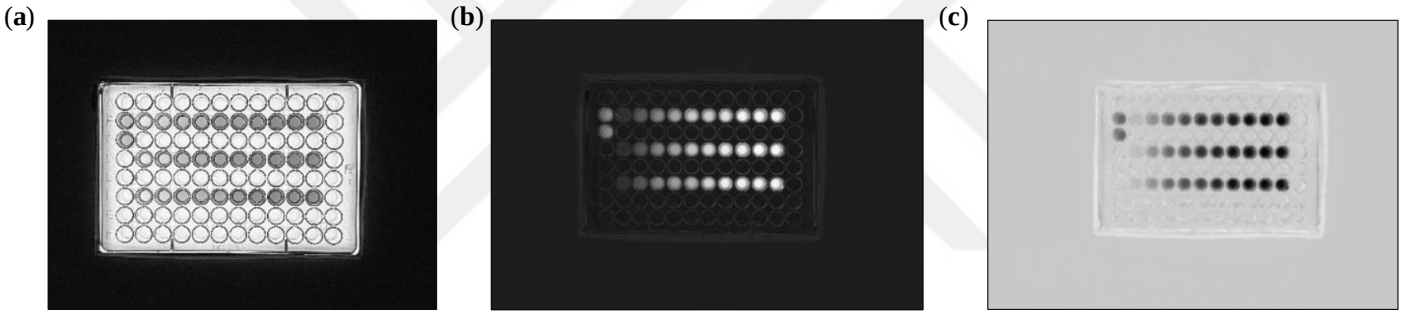


Figure 27. LAB color stack chanels: (a) L, (b) A, and (c) B.

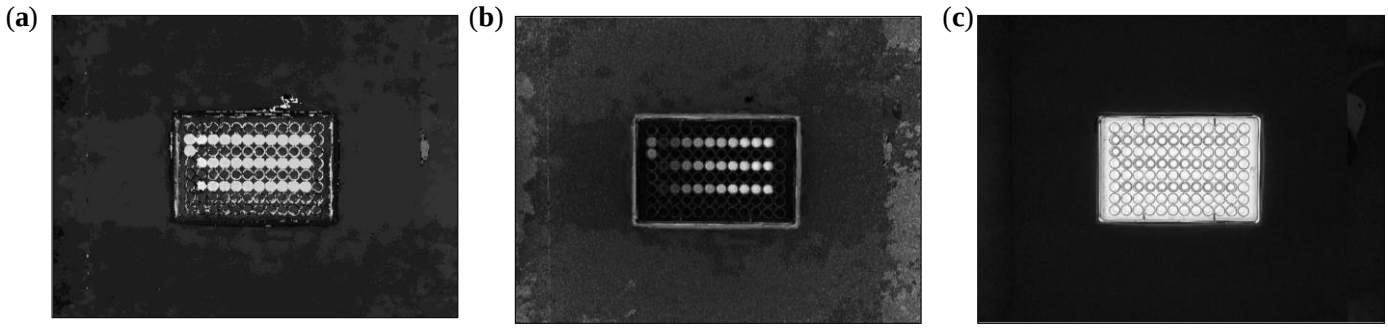


Figure 28. HSB Color models; (a):Hue, (b): Saturation, and (c) Brightness.

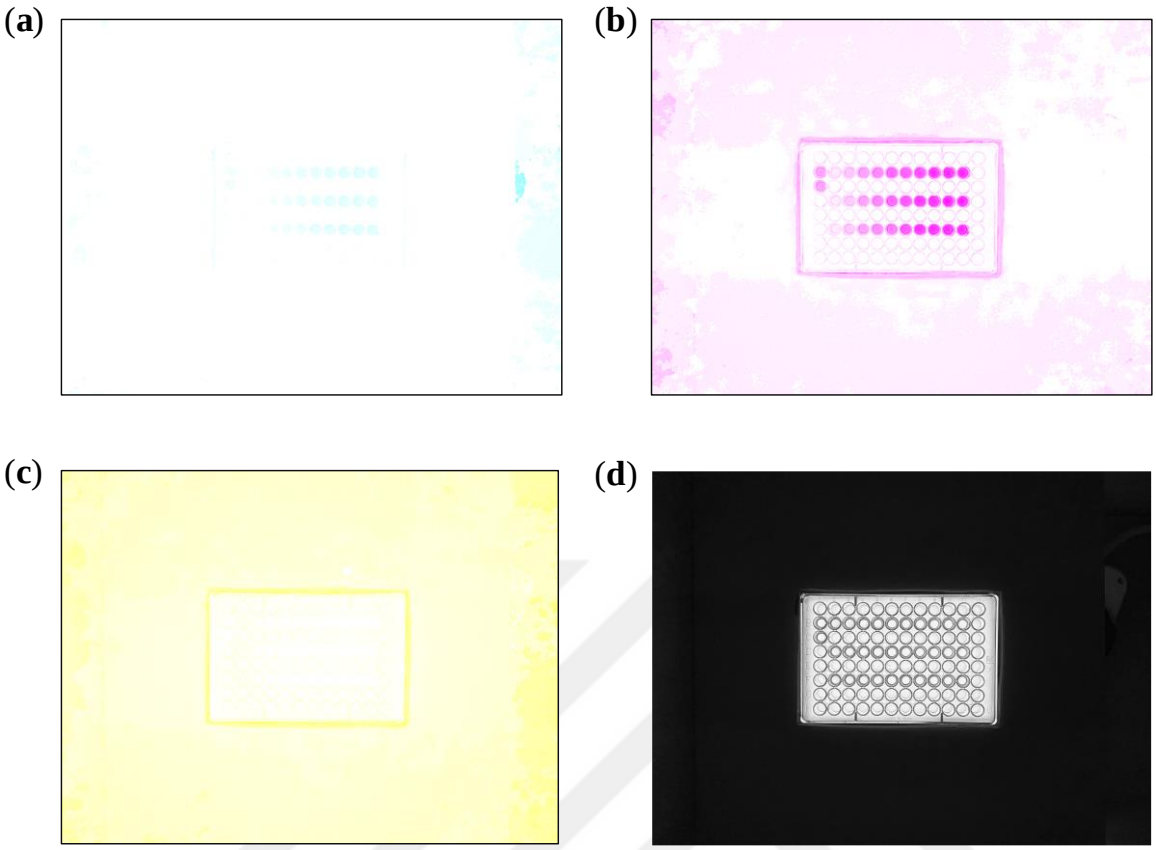


Figure 29. CMYK color model; (a) Cyan, (b) Magenta, (c) Yellow, and (d) Key.

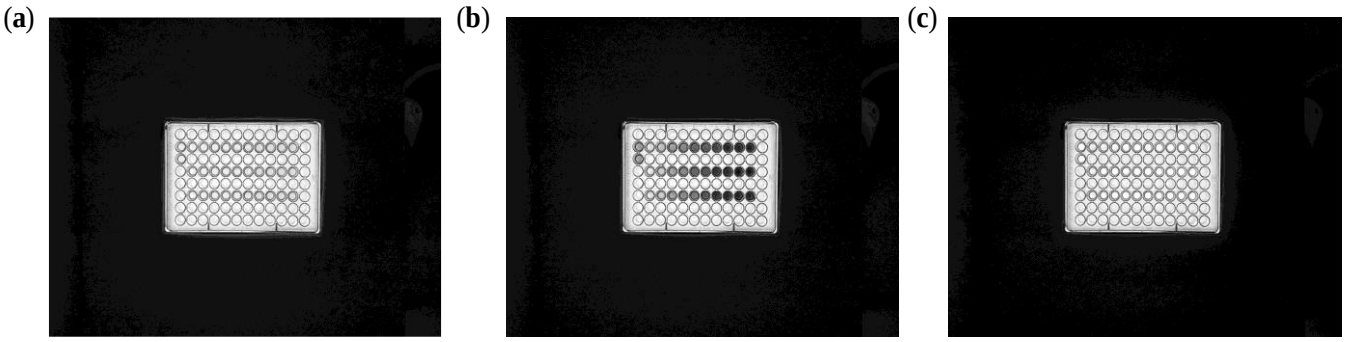


Figure 30. RGB Color model; (a): Red, (b): Green, and (c): Blue.

In the context of LAB color models, the A channel demonstrates a significantly higher correlation compared to the L and B channels, as evidenced by the R-squared values obtained from a correlation analysis. Specifically, the R squared value for the A channel is 0.9907, indicating an exceptionally high degree of correlation. This is notably higher than the R-squared values for the L and B channels, which are 0.9811 and 0.9696 respectively (Figure 31). These values suggest that while all three channels exhibit strong correlations, the A channel's correlation is the most pronounced, potentially implying a greater consistency or predictive accuracy in the color space represented by the A channel relative to the L and B channels.

In the HSB color model, the Saturation channel exhibits a significantly higher correlation to the CPC-Calcium complexed color compared to the Hue and Brightness channels, with an R-squared value of 0.9887, whereas Hue and Brightness have R-squared values of 0.5303 and 0.7561, respectively (Figure 32). This strong correlation is attributable to the fact that as the concentration of calcium increases, the intensity of the color intensifies, leading to a corresponding increase in saturation. In contrast, this increase in color intensity does not produce a proportionate change in the brightness and hue, indicating that these channels are less effective in capturing variations in calcium concentration. Consequently, within the HSB model, the Saturation channel serves as a reliable indicator of the CPC-Calcium complexed color, making it a preferred metric for accurate measurement and analysis.

In the context of analyzing the relationship between color intensity and calcium concentration using the RGB color model, the Green (G) channel demonstrated a significantly higher correlation compared to the Red (R) and Blue (B) channels. Specifically, the G channel exhibited an R-square value of 0.9917, indicating an exceptionally strong correlation, whereas the R and B channels had R-square values of 0.9813 and 0.6204, respectively. This pronounced difference highlights the superior sensitivity of the Green channel to variations in calcium concentration. Consequently, the Green channel was selected for further analysis due to its high correlation with changes in color intensity, suggesting that it is the most reliable indicator within the RGB model for detecting variations in calcium levels.

Within the CMYK color model, the Magenta (M) channel emerged as the sole viable option for determining calcium concentration using the proposed method. The conversion of images to the Cyan (C) and Yellow (Y) channels proved ineffective for analysis, as these

channels lacked clarity and did not exhibit any correlation with the method Figure 29. In contrast, the Magenta channel displayed a robust correlation, with an R-square value of 0.9881 (Figure 34), indicating its suitability for accurate calcium detection. Although the Key (K) channel showed some correlation, it was not sufficiently reliable for analytical purposes. Consequently, the magenta channel is the preferred choice for analysis when using the CMYK color model due to its strong correlation and reliability in reflecting calcium concentration changes.

**(a)**

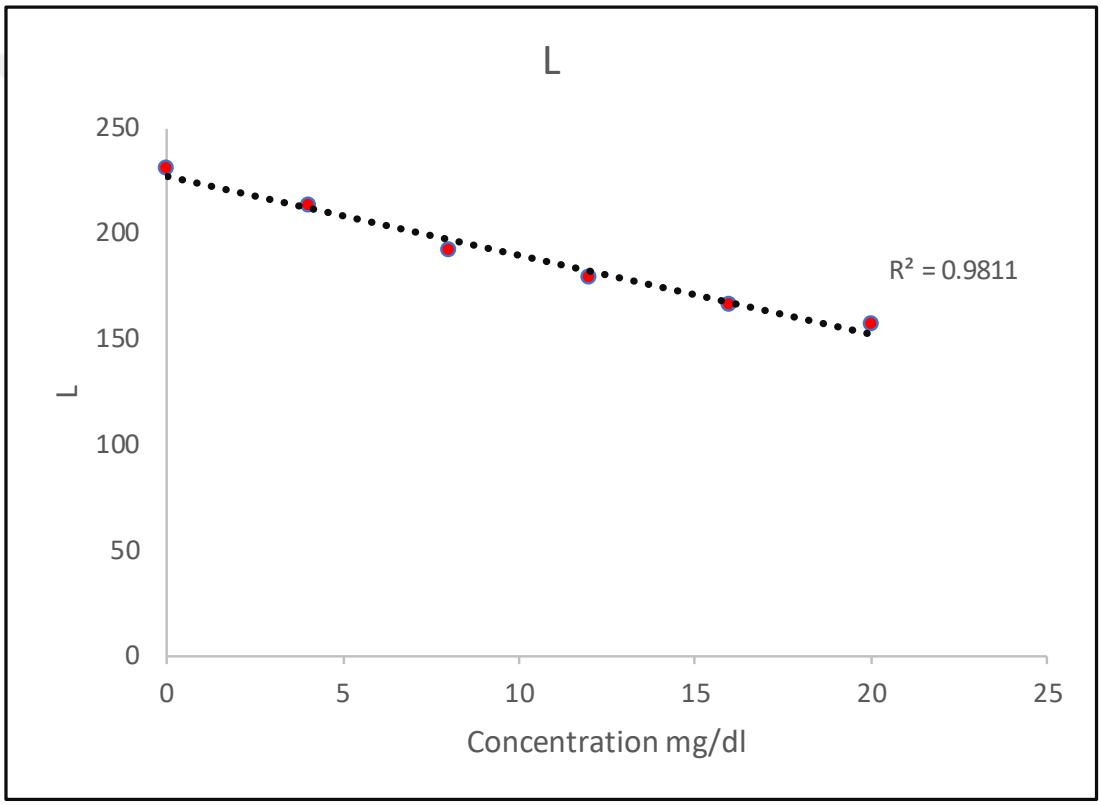

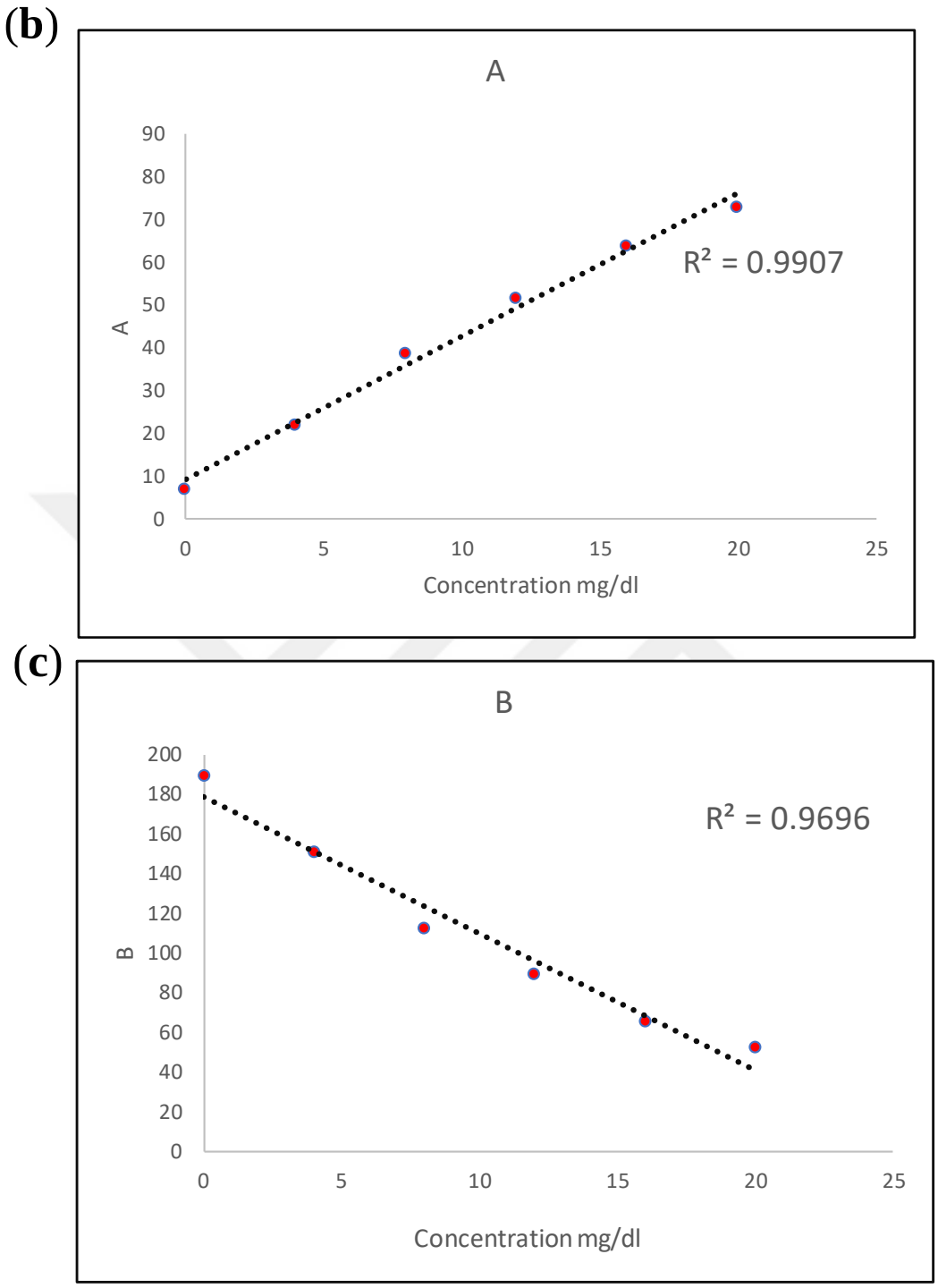


Figure 31. Calibration curve between LAB color channels and concentratoin of standard solutions; (a) L channel, (b) A channel, and (c) B channel.

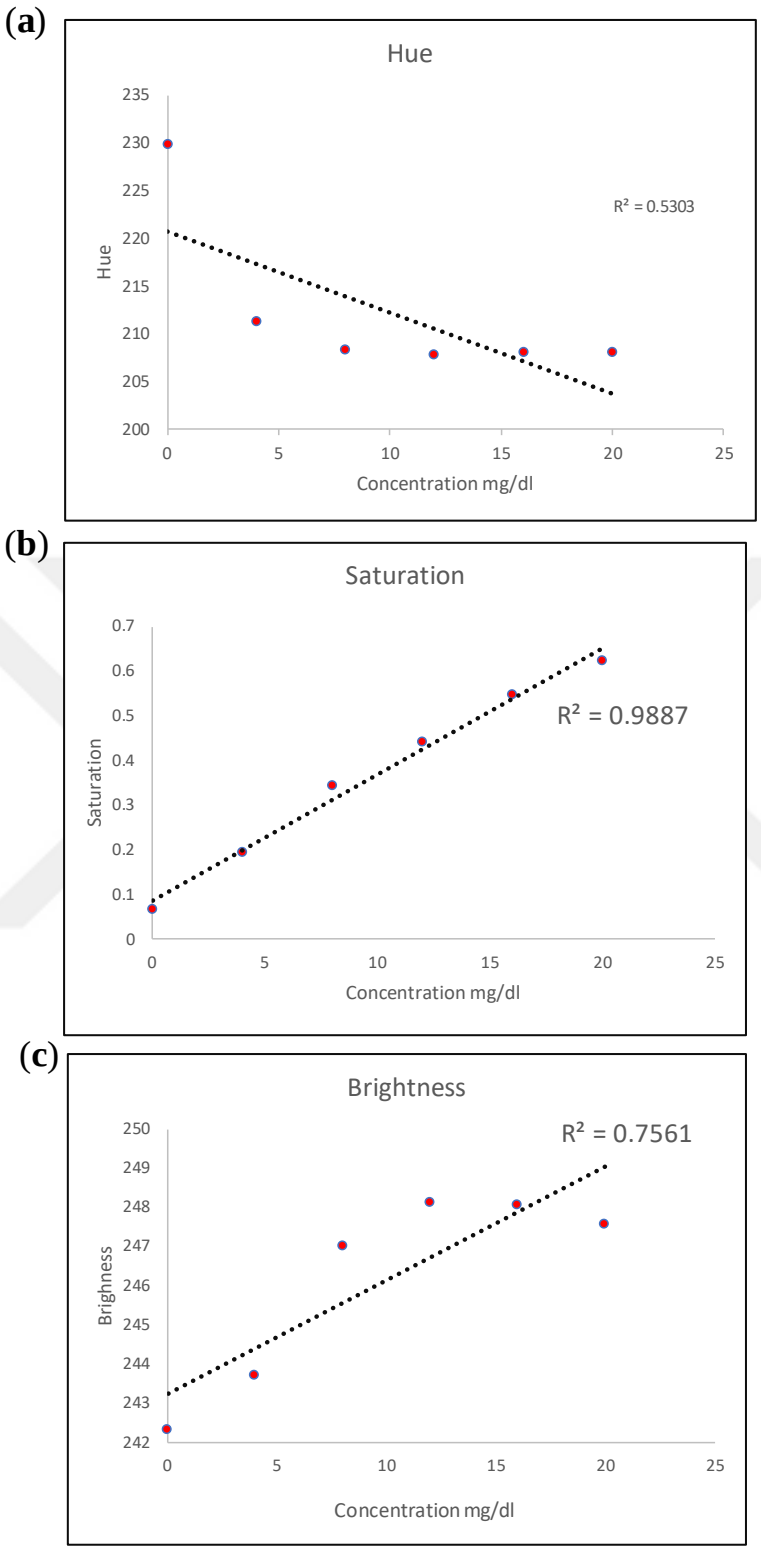


Figure 32. Calibration curve between HSB color channels and concentratoin of standard solutions; (a) Hue channel, (b) Saturation channel, and (c) Brightness channel.

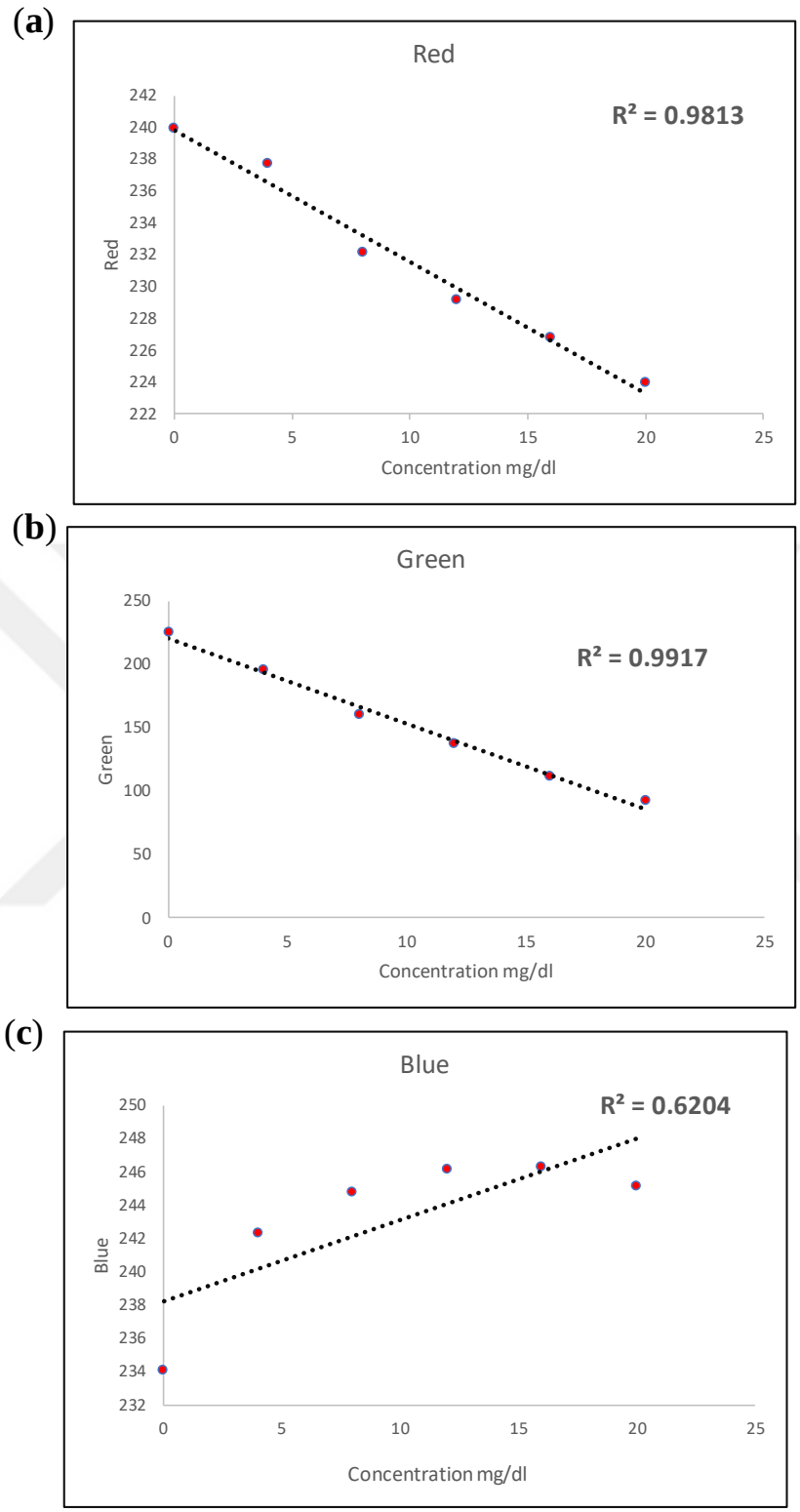


Figure 33.Calibration curve between RGB color channels and concentratoin of standard solutions; (a) Red channel, (b) Green channel, and (c) Blue channel.

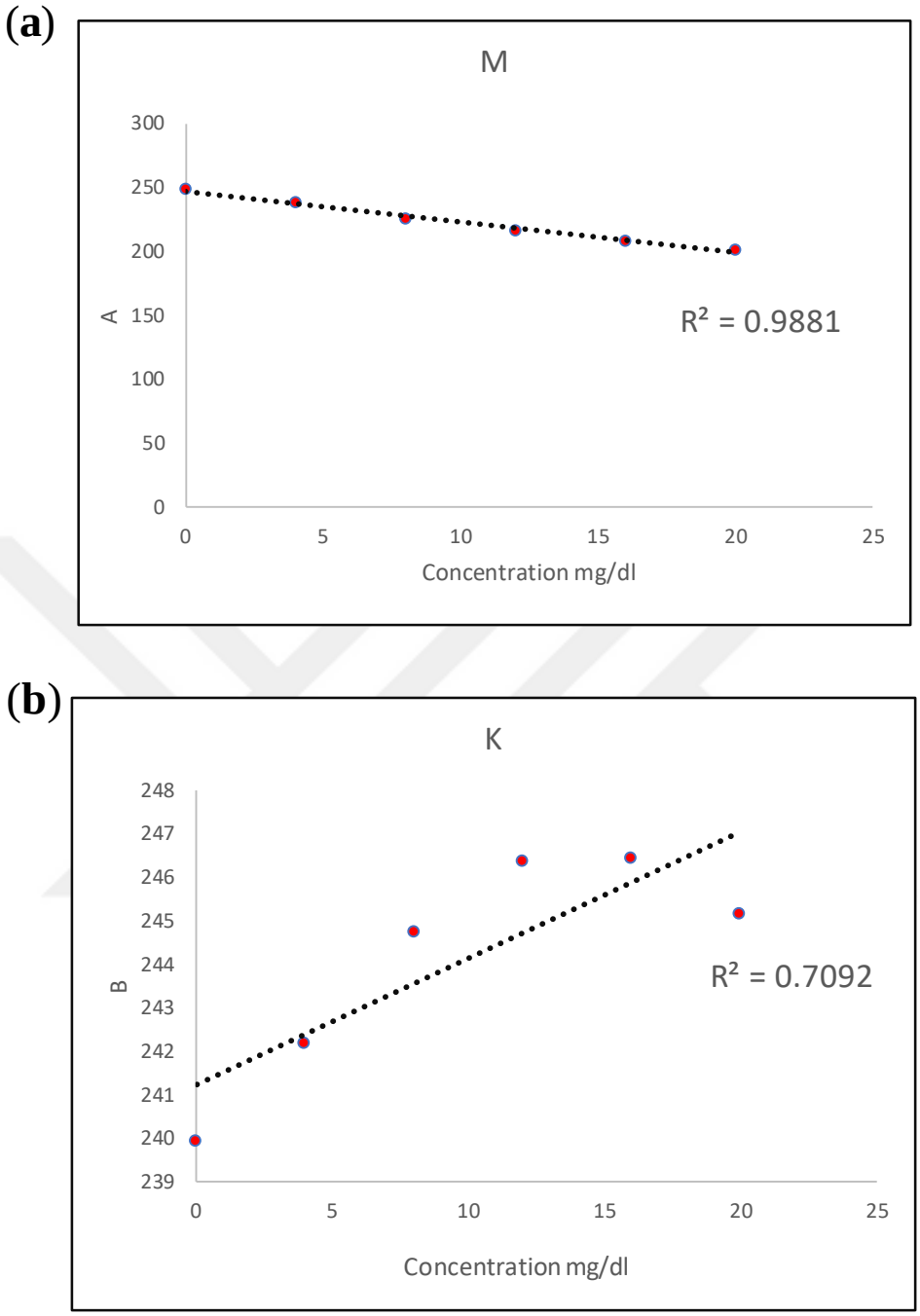


Figure 34. Calibration curve between CMYK color channels and concentratoin of standard solutions; (a) Magenta channel, (b) Key channel.

### 3.1.3. Solution Volume

In the proposed method, the volume of the solution emerged as a critical parameter, particularly in the context of developing a more environmentally friendly and economical approach to calcium measurement. Traditional spectrophotometric methods require a minimum solution volume of 1000 µl. However, through extensive preliminary experiments, we adopted the use of a microwell plate, which accommodates reaction solutions of up to 250 µl. This adaptation not only significantly reduces the required volume of the solution but also aligns with eco-friendly and sustainable practices. Numerous tests were conducted to evaluate the impact of solution volume on the analytical performance, ensuring that the reduced volume did not compromise the accuracy and reliability of the calcium measurements.

We further investigated the analytical performance using varying volumes of solution 100, 150, 200, and 250 µl in the microwell plate. Our findings revealed that the analytical performance remained consistent across these different solution volumes. This was substantiated by plotting calibration curves across all color models and solution volumes, consistently yielding R-square values exceeding 0.99 (Figure 35-32). These high R-square values across all tested volumes confirm that the method is robust and reliable regardless of the solution volume used. Therefore, the analysis of calcium can be confidently conducted with any of these solution volumes without compromising the accuracy and reliability of the results.

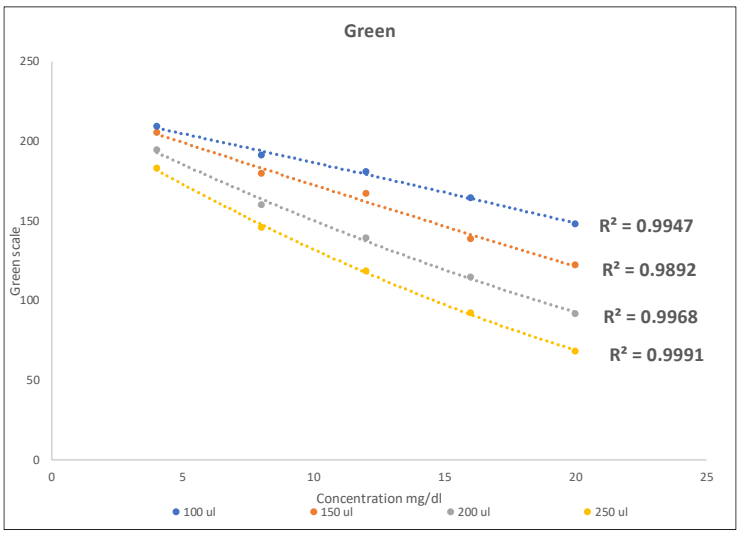


Figure 35. Graph shows the effect of Solution volume with Green respose.

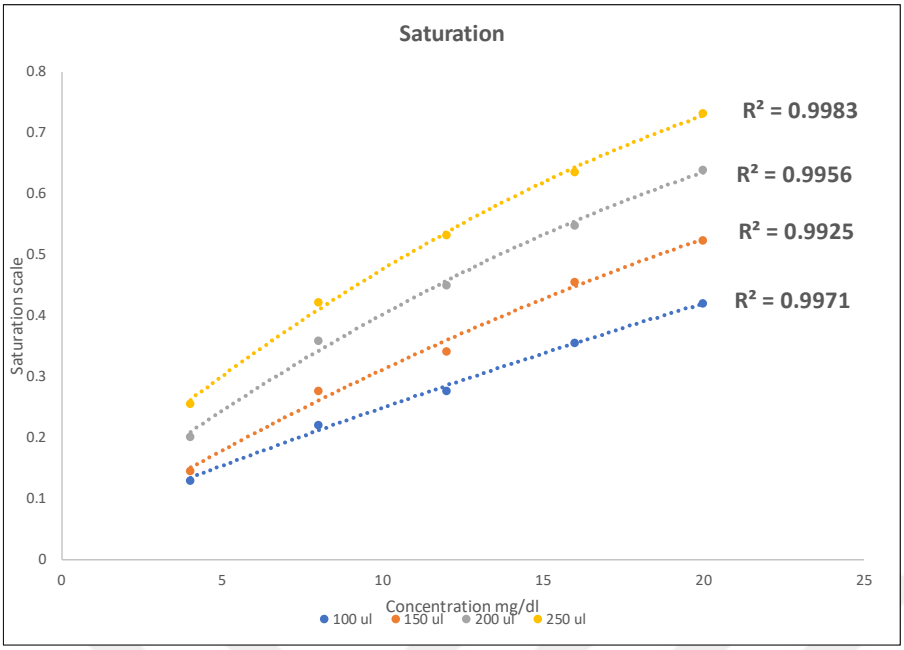


Figure 36. Graph shows the effect of Solution volume with Saturation respose.

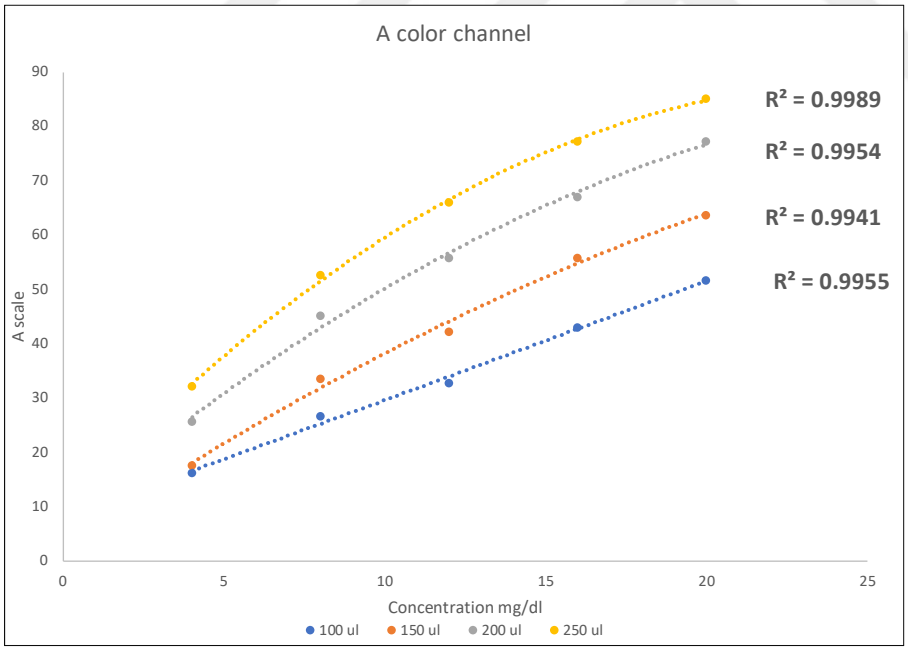


Figure 37. Graph shows the effect of Solution volume with A channel respose

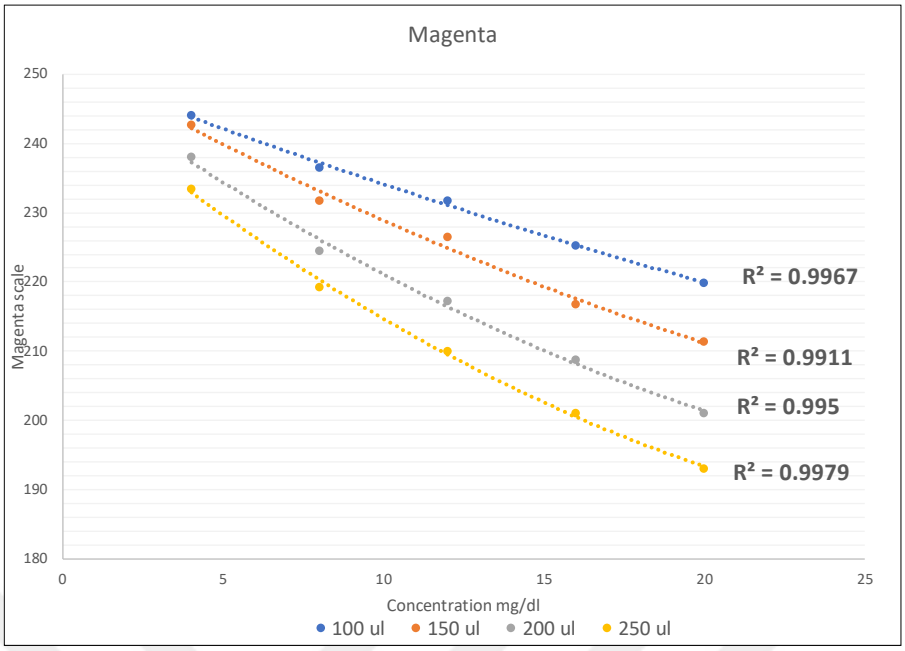


Figure 38. Graph shows the effect of Solution volume with Magenta.

### 3.1.4. Distance Between Detection Camera And The Sample Solutions

The most crucial stage of this proposed method was the photography process, as the entire analysis and analytical performance hinged on the quality of the images captured. For the photos to be reliable, they needed to be exceptionally clear and taken in an optimal environment. A key parameter in achieving this clarity was the distance between the camera and the microwell plate containing the solution. To determine the optimal distance, several tests were conducted within the range of 15 to 35 cm. Distances less than 15 cm resulted in blurry images with shallow depth, while distances greater than 35 cm caused focus issues and a lack of resolution. Through these tests, the optimal range was found to be between 15 and 35 cm.

Within the proposed range of 15 to 35 cm, the analytical performance remained consistent across all distances, as evidenced by the calibration curves and R-square values. However, at a distance of 25 cm, the performance was notably superior in most color models, yielding higher R-square values, which indicate a stronger correlation and greater accuracy in the analysis. This optimal distance of 25 cm not only minimized issues related to blurriness and depth but also maximized the resolution and clarity of the captured images, ensuring the reliability of the analytical results. Consequently, 25 cm was selected as the optimal distance

between the detector and the solution during photo capturing. This selection is crucial as it enhances the precision and dependability of the subsequent analyses, thereby improving the overall efficacy of the proposed method. Further, this distance ensures that the conditions are reproducible and standardized, which is essential for the consistency and validity of the analytical outcomes.

**(a)**

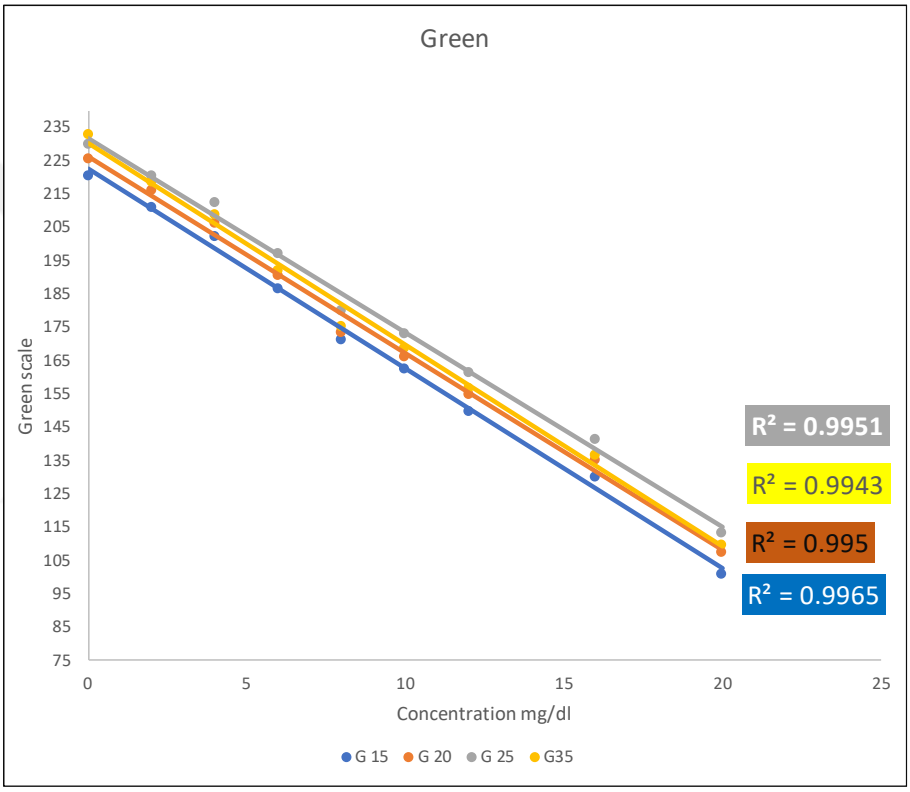

**(b)**

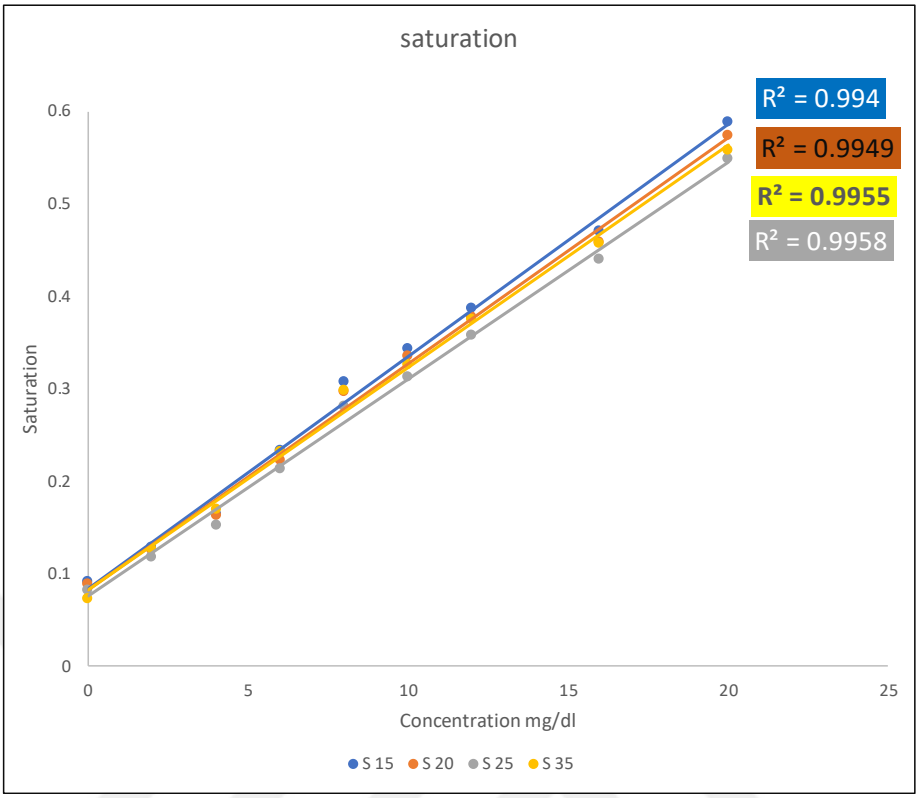
saturation
R² = 0.994
R² = 0.9949
R² = 0.9955
R² = 0.9958
Saturation
0.6
0.5
0.4
0.3
0.2
0.1
0
0
5
10
15
20
25
Concentration mg/dl
S 15
S 20
S 25
S 35

**(c)**

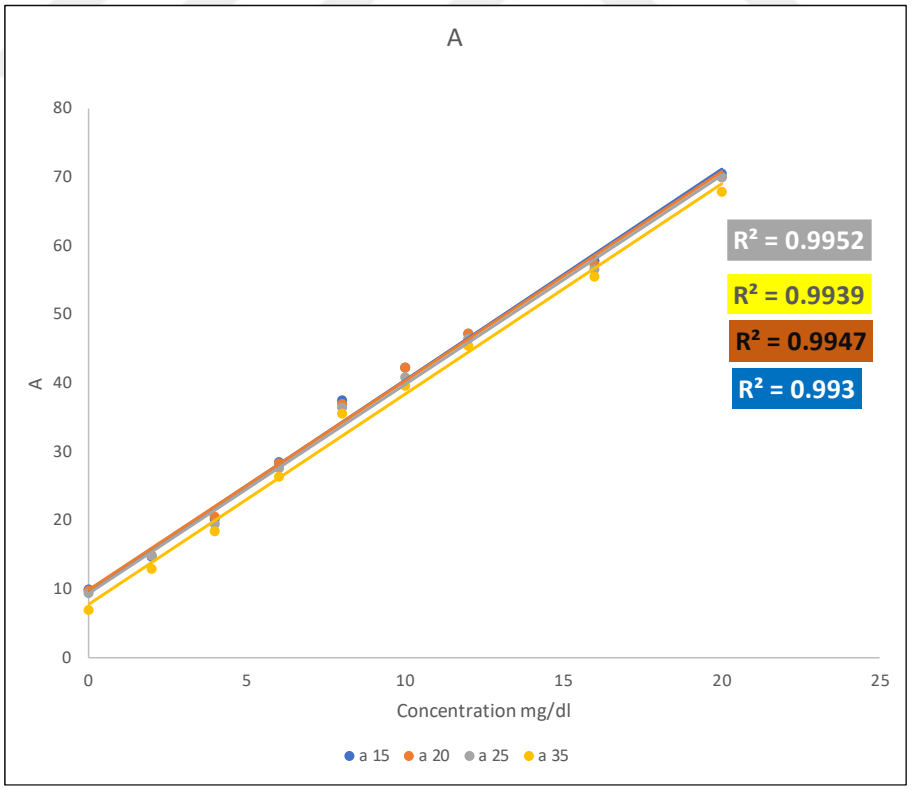
A
R² = 0.9952
R² = 0.9939
R² = 0.9947
R² = 0.993
A
80
70
60
50
40
30
20
10
0
0
5
10
15
20
25
Concentration mg/dl
a 15
a 20
a 25
a 35

**(d)**

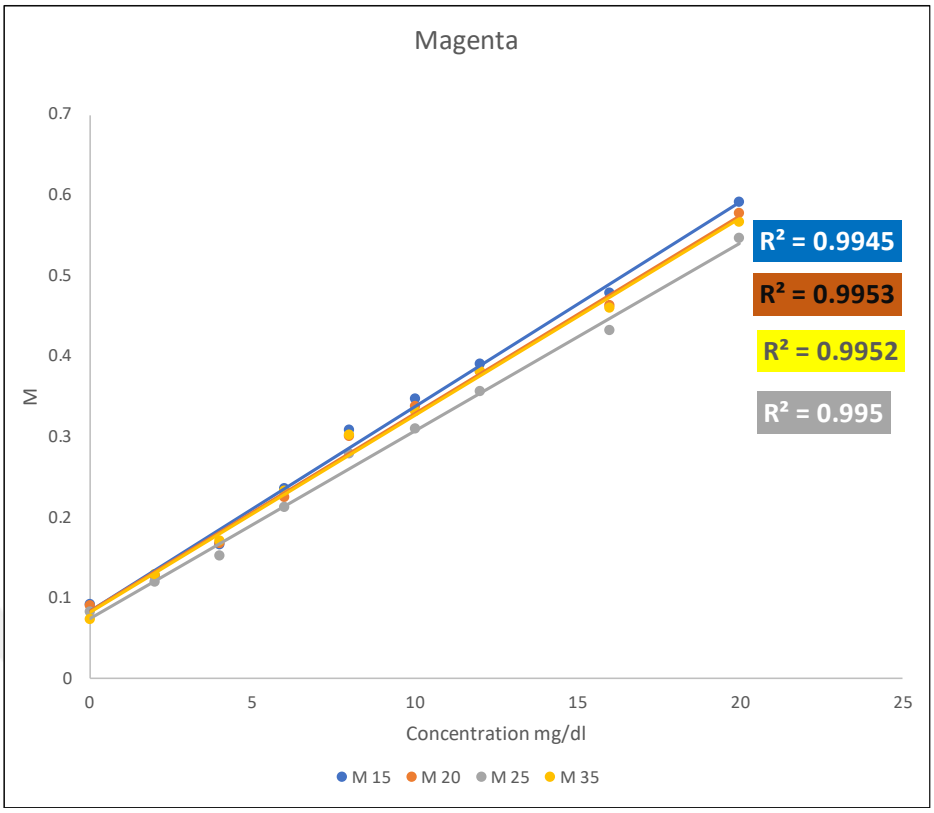


Figure 39. Effect of Distance between Detector camera and solution; (a) Green, (b) Saturation, (c) A color channel, and (d) Magenta.

### 3.1.5. Distance Between Source of Light And The Sample Solutions

Numerous tests were conducted to evaluate the impact of varying distances between the light source and the microwell plate containing the solution, with distances ranging from 0 to 6.5 cm. Following extensive calibration and analysis using ImageJ software, it was established that a distance of 3 cm was optimal. This conclusion was supported by the R-square values obtained during calibration, which demonstrated greater accuracy at 3 cm compared to distances of 0 cm or 6.5 cm. This optimization was essential for improving the precision of calcium quantification in my study, ensuring more reliable and accurate results.

**(a)**

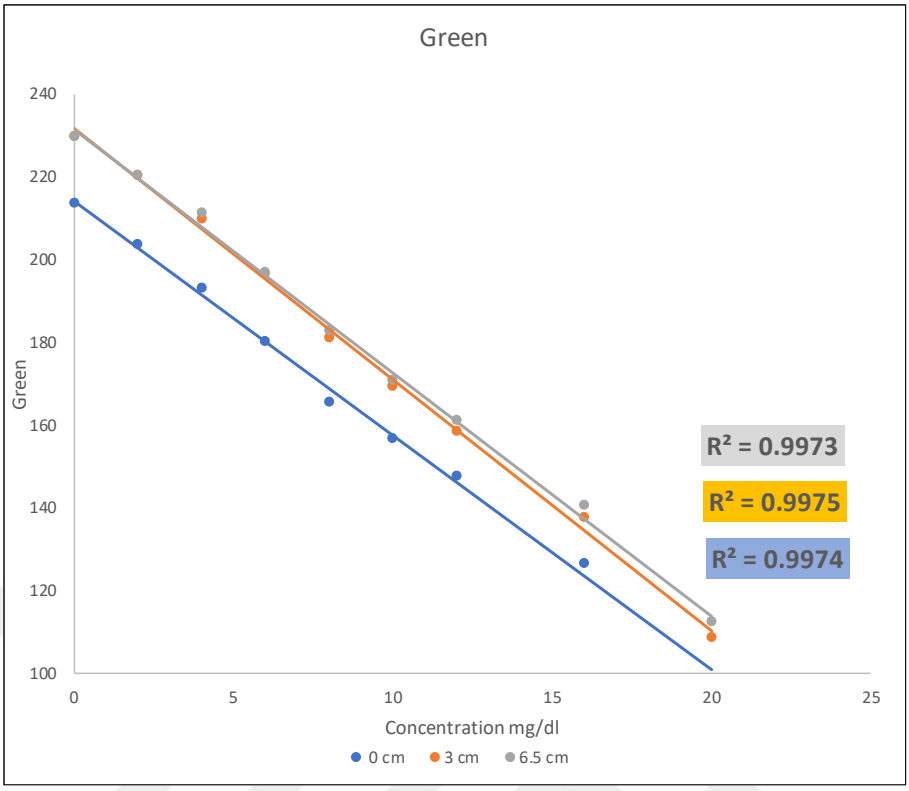
Green
240
220
200
180
160
140
120
100
Green
0
5
10
15
20
25
Concentration mg/dl
0 cm
3 cm
6.5 cm
R² = 0.9973
R² = 0.9975
R² = 0.9974

**(b)**

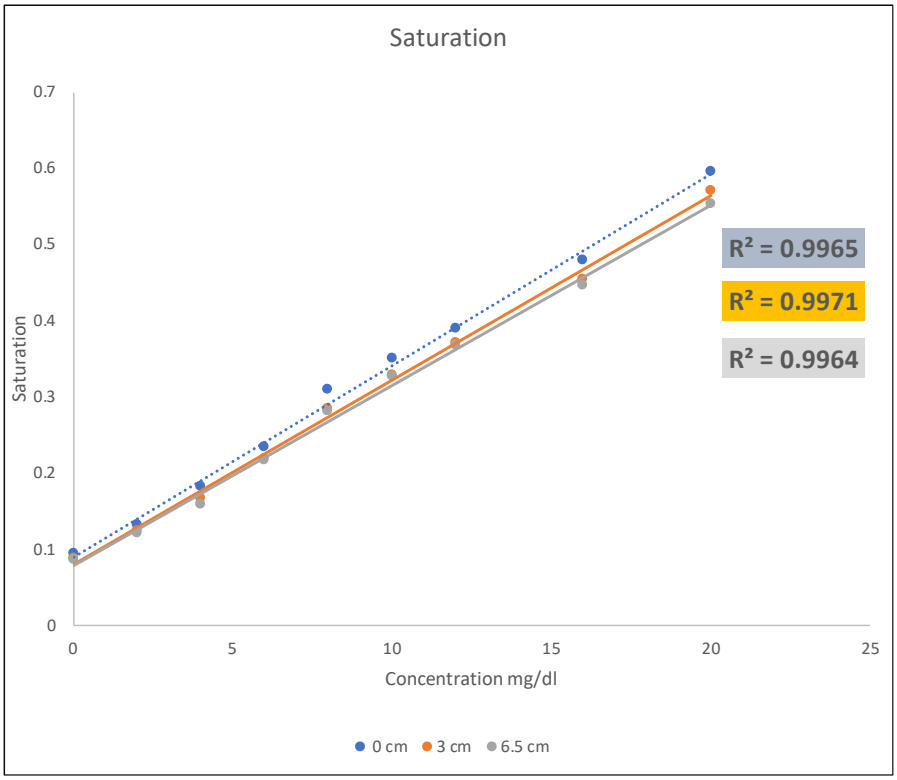
Saturation
0.7
0.6
0.5
0.4
0.3
0.2
0.1
0
Saturation
0
5
10
15
20
25
Concentration mg/dl
0 cm
3 cm
6.5 cm
R² = 0.9965
R² = 0.9971
R² = 0.9964

**(c)**

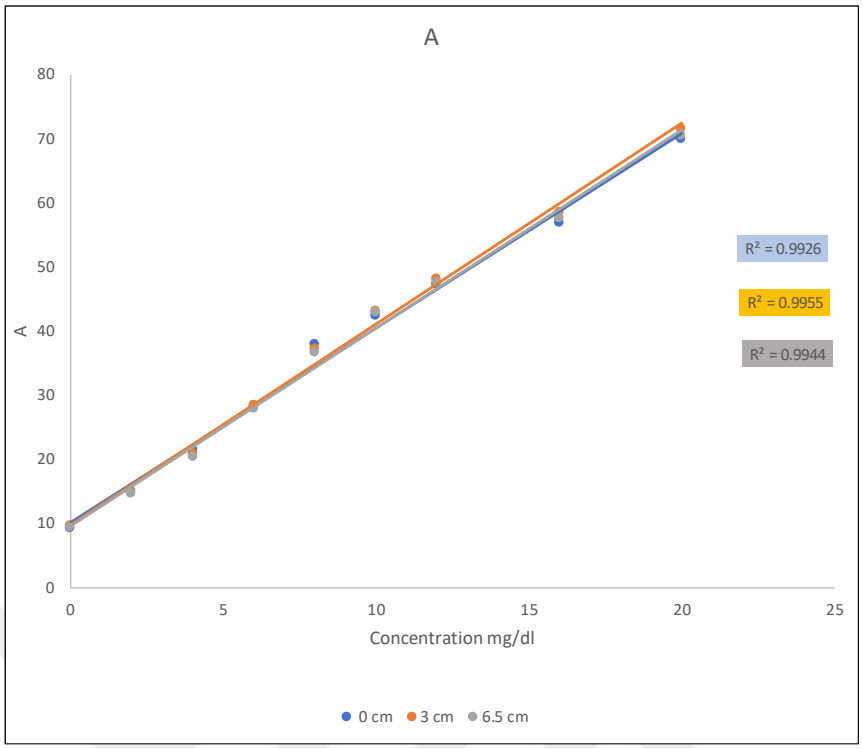


**(d)**

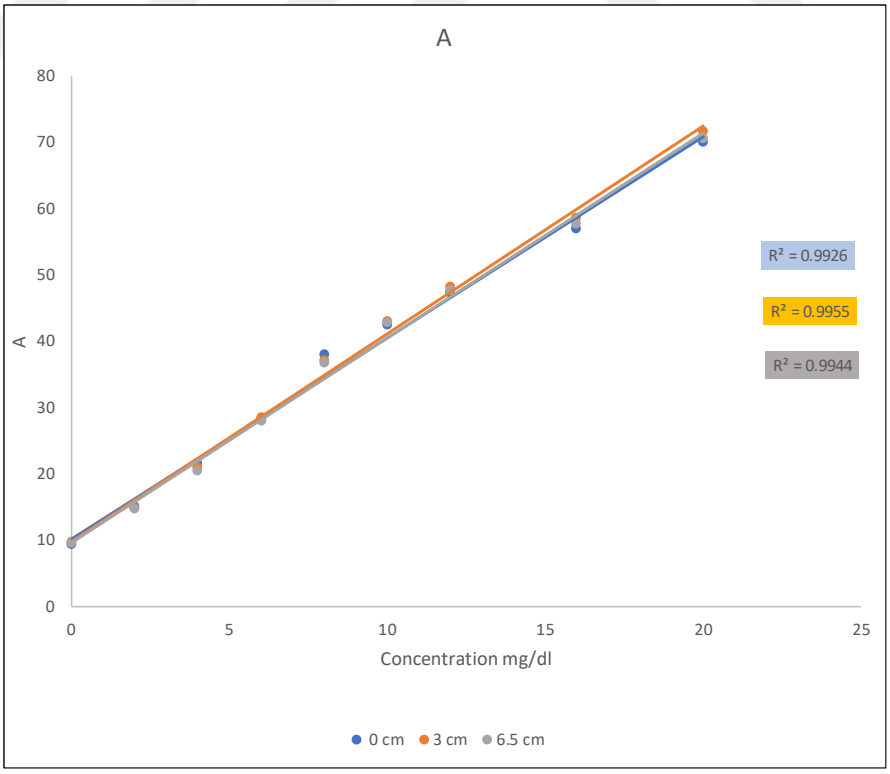


Figure 40. Distance between Source of light and Solution; (a) Green, (b) Saturation, (c) A, and (d) Magenta

### 3.1.6. Reaction Time

To ensure the optimal timing for capturing images after initiating the reaction and to clarify the reaction kinetics, several tests were conducted using three different concentrations: low (6 mg/dl), normal (10 mg/dl), and high (14 mg/dl). The results, illustrated in the graph, show that for all color models, the reaction between $Ca^{2+}$ ions and the CPC reagent reaches completion within 10 minutes. Beyond this point, the color intensity gradually diminishes. Therefore, it can be concluded that photographs for analysis should be taken 10 minutes after the reaction starts to ensure accuracy and consistency in the observed color changes.

**(a)**

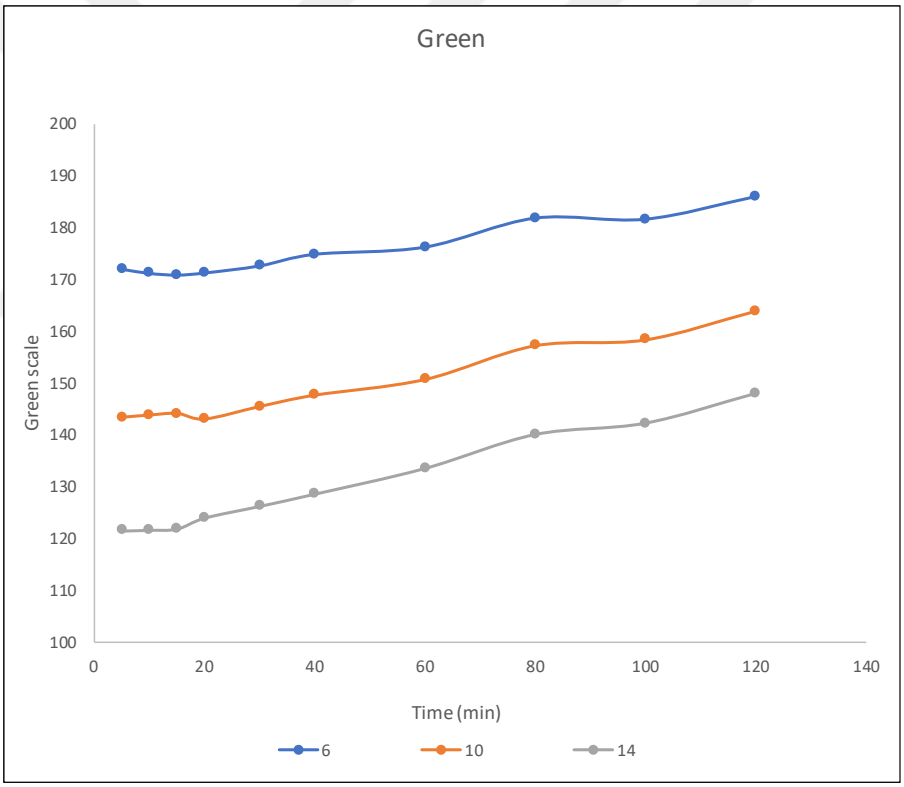

**(b)**

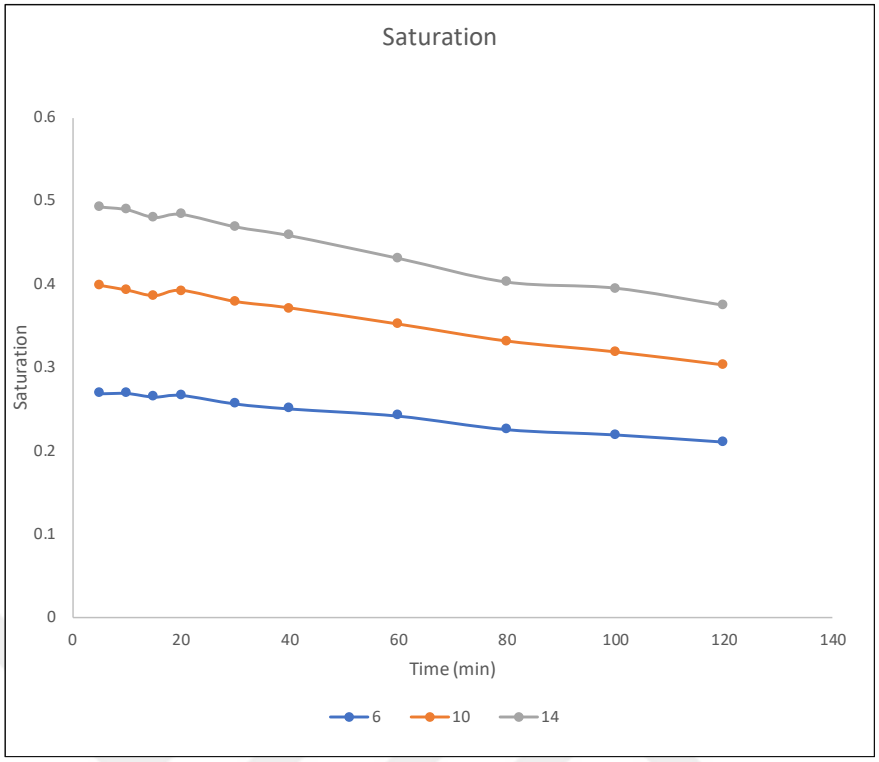
Saturation
Saturation
0.6
0.5
0.4
0.3
0.2
0.1
0
0
20
40
60
80
100
120
140
Time (min)
6
10
14

**(c)**

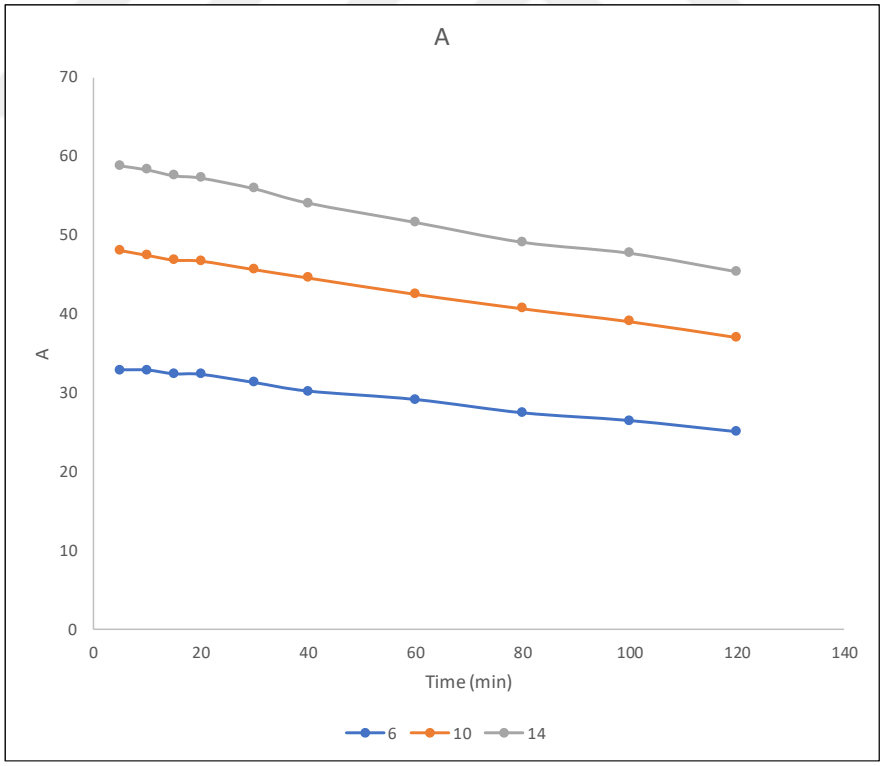
A
A
70
60
50
40
30
20
10
0
0
20
40
60
80
100
120
140
Time (min)
6
10
14

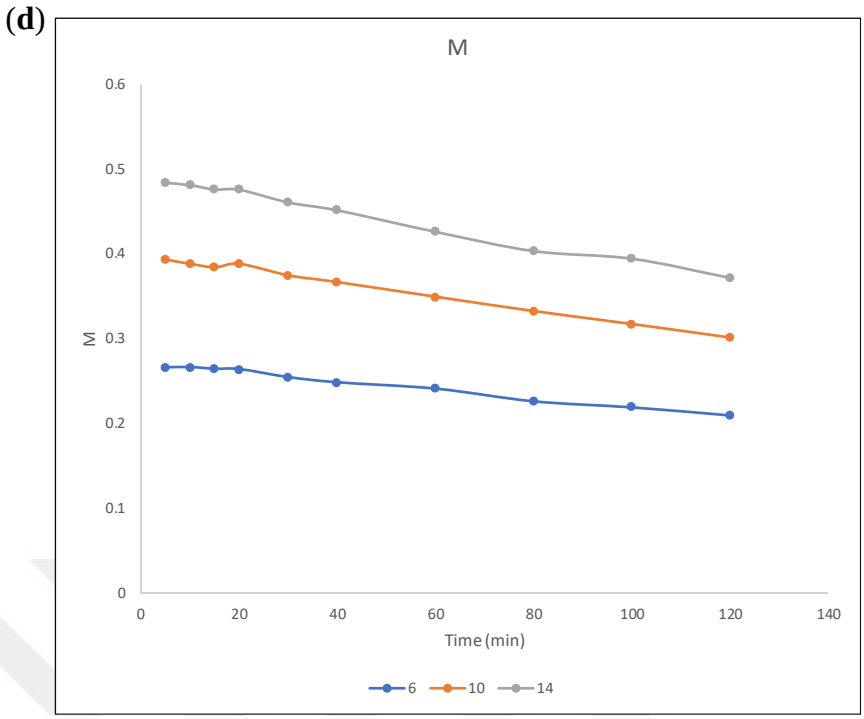


Figure 41. Time of reaction (a) Green, (b) Saturation, (c) A, and (d) Magenta

### 3.1.7. Contrast

After the photos were taken, but before analysis with Image J software, their contrast was deliberately altered to levels significantly lower and higher than normal (-99 and +99, respectively). These modified versions were then compared to the original, unaltered photos. The analysis revealed that adjusting the contrast negatively impacted the results, as indicated by a decrease in the R-square values and an increase in the standard deviation (Figure 43). Consequently, the original photos, without any contrast adjustments, demonstrated superior analytical performance with higher R-square values and lower standard deviation.

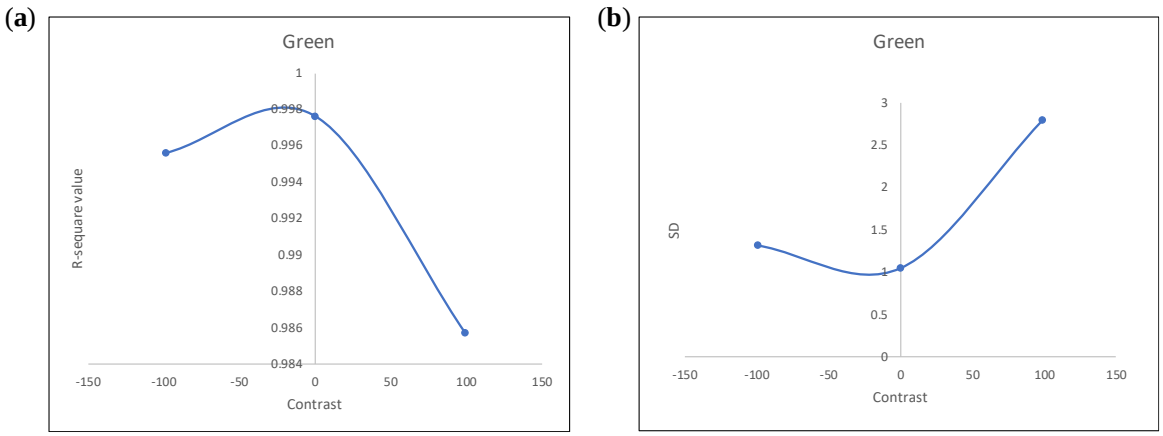


Figure 42. Effect of contrast (a) R-Square (b) Standard deviation.

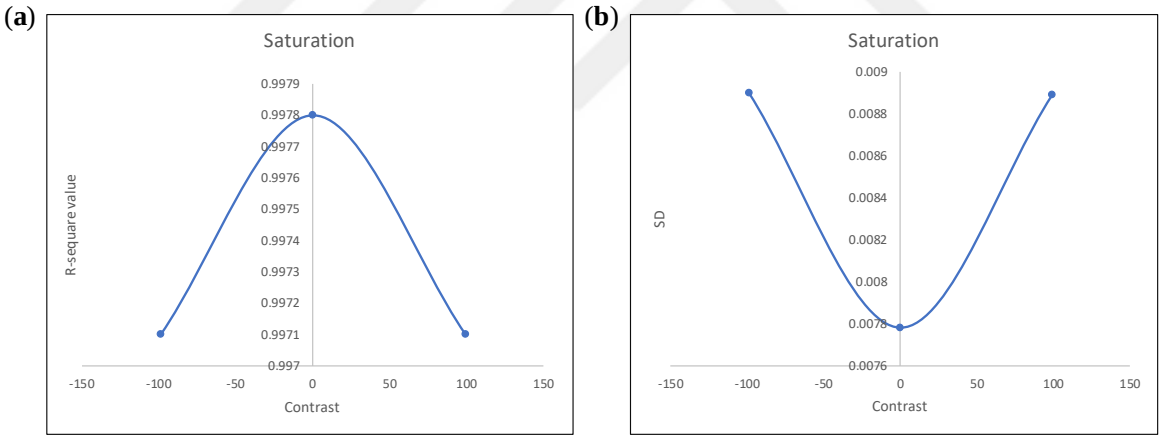


Figure 43. Effect of contrast (a) R-Square (b) Standard deviation.

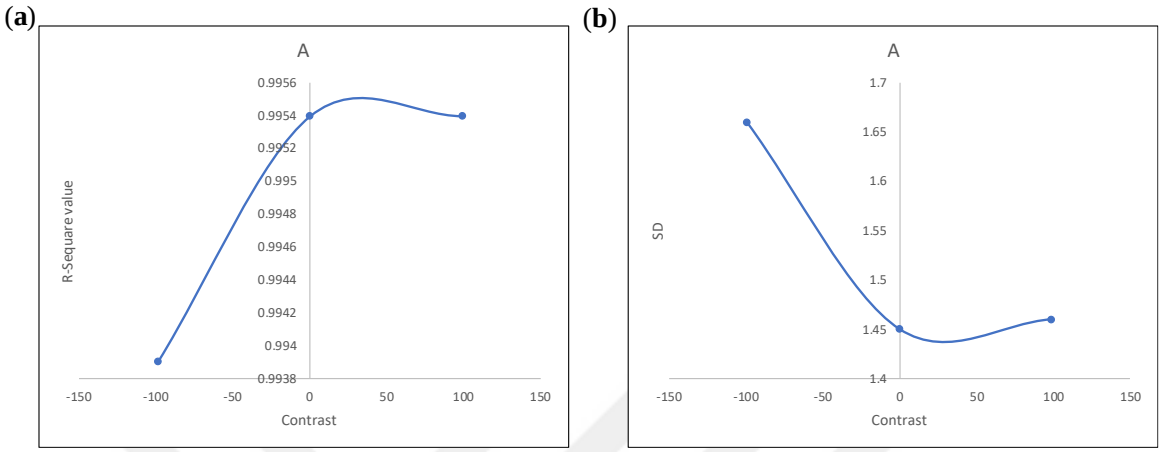


Figure 44. Effect of contrast analyzed in A color channel (a) R-Square (b) Standard deviation.

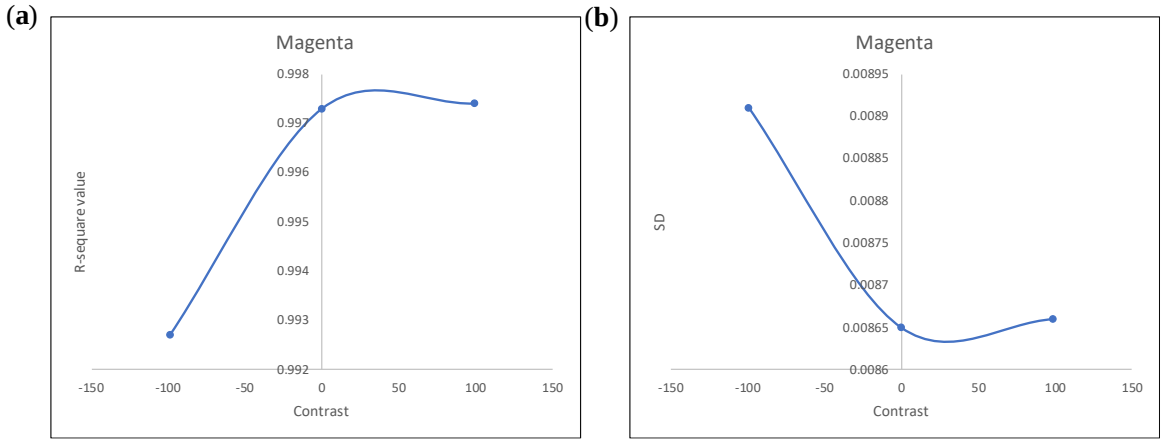


Figure 45. Effect of contrast analyzed in Magenta color channel (a) R-Square (b) Standard deviation.

### 3.1.8. Brightness

In our study, we also investigated the impact of post-capture brightness adjustments on the performance of the proposed method. We tested two levels of brightness: low (-50) and high (+50). Both adjusted images were analyzed and compared to the original. The results indicated that changing the brightness negatively affected the analytical performance in the Green, A, and Magenta color channels (Figure 46, Figure 48, and Figure 49). However, increasing the brightness positively influenced the Saturation color channel, with the performance for Saturation being better at high brightness compared to both low and normal brightness levels (Figure 47).

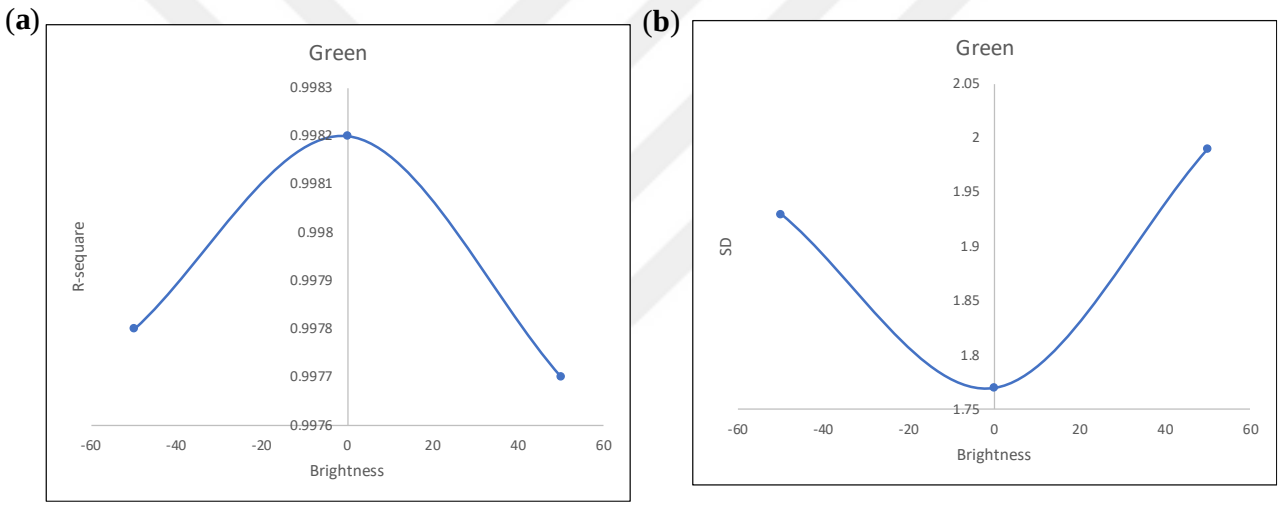


Figure 46. Effect of Brightness (a) R-sequare, (b) SD. Analyzed in Green color channel

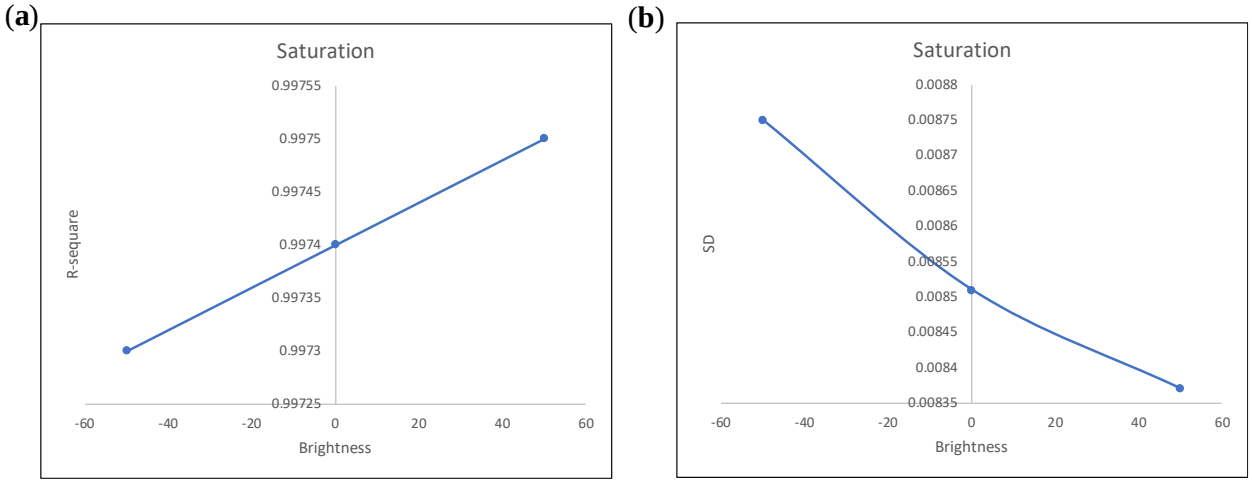


Figure 47. Effect of Brightness (a) R-sequare, (b) SD. Analyzed in Saturation color channel

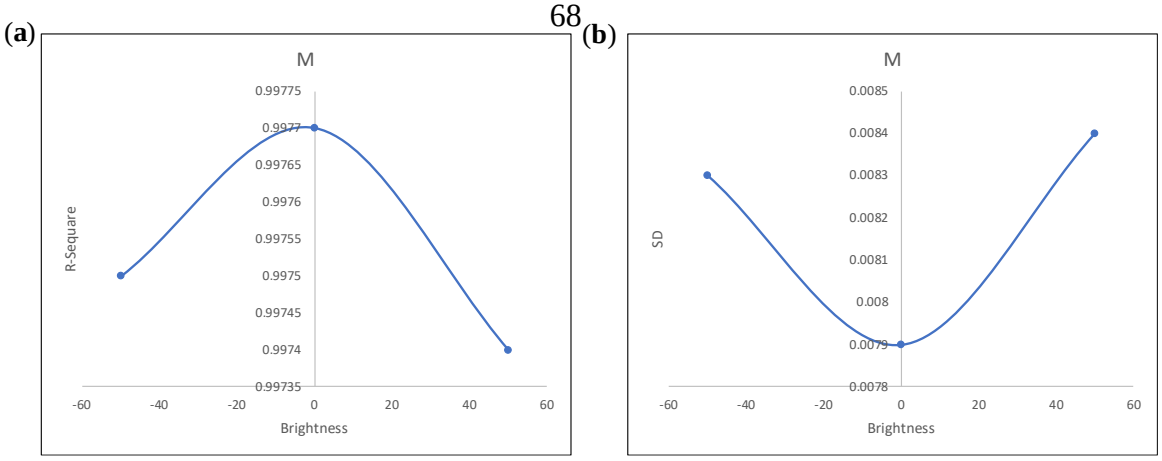


Figure 48. Effect of Brightness (a) R-sequare, (b) SD. Analyzed in Magenta color channel

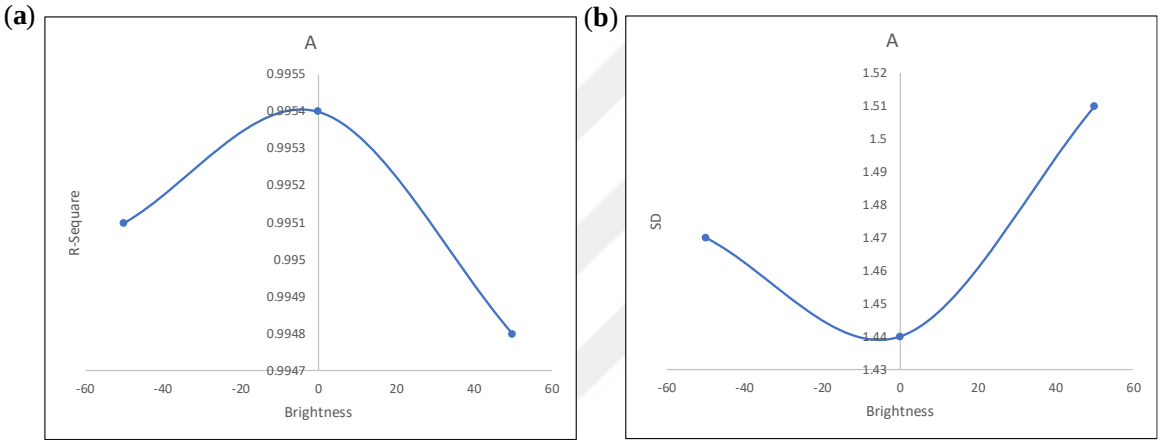


Figure 49. Effect of Brightness (a) R-sequare, (b) SD. Analyzed in A channel

### 3.1.9. Selecting the Microwell Plate Types

Microwell plates come in various sizes and types, with the two primary types being flat bottom plates and round bottom plates. To evaluate their performance, a specific experiment was conducted in which a single concentration of 10 mg/dl of calcium ions was prepared and analyzed five times using each type of plate. The results indicated that flat bottom plates provided superior repeatability and less fluctuation in measurements compared to round bottom plates. This conclusion was supported by the analysis of the percentage relative standard deviation (%RSD), which demonstrated that flat bottom plates offer more consistent and reliable results for this type of assay.

The flat bottom plate was selected as the optimal type for the proposed method due to its superior performance compared to the round bottom plate (Table 7). This preference is

attributed to the reduced fluctuation of the bottom layer when exposed to light from the source, ensuring an even distribution of light across the entire surface area. Consequently, all microwells in the flat bottom plate receive and divide the light uniformly, leading to more consistent and reliable analytical results.

Table 7. Comparison between two types of microwell plates.

| | %RSD | | | |
|---|---|---|---|---|
| **Plate Types** | **Green** | **Saturation** | **A** | **Magenta** |
| Flat Botton | 1.46 | 1.24 | 2.05 | 1.20 |
| Round Botton | 2.04 | 1.61 | 1.34 | 1.67 |

### 3.1.10. Keeping the Solution during Incubation Time

In the period between starting the reaction and transferring the solution to the microwell plate, we're conducting a detailed study to determine the best way to handle the solution during this "Incubation" phase. Specifically, we're exploring whether it's more effective to keep the solution in a designated box or to leave it in the standard room environment. Our goal is to ensure the stability of the reaction and minimize any external factors that could affect the outcome. This investigation is crucial for maximizing the reliability and accuracy of our experimental results.

In our experiment, a singular concentration was meticulously prepared and analyzed five times, employing both in-box and external incubation methods. Remarkably, the results yielded similar %RSD values for both approaches, indicating consistency in our measurements. However, intriguingly, incubation outside of the box demonstrated slightly superior outcomes in terms of %RSD with UV/Vis methods and most color models in Image J, except for A color stack that has better results with the inside of the incubation approach. This phenomenon led us to deduce that maintaining the solution reaction outside the box, within a standard room environment, during the incubation period. The comparison between both ways of incubation is summarized in the Table 8 bellow.

Table 8. Comparison of two ways of incubation process.

| | %RSD | | | | |
|---|---|---|---|---|---|
| **Plate Types** | **UV/Vis** | **Green** | **Saturation** | **A** | **Magenta** |
| Inside of box | 1.24 | 1.23 | 0.694 | 0.82 | 0.79 |
| Outside | 0.81 | 1.30 | 0.515 | 0.31 | 0.49 |

## 3.2. Validation Experimental Results

### 3.2.1. Linear Range

To establish the linear range of the proposed method, a series of standard solutions ranging from 0.0 to 100 mg/dl were prepared and analyzed (Figure 50). Upon constructing the calibration curves for each color model, it was determined that the method exhibited linearity within the 0.0 to 20 mg/dl range (Figure 51). This confirmed linearity simplifies the application of the method to real serum samples, as it encompasses a broader range than the pathogenic levels of serum calcium, thereby ensuring accurate and reliable measurement across a relevant concentration spectrum.

**(a)**

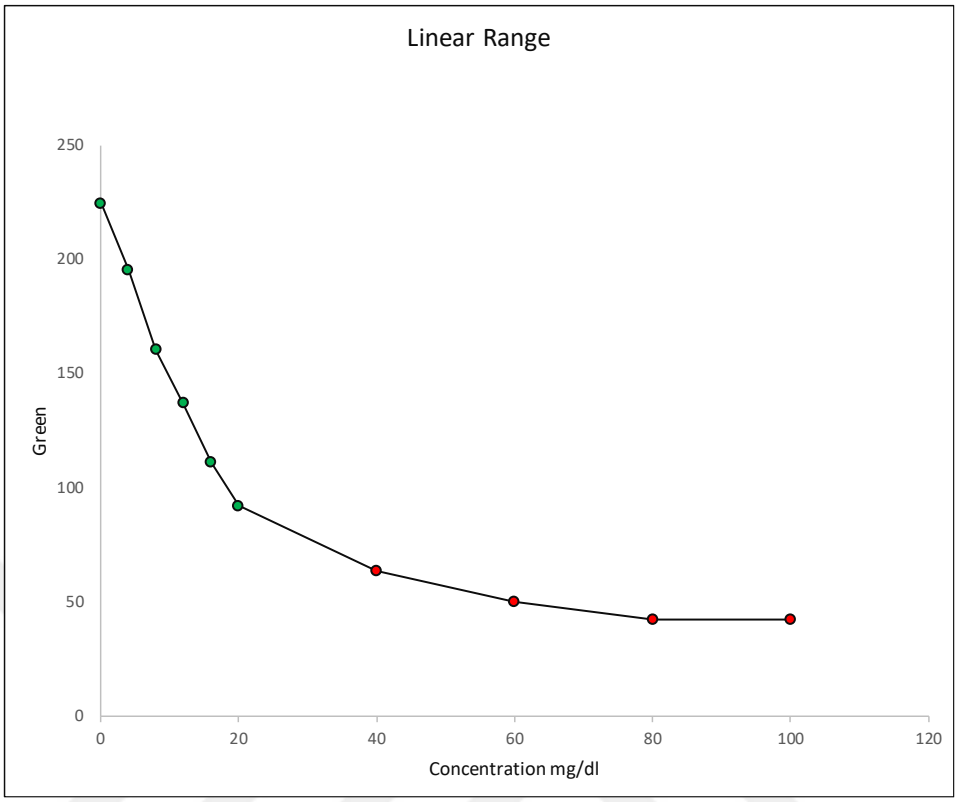
Linear Range
Green
250
200
150
100
50
0
0
20
40
60
80
100
120
Concentration mg/dl

**(b)**

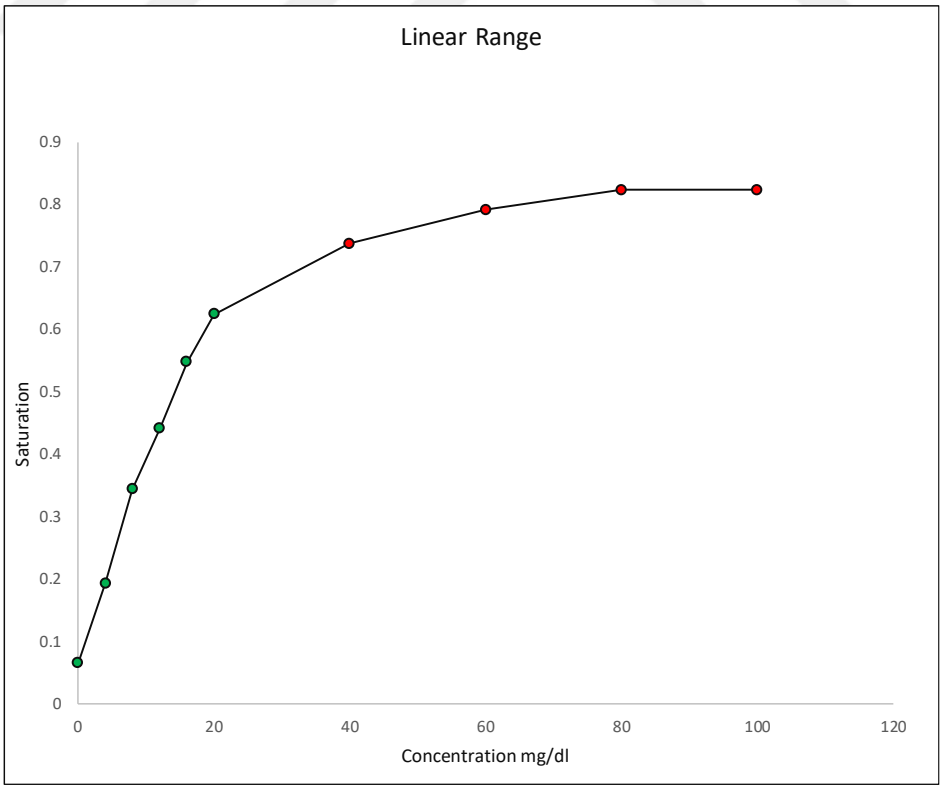
Linear Range
Saturation
0.9
0.8
0.7
0.6
0.5
0.4
0.3
0.2
0.1
0
0
20
40
60
80
100
120
Concentration mg/dl

**(c)**

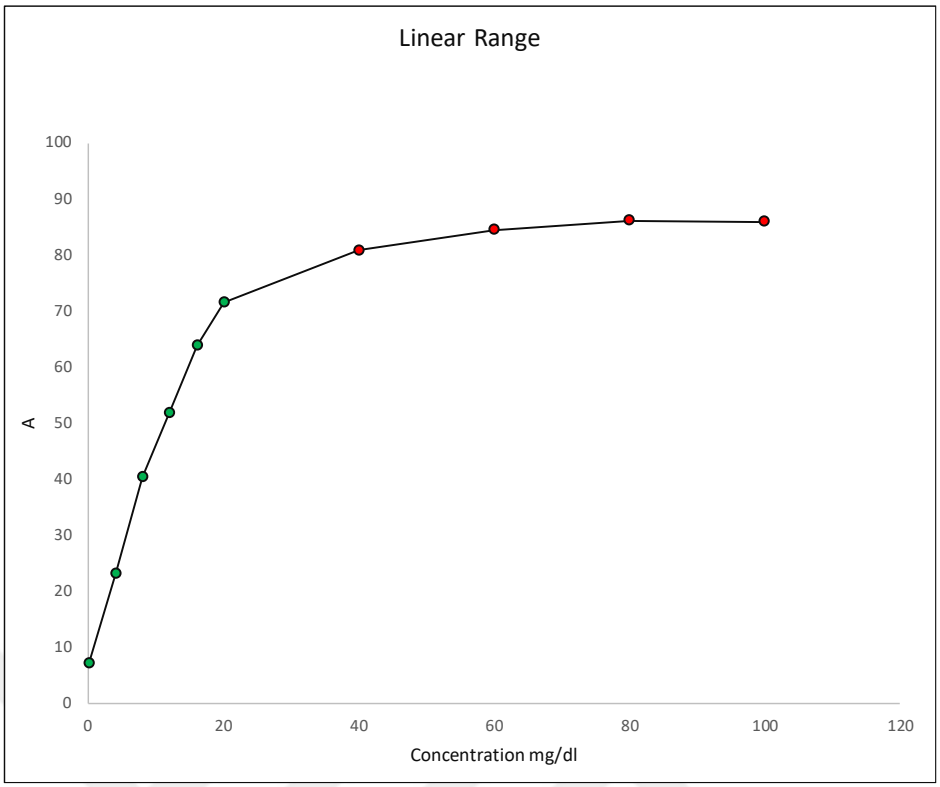


**(d)**

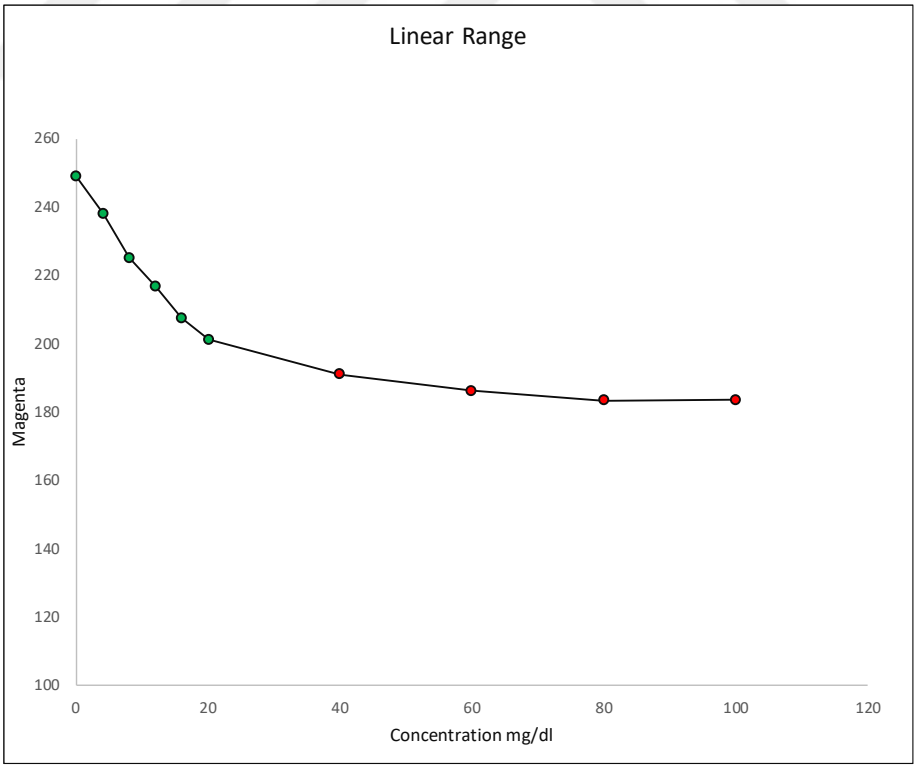


Figure 50. Calibration curve of standard solution from 0.0 to 100 mg/dl; (a) Green, (b) Saturation, (c) A, and (d) Magenta

(a)

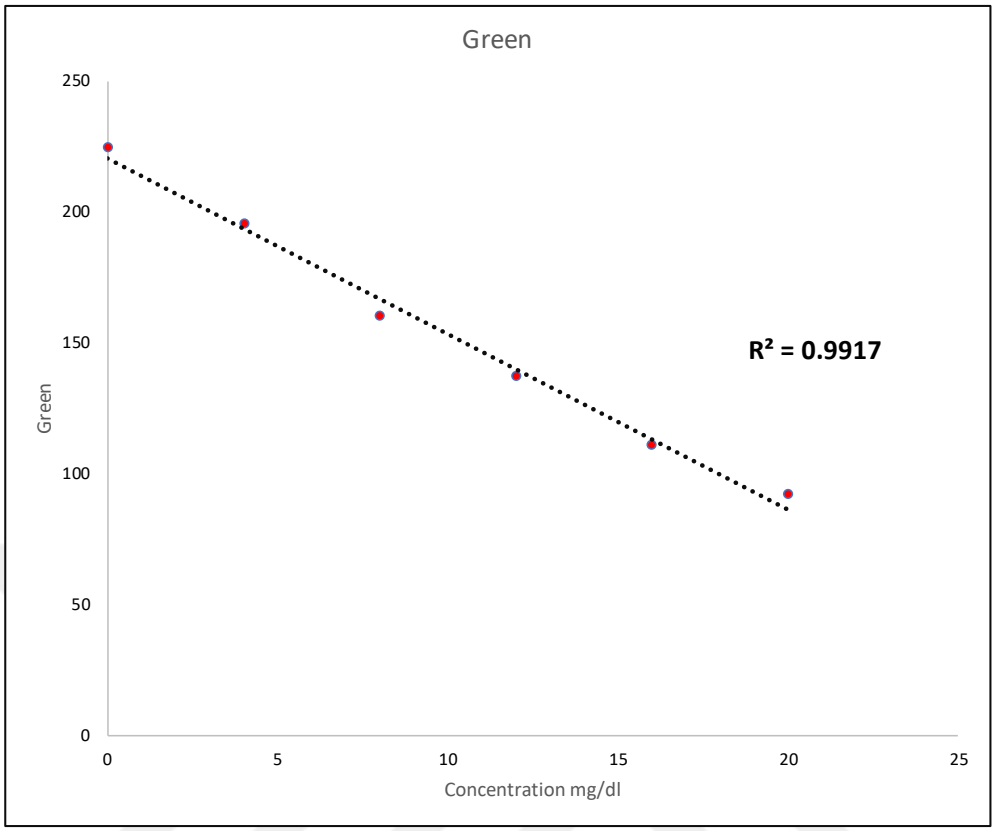
Green
250
200
150
100
50
0
Green
0
5
10
15
20
25
Concentration mg/dl
R² = 0.9917

(b)

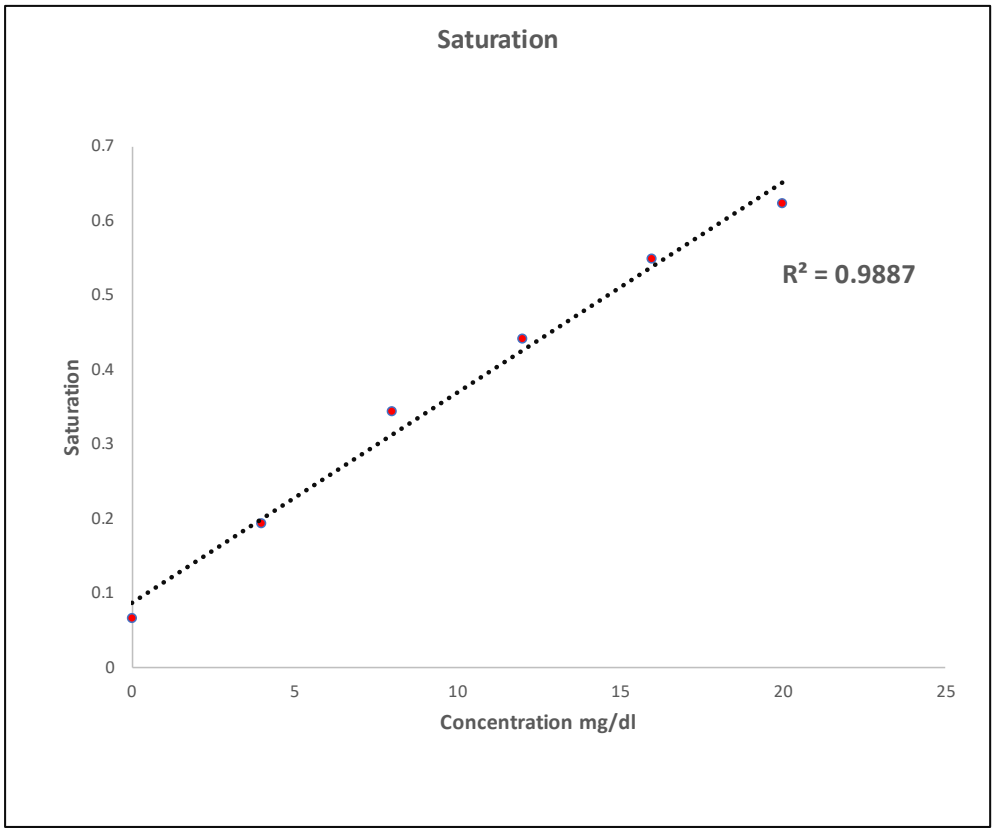
Saturation
0.7
0.6
0.5
0.4
0.3
0.2
0.1
0
Saturation
0
5
10
15
20
25
Concentration mg/dl
R² = 0.9887

(c)

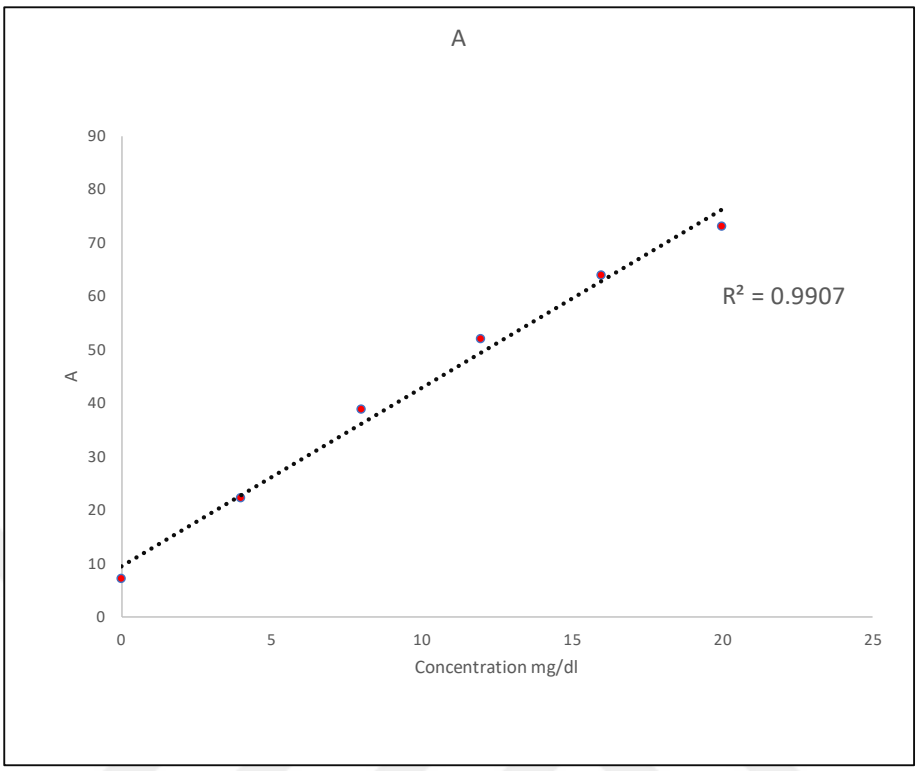


(d)

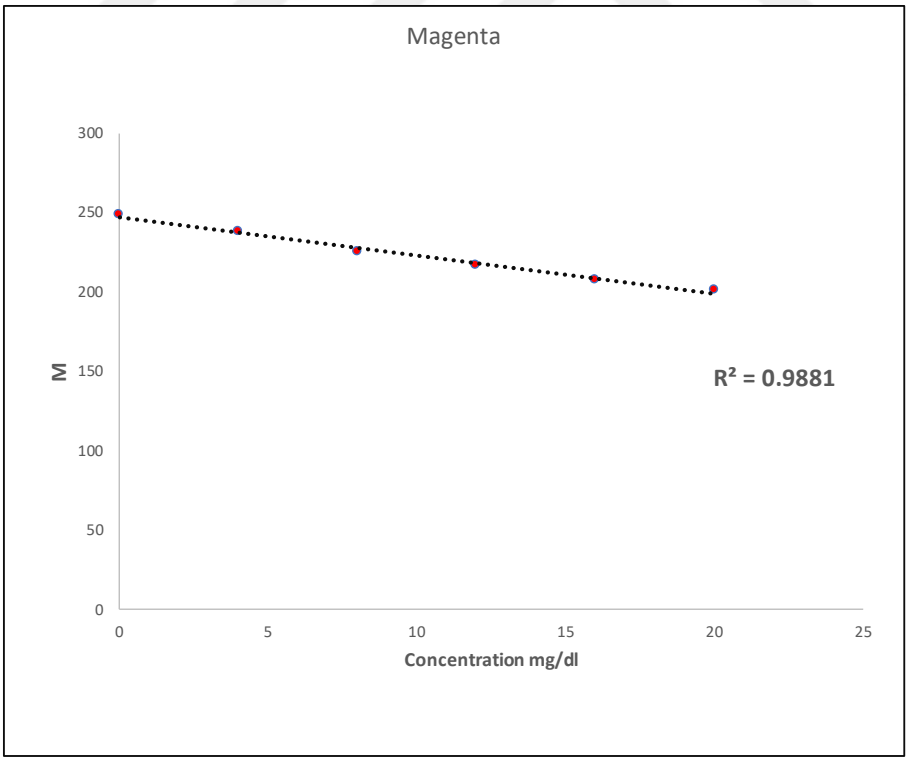


Figure 51. Calibration curve of standard solution from 0.0 to 20.0 mg/dl; (a) Green, (b) Saturation, (c) A, and (d) Magenta

### 3.2.2. Analytical performance LOD and LOQ

The limit of detection (LOD) and limit of quantitation (LOQ) were determined using specific mathematical formulas, with LOD calculated as 3Sb/m and LOQ as 10Sb/m. In these formulas, Sb refers to the standard deviation of the intercept of the calibration curve, which reflects the variability of the baseline measurement. The parameter m represents the slope of the regression equation, indicating the sensitivity of the method to changes in analyte concentration. This approach ensures precise and accurate quantification by accounting for both the inherent variability in the measurement process and the response of the analytical method.

All color models were employed to calculate the LOD and LOQ and were subsequently compared to the traditional UV-spectroscopy method. The proposed method utilizing Image J for color channel saturation demonstrates exceptional analytical performance in determining calcium, with LOD and LOQ values of 0.41 and 1.37 respectively, which are the lowest among all tested color models. Despite this, all color models exhibit robust LOD and LOQ values within acceptable ranges, indicating their reliability. Compared to the traditional UV method, this innovative approach shows superior analytical capabilities, reinforcing its effectiveness for precise calcium determination. The results are summarized in Table 9 below.

Table 9. Comparison of LOD and LOQ for both methods and color channels.

| **Methods** | **LOD** mg/dl | **LOQ** mg/dl |
|---|---|---|
| UV/Vis | 0.49 | 1.64 |
| Green | 0.46 | 1.56 |
| Saturation | 0.41 | 1.37 |
| A | 0.66 | 2.22 |
| Magenta | 0.44 | 1.49 |

### 3.2.3. Repeatability And Precision

The repeatability and precision of the proposed method were assessed by examining the percent relative standard deviation (%RSD) for both intra-day and inter-day measurements. When compared to the traditional UV-Vis method, all color channels demonstrated acceptable deviation. This indicates a strong correlation between the two methods, as reflected in the summarized results in the Table 10 below. Notably, the proposed method showed a very good comparison to the UV-Vis method, suggesting its reliability and accuracy in delivering consistent results, thereby validating its use as an alternative analytical technique.

Table 10. Interday and intraday comparation between all color models and Uv/Vis method.

| | %RSD* | |
|---|---|---|
| Method | Intraday | Interday |
| UV/Vis | 1.24 | 1.38 |
| Green | 1.28 | 2.85 |
| Saturation | 0.73 | 2.12 |
| A | 0.79 | 1.72 |
| Magenta | 0.80 | 3.35 |

** Percent Relative Standard Deviation*

### 3.2.4. Recovery

The addition-recovery test was conducted to evaluate the matrix effect by spiking a blood sample with 1.06 mg/dl of standard calcium ions solution and analyzing it using the proposed calcium assay. The absolute recovery was determined by calculating the percentage yield of the spiked concentrations. As shown in Table 11, the absolute recovery rates for UV-Vis, Green, Saturation, A, and Magenta methods at the specified concentration were 99.17%, 106.41%, 104.64%, 97.30%, and 101.82%, respectively, indicating varying degrees of accuracy and precision in the assay's performance across different analytical methods.

Table 11. Percentage recoveries of calcium ions from serum

| Added concentration: 1.06 mg/dl | | |
|---|---|---|
| **Methods** | **Found** (mg/dl) | **Percent Recovery %** |
| UV/Vis | 1.05 | 99.17 |
| Green | 1.12 | 106 |
| Saturation | 1.10 | 104.6 |
| A | 1.03 | 97.3 |
| Magenta | 1.07 | 101.8 |

### 3.2.5. Selectivity and Specificity

In the o-Cresol Phthalein Complexone (o-CPC) method, managing the interference of magnesium ions in calcium measurement is crucial. This challenge is addressed by adjusting the solution's pH to mitigate competitive binding. To evaluate the effectiveness of this optimized method for accurately determining serum calcium levels, a rigorous investigation was conducted using a spiking experiment. This involved adding known concentrations of magnesium ions to serum samples and assessing their impact on calcium measurements. By analyzing calcium concentrations before and after the addition of magnesium, the study effectively quantified any deviations, demonstrating the method's robustness in minimizing magnesium interference.

The results indicate that the addition of 1 mg/dl of magnesium has a negligible effect on calcium measurement (Table 12). Given the narrow normal and pathogenic ranges of serum magnesium, these findings validate the reliability of the o-Cresol Phthalein Complexone (o-CPC) method under the same conditions. Consequently, the impact of magnesium can be considered insignificant, allowing it to be effectively ignored in calcium assays, thereby affirming the accuracy and dependability of the optimized method for clinical applications.

Table 12. Selectivity and specificity of the UV/Vis and Image J method.

| **Method** | **Unspiked** mg/dl | **Spiked*** mg/dl | **% affected** |
|---|---|---|---|
| UV/Vis | 8.54 | 8.67 | 101 |
| Green | 8.46 | 8.26 | 98 |
| Saturation | 8.61 | 8.34 | 97 |
| A | 8.81 | 8.62 | 98 |
| Magenta | 8.99 | 8.78 | 98 |

** 1 mg//dl of Magnesium added.*

### 3.3. Determination of Calcium in Serum

To evaluate the applicability of the proposed method for quantifying calcium in serum, an independent study was conducted using a UV-Vis spectrophotometer. The accuracy of the proposed method was validated through a statistical comparison of results obtained from both techniques. This comparative analysis demonstrated that the proposed method yielded results consistent with those of the UV-Vis spectrophotometer, thus confirming its reliability and accuracy for serum calcium quantification. The successful validation through statistical comparison underscores the proposed method's efficacy and potential for broader application in clinical and laboratory settings.

The analysis involved utilizing 40 samples, which included controls, to determine calcium levels using both the proposed method and the UV-Vis method. Additionally, Image J software was employed, utilizing four color channels across four distinct models: Green, Saturation, A, and Magenta. The outcomes obtained from these four-color models, alongside those from the UV-Vis methods, are consolidated in the Table 13 below for comparative evaluation.

The relationship between color channels and UV-Vis methods is pivotal for accurately determining analytes in diverse samples. Among these channels, the green channel stands out for its exceptional correlation with UV-Vis techniques. Empirical evidence, gleaned from an analysis of 40 real samples, reveals a striking correlation coefficient of approximately 0.98, affirming the robustness of this association. However, it is essential to

recognize the utility of alternative color channels, which offer viable options for analytical procedures. Nevertheless, the unequivocal reliability of the green color model in identifying analytes, notably calcium in serum samples, underscores its indispensable role as a preferred methodological approach within the realm of analytical chemistry.

Table 13. Concentration of calcium in serum samples

| Samples ID | UV/Vis mg/dl | Image J | | | |
|---|---|---|---|---|---|
| | | Green mg/dl | Saturation mg/dl | A mg/dl | Magenta mg/dl |
| 10019396753 | 11.4 | 11.0 | 11.2 | 11.1 | 11.2 |
| 10019402493 | 11.6 | 11.2 | 11.6 | 11.6 | 11.6 |
| 10019403096 | 10.9 | 11.2 | 11.4 | 11.3 | 11.3 |
| 10019400026 | 9.0 | 8.7 | 9.2 | 9.6 | 9.4 |
| 10019400138 | 9.1 | 9.0 | 9.7 | 11.0 | 10.2 |
| 10019399978 | 7.0 | 7.2 | 7.7 | 8.8 | 8.2 |
| 10019413816 | 19.9 | 20.1 | 20.2 | 19.3 | 22.1 |
| 10019411688 | 8.4 | 8.3 | 8.6 | 8.7 | 8.7 |
| 10019412655 | 8.1 | 8.4 | 8.6 | 8.8 | 8.7 |
| 10019397724 | 9.1 | 9.2 | 9.4 | 9.6 | 9.5 |
| 10019397254 | 10.1 | 10.1 | 10.4 | 10.4 | 10.5 |
| 10019396890 | 8.4 | 8.8 | 9.0 | 10.13 | 9.5 |
| 10019398571 | 9.9 | 10.4 | 10.6 | 10.0 | 10.8 |
| 10019396614 | 10.5 | 10.3 | 10.7 | 10.7 | 10.8 |
| 10019398061 | 9.2 | 9.1 | 9.4 | 9.5 | 9.5 |
| 10019396877 | 9.5 | 9.1 | 9.2 | 9.2 | 9.2 |
| 10019397205 | 10.3 | 10.1 | 10.7 | 10.6 | 10.8 |
| 10019398095 | 9.3 | 9.9 | 10.1 | 9.8 | 10.2 |
| 10019397424 | 10.1 | 10.2 | 10.7 | 10.8 | 10.9 |
| 10019397756 | 10.3 | 10.6 | 10.8 | 10.8 | 10.7 |
| 10019397286 | 9.6 | 9.6 | 9.7 | 9.7 | 9.8 |
| 10019397126 | 9.7 | 10.3 | 10.4 | 10.1 | 10.5 |
| 10019397077 | 9.9 | 10.2 | 10.4 | 10.1 | 10.6 |
| 10019397047 | 9.3 | 9.0 | 9.3 | 9.3 | 9.3 |
| 10019396929 | 9.4 | 10.0 | 9.3 | 9.2 | 9.5 |
| 10019397999 | 9.0 | 9.0 | 9.2 | 9.4 | 9.3 |
| 10019396998 | 9.4 | 9.8 | 9.2 | 9.1 | 9.5 |
| 10019397578 | 9.7 | 9.6 | 9.8 | 10.0 | 9.8 |
| 10019396628 | 9.4 | 9.4 | 9.1 | 9.5 | 9.2 |
| 10019398057 | 9.8 | 9.9 | 9.9 | 10.0 | 10.0 |
| 10019412941 | 11.4 | 11.7 | 11.8 | 11.7 | 12.5 |
| 10019413751 | 10.9 | 11.3 | 11.4 | 11.3 | 11.8 |
| 10019413529 | 11.6 | 12.1 | 12.0 | 11.8 | 12.6 |
| 10019413509 | 11.3 | 11.4 | 11.5 | 11.3 | 11.2 |
| 10019413909 | 11.1 | 11.5 | 11.1 | 10.9 | 11.8 |
| 10019413740 | 7.9 | 7.6 | 8.2 | 9.2 | 5.5 |
| 10019412547 | 11.1 | 11.2 | 10.6 | 10.5 | 11.2 |
| Control 1 | 10.6 | 10.6 | 10.6 | 10.6 | 10.6 |
| Control 2 | 9.9 | 10.0 | 10.2 | 10.1 | 10.2 |
| Control 3 | 13.1 | 12.8 | 11.9 | 12.1 | 11.9 |

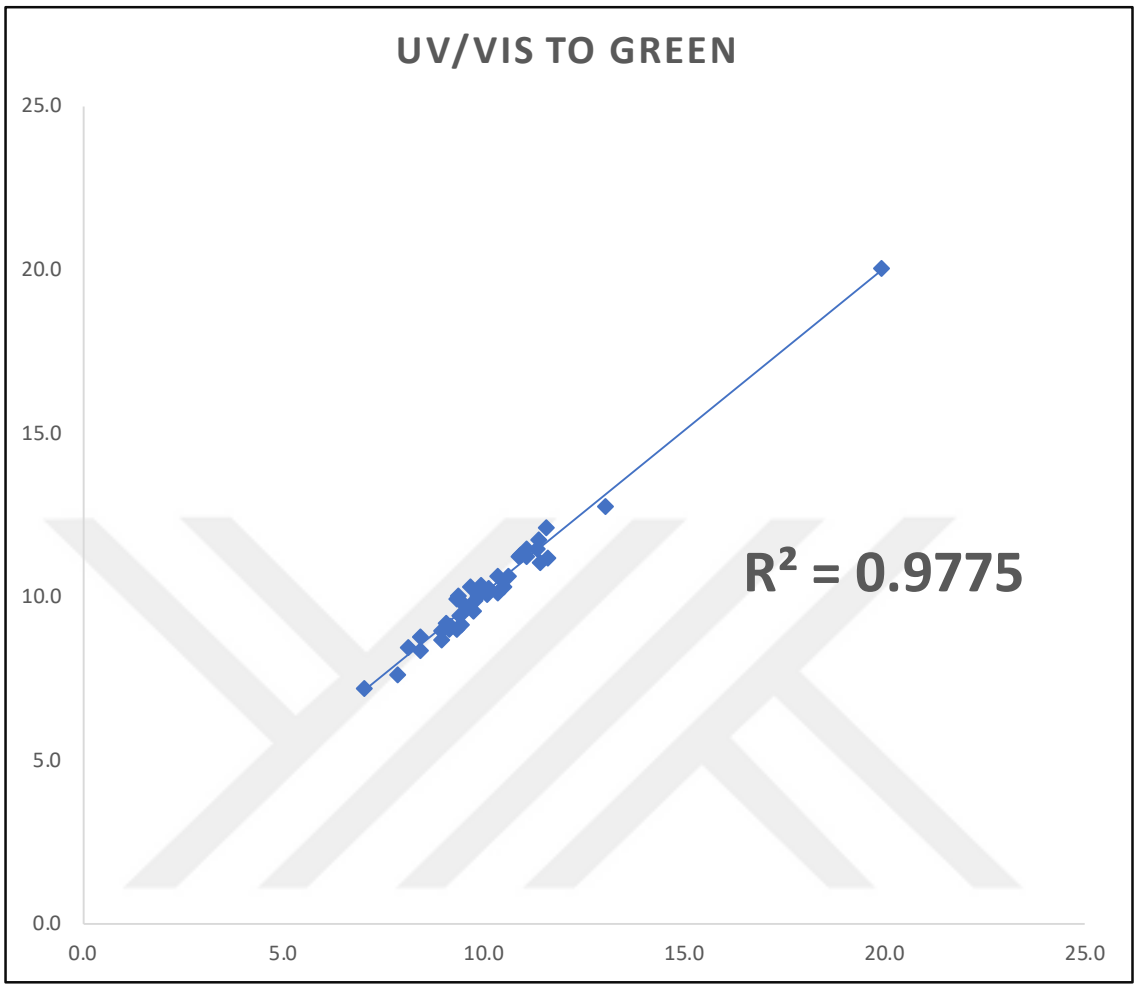


Figure 52. Comparastion of UV with Green color model.

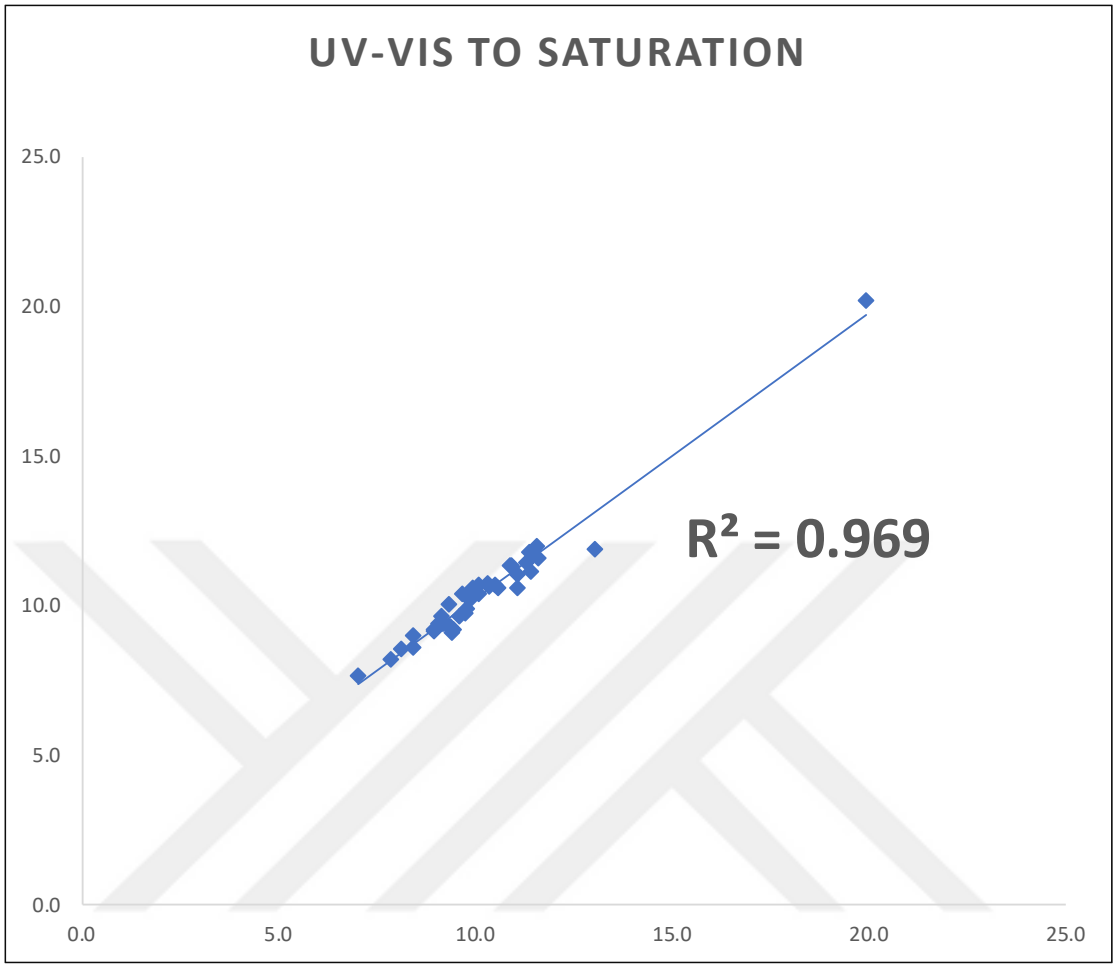


Figure 53 Comparastion of UV with Saturation color model.

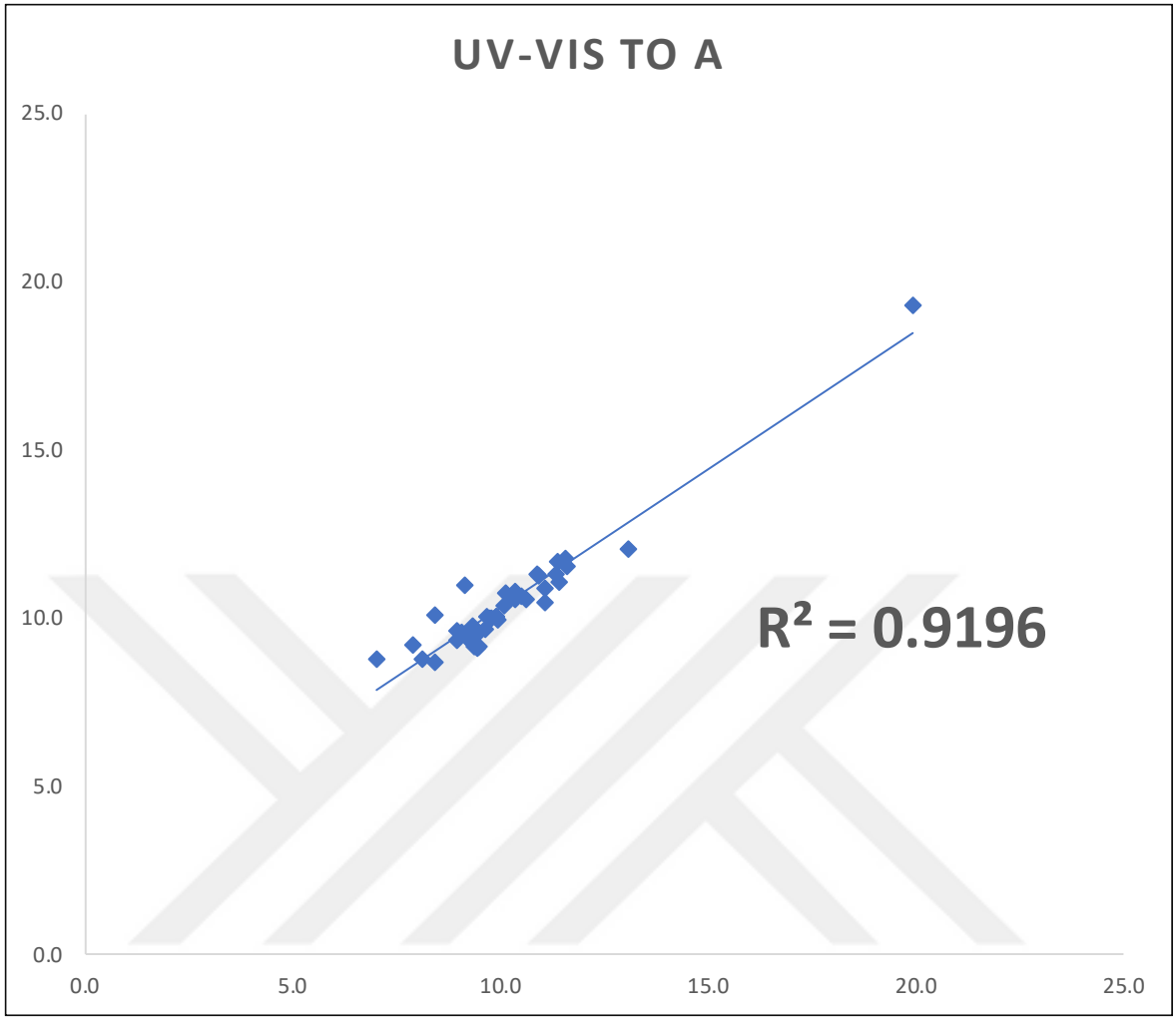


Figure 54. Comparison of UV with A color model.

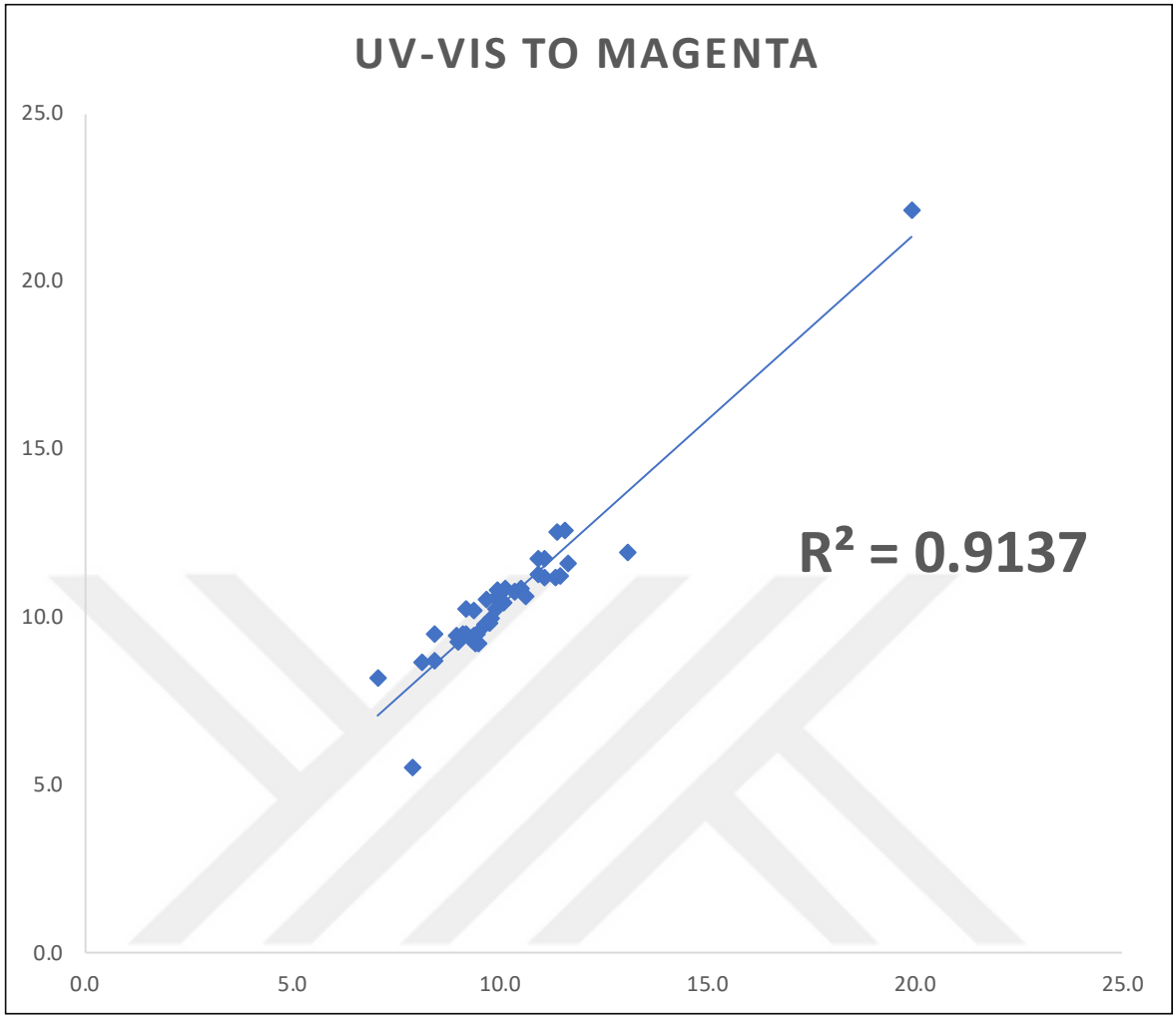


Figure 55. Comparastion of UV with Magenta color model.

## 4. CONCLUSION

This study demonstrates the practicality of utilizing smartphone digital image colorimetry as an alternative to spectrophotometry for the colorimetric detection of calcium in serum. Employing the o-Cresol Phthalein Complexone (CPC) method, a colored complex was formed to facilitate colorimetric detection. The estimated calcium levels obtained through the proposed method were compared with those from an independent study using UV-Vis spectrophotometry, revealing a high degree of statistical concordance. This confirms the reliability and accuracy of the smartphone-based method. Furthermore, this innovative approach offers significant advantages, including simplicity, affordability, broad availability, minimal energy requirements, portability, and environmental friendliness. These attributes make it an ideal solution for calcium determination in serum, especially in resource-limited laboratories and low-income countries, expanding access to essential diagnostic tools.

## 5. REFERENCE


Akar, Z. & Burnaz, N. A. 2019. A new colorimetric method for CUPRAC assay with using of TLC plate. *LWT,* 112**,** 108212.

Baker, S. & Worthley, L. 2002. The essentials of calcium, magnesium and phosphate metabolism: part I. Physiology. *Critical Care and Resuscitation,* 4**,** 301-306.

Bıswas, P., Karan, P., Pal, S., Ghosh, A. K. & Chakraborty, S. 2023. Smartphone-Interfaced Serum Calcium Level Quantification on a Simple Paper Strip Assay for Diagnostics at Extreme Point of Care. *IEEE Journal on Flexible Electronics*.

Bronner, F. 2003. Mechanisms of intestinal calcium absorption. *Journal of cellular biochemistry,* 88**,** 387-393.

Caglar, P., Tuncel, S., Malcık, N., Landers, J. & Ferrance, J. 2006. A microchip sensor for calcium determination. *Analytical and bioanalytical chemistry,* 386**,** 1303-1312.

Cao, F.-J., Cheng, H.-H., Ma, S.-X., Jıao, F. & Dong, D.-M. 2022. Three-channel smartphone-based aptamer sensor for multiplexed detecting antibiotics in water through resonance light scattering. *Sensing and Bio-Sensing Research,* 38**,** 100533.

URL-1. (2024, July 24). Corel: http://product.corel.com/help/Designer/540235012/Main/EN/Documentation/Corel-DESIGNER-Understanding-color-models.html. Has been taken.

Dadı, M., Yasır, M., Dadı, M. & Yasır, M. 2022. Spectroscopy and Spectrophotometry: principles and applications for colorimetric and related other analysis. *Colorimetry,* 1**,** 81-102.

Dash, P., Tıwarı, R., Nayak, S. & Mangaraj, M. 2022. Impact of Time Delay in the Analysis of Serum Ionized Calcium, Sodium, and Potassium. *Journal of Laboratory Physicians,* 14**,** 373-376.

De Olıveıra, L. L. G., De Olıveıra, P. L. P., Francescantonıo, P. L. C. & De Albuquerque, E. S. 2018. Total Cholesterol Determination Using Digital Image Processing.

Elagamy, S. H., Adly, L. & Abdel Hamıd, M. A. 2023. Smartphone based colorimetric approach for quantitative determination of uric acid using Image J. *Scientific Reports,* 13**,** 21888.

Fatonı, A., Anggraenı, M. D. & Dwıasi, D. W. 2019. Easy and low-cost chitosan cryogel-based colorimetric biosensor for detection of glucose. *Journal of analytical chemistry,* 74**,** 933-939.

Favus, M. J., Bushınsky, D. A. & Lemann Jr, J. 2006. Regulation of calcium, magnesium, and phosphate metabolism. *Primer on the metabolic bone diseases and disorders of mineral metabolism,* 6**,** 76-83.

Hall, J. E. 2015. *Pocket Companion to Guyton & Hall Textbook of Medical Physiology E-Book: Pocket Companion to Guyton & Hall Textbook of Medical Physiology E-Book,* Elsevier Health Sciences.

Khazaı, N., Judd, S. E. & Tangprıcha, V. 2008. Calcium and vitamin D: skeletal and extraskeletal health. *Current rheumatology reports,* 10**,** 110-117.

Lı, X.-D. & Zhaı, Q.-Z. 2020. Spectrophotometric Determination of Calcium with Dibromo-p-methylsulfonazo. *Journal of Chemistry,* 2020**,** 1-4.

Lorentz, K. 1982. Improved determination of serum calcium with 2-cresolphthalein complexone. *Clinica Chimica Acta,* 126**,** 327-334.

Markus, V., Dalmızrak, O., Edebal, O. H., Al-Nıdawı, M. & Caleb, J. 2023. Smartphone digital image colorimetry for quantification of serum proteins. *Analytical Methods,* 15**,** 5018-5026.

Mıchaylova, V. & Ilkova, P. 1971. Photometric Determination Of Micro Amounts Of Calcium With Arsenazo Iıı. *Analytica Chimica Acta,* 53**,** 194-198.

Morgan, B. R., Artıss, J. D. & Zak, B. 1993. Calcium determination in serum with stable alkaline Arsenazo III and triglyceride clearing. *Clinical chemistry,* 39**,** 1608-1612.

Mount, D. 2008. Disorders of potassium balance. *Brenner and Rector's the kidney***,** 547-587.

Nguyen, P. T., Kım, Y. I. & Kım, M. I. 2020. Reagent-free colorimetric cholesterol test strip based on self color-changing property of nanoceria. *Frontiers in chemistry,* 8**,** 798.

Olansky, A. S., Parker Jr, L. R., Morgan, S. L. & Demıng, S. N. 1977. Automated development of analytical chemical methods: The determination of senun calcium by the cresolphthalein complexone method. *Analytica Chimica Acta,* 95**,** 107-133.

Ríos-Reına, R. & Azcarate, S. M. 2022. How chemometrics revives the UV-Vis spectroscopy applications as an analytical sensor for spectralprint (nontargeted) analysis. *Chemosensors,* 11**,** 8.

Rosol, T. J. & Capen, C. C. 1997. Calcium-regulating hormones and diseases of abnormal mineral (calcium, phosphorus, magnesium) metabolism. *Clinical biochemistry of domestic animals.* Elsevier.

Schındelın, J., Rueden, C. T., Hıner, M. C. & Elıceırı, K. W. 2015. The ImageJ ecosystem: An open platform for biomedical image analysis. *Molecular reproduction and development,* 82**,** 518-529.

Schrıer, R. W. 1990. Body fluid volume regulation in health and disease: a unifying hypothesis. *Annals of internal medicine,* 113**,** 155-159.

Severenghaus, J. & Ferrebee, J. 1950. Calcium determination by flame photometry; methods for serum, urine, and other fluids.

Shrımanker, I. & Bhattaraı, S. 2019. Electrolytes.

Sıvakumar, R. & Lee, N. Y. 2021. Recent progress in smartphone-based techniques for food safety and the detection of heavy metal ions in environmental water. *Chemosphere,* 275**,** 130096.

Smıth, M. 2010. Disorders of sodium balance. *Core Topics in Endocrinology in Anaesthesia and Critical Care*.

Stern, J. & Lewıs, W. 1957. The colorimetric estimation of calcium in serum with O-cresolphthalein complexone. *Clinica Chimica Acta,* 2**,** 576-580.

Torıbıo, R. E. 2011. Disorders of calcium and phosphate metabolism in horses. *Veterinary Clinics: Equine Practice,* 27**,** 129-147.

Vargas-Muñoz, M., Morales, J., Cerdà, V., Ferrer, L. & Palacıo, E. 2023. Paper sensor-based method using a portable 3D-printed platform and smartphone-assisted colorimetric detection for ammonia and sulfide monitoring in anaerobic digesters and wastewater. *Microchemical Journal,* 188**,** 108469.

Vasudevan, D. M., Sreekumarı, S. & Vaıdyanathan, K. 2013. *Textbook of biochemistry for medical students,* JP Medical Ltd.

Wıllıs, J. 1960. Determination of calcium in blood serum by atomic absorption spectroscopy. *Nature,* 186**,** 249-250.

Wınarno, G. N. A., Prıbadı, A., Marulı, H. J., Achmad, E. D., Anwar, R., Mose, J. C., Nısa, A. S. & Trıanasarı, N. 2021. Ratio of serum calcium to magnesium levels on pregnancy with and without preeclampsia. *Medical Science Monitor: International Medical Journal of Experimental and Clinical Research,* 27**,** e932032-1.

Yam, K. L. & Papadakıs, S. E. 2004. A simple digital imaging method for measuring and analyzing color of food surfaces. *Journal of food engineering,* 61**,** 137-142.

Zhao, T., Lıang, X., Guo, X., Yang, X., Guo, J., Zhou, X., Huang, X., Zhang, W., Wang, Y. & Lıu, Z. 2023. Smartphone-based colorimetric sensor array using gold nanoparticles for rapid distinguishment of multiple pesticides in real samples. *Food Chemistry,* 404**,** 134768.

Zhong, J. & Wang, X. 2019. *Evaluation technologies for food quality,* Woodhead Publishing.

## RESUME

Amad Younis After completing middle school at the Chra School, he began his high school education at Brayaty High School in 2009. Upon graduating from high school, he enrolled in the University of Duhok, Department of Chemistry, in the 2012-2013 academic year and graduated in 2017 with excellent marks. Immediately after graduation, he began working at the same university in the position of assistant researcher. He is fluent in four languages: Kurdish, Arabic, Turkish, and English.